POLARIZED ELECTRONIC SPECTRA FOR THE CRYSTALS OF THREE COMPOUNDS, POTASSIUM TETRABROMOPLATINATE(II) DIHYDRATE, TETRAETHYLAMMONIUM HEXABROMODIPLATINATE(II), AND TETRA-μ-GLYCINE-DIMOLYBDENUM(II) SULFATE TETRAHYDRATE

Timothy Joseph Peters

Ph.D. Thesis Submitted to Iowa State University

MASTER

Ames Laboratory, ERDA

Iowa State University

Ames, Iowa 50011

Date Transmitted: June 1977

PREPARED FOR THE U.S. ENERGY RESEARCH AND DEVELOPMENT ADMINISTRATION UNDER CONTRACT NO. W-7405-eng-82

DISCLAIMER

This report was prepared as an account of work sponsored by an agency of the United States Government. Neither the United States Government nor any agency Thereof, nor any of their employees, makes any warranty, express or implied, or assumes any legal liability or responsibility for the accuracy, completeness, or usefulness of any information, apparatus, product, or process disclosed, or represents that its use would not infringe privately owned rights. Reference herein to any specific commercial product, process, or service by trade name, trademark, manufacturer, or otherwise does not necessarily constitute or imply its endorsement, recommendation, or favoring by the United States Government or any agency thereof. The views and opinions of authors expressed herein do not necessarily state or reflect those of the United States Government or any agency thereof.

DISCLAIMER

Portions of this document may be illegible in electronic image products. Images are produced from the best available original document.

Polarized electronic spectra for the crystals of three

compounds, potassium tetrabromoplatinate(II) dihydrate,

tetraethylammonium hexabromodiplatinate(II), and

tetra-μ-glycine-dimolybdenum(II) sulfate
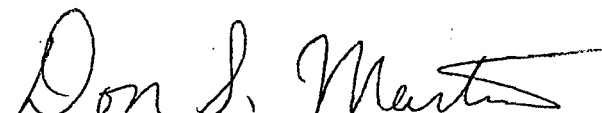
tetrahydrate

by

Timothy Joseph Peters

A Dissertation Submitted to the

Graduate Faculty in Partial Fulfillment of

The Requirements for the Degree of

DOCTOR OF PHILOSOPHY

Department: Chemistry
Major: Physical Chemistry

Approved:

In Charge of Major Work

For the Major Department

For the Graduate College

Iowa State University
Ames, Iowa

1977

TABLE OF CONTENTS

Polarized electronic spectra for the crystals of three
compounds, potassium tetrabromoplatinate(II) dihydrate,
tetraethylammonium hexabromodiplatinate(II), and
tetra-μ-glycine-dimolybdenum(II) sulfate
tetrahydrate*

Timothy Joseph Peters

Under the supervision of Don S. Martin, Jr.
From the Department of Chemistry
Iowa State University

Crystals of $K_2PtBr_4 \cdot 2H_2O$ have an orthorhombic unit cell with a = 8.31(2) Å, b = 13.73(3) Å and c = 4.84(1) Å.

The polarized absorption spectra for $K_2PtBr_4 \cdot 2H_2O$, $[N(C_2H_5)_4]_2Pt_2Br_6$, and $Mo_2(O_2CCH_2NH_3)_4(SO_4)_2 \cdot 4H_2O$ have been recorded at 300 and 15K. In $K_2PtBr_4 \cdot 2H_2O$ the bands at 24,000 and 27,000 cm^{-1} in both a- and b-polarizations appear to be vibronically induced. The energy spacing of the vibrational structure was noted to be somewhat higher at 180 cm^{-1} than for the analogous structure of K_2PtBr_4. The presence of a $PtBr_6^{2-}$ impurity gave rise to red sections, which evidently were due to the electron transfer,

Pt(IV)←Pt(II), occurring in c-polarization. Very weak spin-forbidden bands were observable in all three polarizations below 23,500 cm^{-1}. In the crystal spectra of $[N(C_2H_5)_4]_2Pt_2Br_6$ the transitions were defined with respect to the three molecular axes of the $Pt_2Br_6^{2-}$ ion. Excited states were assigned under the D_{2h} point group symmetry of the ion. The delocalization of the d electrons gave rise to strongly enhanced intensities for both spin-forbidden and spin-allowed d←d transitions. The M←L charge-transfer transitions occur at lower energies in the case of $Pt_2Br_6^{2-}$ than in $PtBr_4^{2-}$. These charge transfer transitions were found from the polarizations to originate from the terminal bromides. The crystal spectra of $Mo_2(O_2CCH_2NH_3)_4(SO_4)_2 \cdot 4H_2O$ were recorded through the region 20,000 - 25,000 cm^{-1}. The spectra at 15K revealed the vibrational structure in the two recorded polarizations. The electronic transition observed in these spectra was forbidden under the local symmetry of D_{4h}. The crystallographic site symmetry was S_4. The observed transition was attributed to a vibronic excitation. Therefore this transition could not be assigned from the observed data as the electric dipole allowed δ^*←δ transition under D_{4h} symmetry.

I. INTRODUCTION

Polarized crystal absorption spectra have been obtained for the coordination compounds of platinum(II), $K_2PtBr_4 \cdot 2H_2O$ and $[N(C_2H_5)_4]_2Pt_2Br_6$. Absorption spectra have also been recorded for single crystals of the dimeric molybdenum compound, $Mo_2(O_2CCH_2NH_3)_4(SO_4)_2 \cdot 2H_2O$.

Crystals of $K_2PtBr_4 \cdot 2H_2O$ were found to be orthorhombic and absorption spectra were obtainable for light polarized in the a, b, and c directions of the unit cell. In the case of $[N(C_2H_5)_4]_2Pt_2Br_6$, the unit cell was triclinic and crystals show the development of a 001 cleavage face. The extinction directions for this face were found to be very closely aligned to two molecular axes for the $Pt_2Br_6^{2-}$ ion. These molecular axes apparently establish the axes of the optical indicatrix and thus there is very little wavelength dependence for the direction of these axes. The absorption spectra in these extinction directions were recorded. The unit cell of $[Mo_2(O_2CCH_2NH_3)_4](SO_4)_2 \cdot 4H_2O$ is tetragonal and polarized absorption spectra were recorded in the a and c crystal directions.

Electronic spectroscopy has been widely applied to provide information about molecular energy levels and also about crystal interactions (1-4). Absorption spectra have permitted the assignments of the electronic energy states

for $PtCl_4{}^{2-}$. In K_2PtCl_4 this ion occupies a site of full D_{4h} symmetry in a tetragonal unit cell. A rendition of this unit cell looking down the c or stacking axis can be seen in Figure 1.

The interaction of molecules with electromagnetic radiation can be treated by radiation theory (5). This particular theory introduces a time dependent perturbation into the Hamiltonian operator. The perturbation is the result of an interaction between an oscillating electromagnetic field and the system's instantaneous dipole moment. The interaction produces an oscillation between two states of the system. This results in the absorption or emission of radiation of energy, hv, which is the energy of separation of the two states. The rate of an induced-radiative transition is found to be proportional to the energy density of the absorption

As an example of the application of radiation theory consider an arbitrary wave function corresponding to the stationary states of the system written as,

$$\Psi = a_1\Psi_1 + a_2\Psi_2 + \ldots + a_r\Psi_r \tag{1}$$

The functions Ψ_n are then of the form,

$$\Psi_n(q,t) = \phi_n(q)e^{-iE_nt/\hbar} \tag{2}$$

Figure 1. Unit cell of K_2PtCl_4, dashed atoms at $z = \frac{1}{2}$
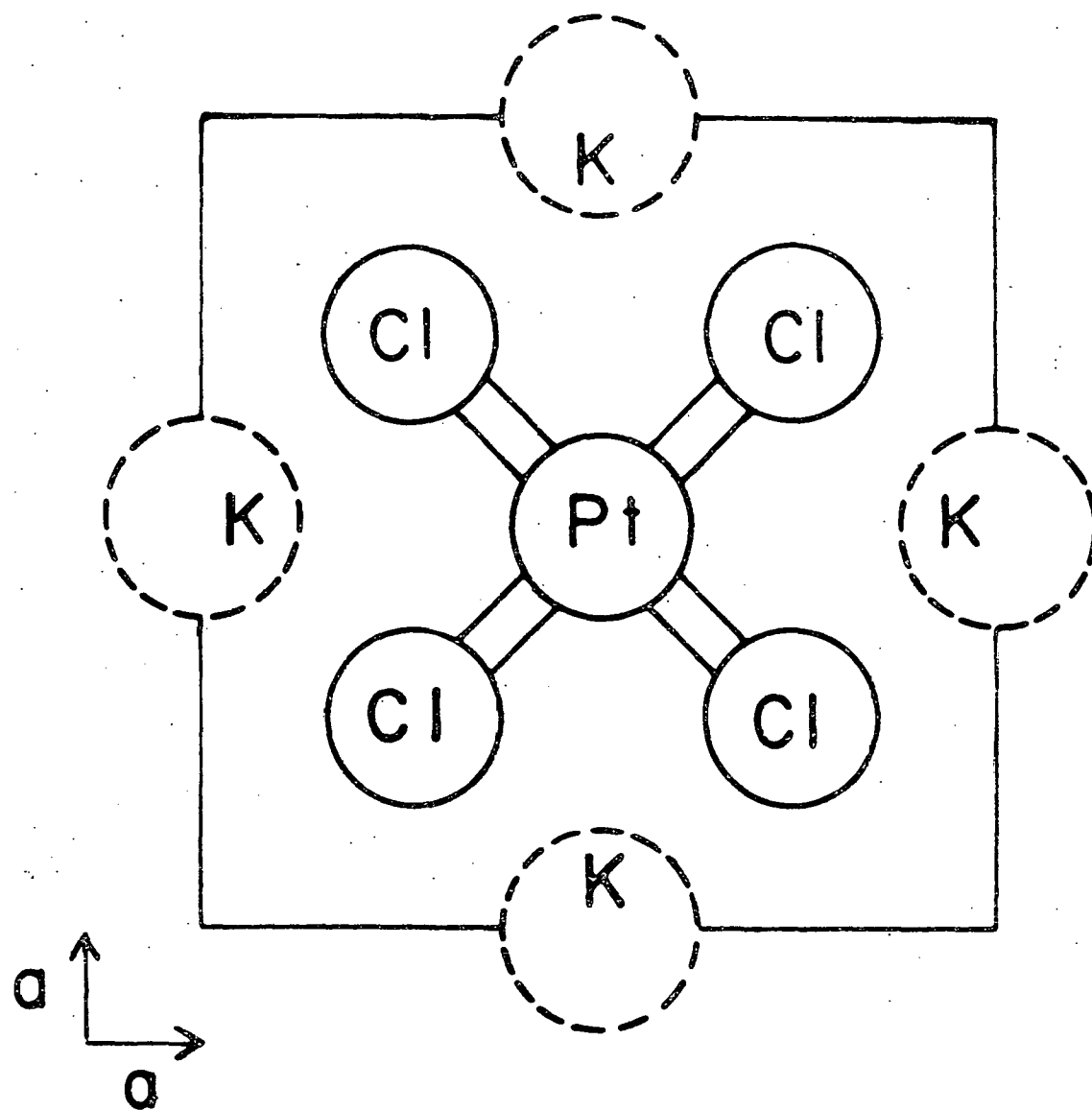
where q represents a set of general coordinates. The
unperturbed Hamiltonian operator, $\hat{H}_o$, operating on this
function gives

$$\hat{H}_o \Psi_n = i\hbar \frac{\partial \Psi_n}{\partial t} = E_n \Psi_n \tag{3}$$

The actual Hamiltonian including the time perturbation can
be expressed as,

$$\hat{H} = \hat{H}_o + \hat{H}' \tag{4}$$

The coefficients, a_n, in the expansion of the arbitrary
wave function vary with time at a rate given by,

$$\frac{da_m}{dt} = \frac{-i}{\hbar} \sum_n a_n H'_{mn}(t) \tag{5}$$

where $H'_{mn}(t)$ is a matrix element calculated from the wave
functions, $\Psi_m(q,t)$ and $\Psi_n(q,t)$. The matrix elements of
$H'_{mn}(t)$ relative to $\phi_m(q)$ and $\phi_n(q)$ give,

$$\frac{da_m}{dt} = \frac{-i}{\hbar} \sum_n a_n H'_{mn} e^{i\omega_{mn} t} \tag{6}$$

where $\omega_{mn} = \frac{(E_m - E_n)}{\hbar}$.

Consider now a perturbing electromagnetic wave propa-
gating in the direction of the z-axis with its electric
vector directed along the x-axis. The energy of this
particular electric vector can be written as

$$E_x = 2E_x^{\,o} \cos(\omega t - 2\pi z/\lambda) \tag{7}$$

From this result the time dependent perturbation operator, H', can then be written as the vector dot-product,

$$\hat{H}' = \mu_x \cdot E_x \tag{8}$$

where μ_x is the x-component of the electric dipole moment. If the wavelength of the radiation is larger than the dimensions of the molecules, then the $2\pi z/\lambda$ term in equation (7) can be dropped. This reduces the expression to the form,

$$\frac{da_m}{dt} = -\frac{2E_x^{\,o}}{\hbar} \sum_n a_n \mu_{mn}^x \cos \omega t \cdot e^{i\omega_{mn} t} \tag{9}$$

where μ_{mn}^x is a matrix element of the dipole in the x-direction. This last expression can be put into exponential form as,

$$\frac{da_m}{dt} = -\frac{E_x^{\,o} i}{\hbar} \sum_n a_n \mu_{mn}^x \left[e^{i(\omega_{mn}+\omega)t} + e^{i(\omega_{mn}-\omega)t} \right] \tag{10}$$

If now the system is in the state, Ψ_n, when $a_n = 1$ and all other a_m-coefficients are zero, then

$$\frac{da_m}{dt} = \frac{-E_x^{\,o} i}{\hbar} \mu_{mn}^x \left[e^{i(\omega_{mn}+\omega)t} + e^{i(\omega_{mn}-\omega)t} \right] \tag{11}$$

This expression can be integrated by assuming that the probability of the system undergoing a transition is small so that a_n is very close to unity. Integration over time with the boundary condition, $a_m = 0$ at $t = 0$, gives

$$a_m = \frac{E_x^{\,\circ}\mu_{mn}^x}{\hbar}\left[\frac{(1-e^{i(\omega_{mn}+\omega)t})}{\omega_{mn}+\omega} + \frac{(1-e^{i(\omega_{mn}-\omega)t})}{\omega_{mn}-\omega}\right] \quad (12)$$

The absorption of a quantum of radiation is represented by the second term in the expression of equation (12). That is, $E_m > E_n$, where E_m is the energy of the final state, then the term with $(\omega_{mn}-\omega)$ in the denominator becomes large since ω_{mn} and ω are nearly equal. The equation for absorption would then be written as,

$$a_m = \frac{E_x^{\,\circ}\cdot\mu_{mn}^x}{\hbar}\frac{(1-e^{i(\omega_{mn}-\omega)t})}{\omega_{mn}-\omega} \quad (13)$$

The probability for the system being in the state, Ψ_m, after a time, t, is given by the product,

$$a_m^*a_m = \frac{(E_x^{\,\circ})^2|\mu_{mn}^x|^2}{\hbar^2 t^{-2}}\frac{\sin^2[(\omega_{mn}-\omega)/2]\cdot t}{[(\omega_{mn}-\omega)/2]^2 t^2} \quad (14)$$

Integration of equation (14) over all radiation frequencies completes the calculation. The transition probability is extremely small except in a small region near ω_{mn} and this permits treating $E_x^{\,\circ}$ as the constant, $E_x^{\,\circ}(\nu_{mn})$, in the integration. The integration is carried out over ω from $-\infty$ to ∞ and gives the result,

$$a_m^*a_m = [E_x^{\,\circ}(\nu_{mn})]^2\cdot|\mu_{mn}^x|^2 t/h \quad (15)$$

where $E_x^{\circ}(\nu_{mn})$ is the electric-vector of the radiation at frequency, ν_{mn}.

The time derivative of $a_m^* a_m$ gives the rate of transition from state-n to state -m and is represented by

$$\frac{d(a_m^* a_m)}{dt} = [E_x^{\circ}(\nu_{mn})]^2 |\mu_{mn}^x|^2 / \hbar^2 \tag{16}$$

Equation (16) can be rewritten in terms of the Einstein coefficient for induced absorption of radiation, B_{nm}, as

$$\frac{d(a_m^* a_m)}{dt} = B_{nm} \, \rho(\nu_{mn}) \tag{17}$$

where $\rho(\nu_{mn})$ is the radiation density. This radiation density can be shown to be equal to $3/2\pi[E_x^{\circ}(\nu)]^2$. This permits the Einstein coefficient for induced absorption to be written as

$$B_{nm} = \frac{2\pi}{3\hbar^2}(|\mu_{mn}^x|^2 + |\mu_{mn}^y|^2 + |\mu_{mn}^z|^2) \tag{18}$$

or

$$B_{nm} = \frac{2\pi}{3\hbar^2}|\mu_{mn}|^2 \tag{19}$$

Equation (19) serves as the basis for the selection rules of an electric dipole transition. The quantity, μ_{mn}, in equation (15) is known as the transition moment. This electric dipole transition moment is defined by the equation

$$\mu_{mn} = \int \Psi_m^*(-e \sum_i \underset{\sim}{r}_i) \Psi_n d\tau_{elec} \qquad (20)$$

where Ψ_n and Ψ_m are the wave functions of the states between which the transition is occurring. The quantity, $\underset{\sim}{r}_i$, is the dipole vector for the ith electron and the summation is taken over all the electrons in the system.

When a light beam of frequency ν penetrates a medium, the absorbance of the radiation is defined as

$$A = \log(I_0/I) \qquad (21)$$

where I_0 and I are intensities of the light beam. The absorption is proportional to the concentration of the molecular species as well as the path length. This relation for the absorption is the well-known Beer-Lambert Law (6) written as

$$A = \epsilon ML \qquad (22)$$

where M is molar concentration and L is path length in cm. The constant of proportionality, ϵ $(cm^{-1}M^{-1})$, serves to characterize the intensity of absorption by the molecular species. The amount of light absorbed is proportional to the number of absorbing molecules.

The extinction coefficient, $\epsilon(\nu)$, is defined by the equation

$$\epsilon(\nu) = \frac{1}{CL} \log_{10}(I_0/I) \qquad (23)$$

The intensity of the beam is proportional to the number of photons/cm^2-sec or the photon flux, Q. A differential of flux, dQ, passing through a differential thickness, dx, may be related to the radiation density, ρ, and the Einstein coefficient, B_{nm}, by the expression,

$$dQ = \frac{B_{nm}(\rho d\nu)}{1000} (M)(N)dx \tag{24}$$

where N is Avogradro's number and M is the molarity. The radiation density, ρ, is related to the photon flux and the energy by the equation

$$\rho d\nu = \frac{Qh\nu_{nm}}{(c/n)} \tag{25}$$

where c here is the speed of light and n is the refractive index. Substitution of this value into equation (24) gives

$$\frac{dQ}{Q} = \frac{B_{nm}h\nu_{nm}}{(c/n)} \cdot \frac{MN}{1000} dx \tag{26}$$

Integration of equation (26) gives the extinction coefficient, $\varepsilon(\nu)$, as

$$\varepsilon(\nu) = \frac{B_{nm}h\nu}{(c/n)} \cdot \frac{MN}{(1000)(2.303)} \tag{27}$$

This expression is normally integrated over dν to account for the fact that absorption occurs over a band of finite width. The value of the extinction coefficient at the

maximum of an absorption band serves to give a rough idea of the transition probability.

The oscillator strength, f, is a better measurement of the transition intensity and includes the integration of absorbance over the energy range in cm^{-1} for the transition band. The definition of oscillator strength is based upon an assignment of unity for the oscillator strength of an oscillator made up of an electron bound to a center of attraction by a Hooke's law force (5). For such a model the Einstein coefficient, B_{nm}, and the integrated extinction coefficient can be calculated. The f-value for an actual transition is calculated by a ratio of its integrated coefficient to the value for f = 1 for the bound electron oscillator. The oscillator strength can then be expressed as the integral,

$$f = 4.32 \times 10^{-9} \int \varepsilon d\bar{\nu} \qquad (28)$$

where $\bar{\nu}$ is in wavenumbers. The magnitude of f depends upon the extent to which an absorption transition is allowed or forbidden. From equation (27) the oscillator strength can be related to the dipole strength, which can be expressed in terms of the transition dipole moment, μ_{mn}. This expression can now be written as

$$f = 1.085 \times 10^{-5} \bar{\nu}_{mn} |\mu_{mn}|^2 \qquad (29)$$

where $\bar{\nu}_{mn}$ equals the transition energy.

The dipole moment operator is written as,

$$\underset{\sim}{d} = - e \sum_i \underset{\sim}{r}_i \tag{30}$$

and is a sum of one-electron operators. Allowed electronic transitions will correspond to one-electron excitations; therefore, the transition dipole moment can be expressed in terms of a one-electron integral such as,

$$\mu = \int u'^* \underset{\sim}{r} \, u^o \, d\tau \tag{31}$$

where the electron can be considered to be excited from the orbital u^o to u'. Selection rules may be ascertained from the symmetries of u^o, u', and $\underset{\sim}{r}$. The product of these three terms in the dipole transition integral must contain the totally symmetric representation in order to give a non-zero integral. The wave function of the molecule can be expressed in the form of a Slater determinant as,

$$\Psi_o = | \ \ldots \ u_i^o S \ \ldots \ |/\sqrt{n!} \tag{32}$$

where S represents the spin wave function of α or β.

In the case of the $PtCl_4^{2-}$ ion in D_{4h} symmetry, the totally symmetric representation would be A_{1g}. The direct product of the symmetry representations of u^o and u' will give the symmetry of the one electron excited state. In the D_{4h} point group the z-component of $\underset{\sim}{d}$ serves as a basis

function for the irreducible representation, A_{2u}, and the x,y-components are basis functions for the degenerate E_u representation. A nonzero transition dipole integral will result for transitions to A_{2u} for z-polarized radiation and for transitions to E_u for x,y-polarization. A dipole transition will be forbidden if the transition is occurring between states of the same parity such as the gerade to gerade d←d transitions. However, d←d transitions are possible as seen in the case of K_2PtCl_4 spectra below 40,000 cm^{-1}. This has generally been explained as the result of inversion symmetry removal for the ion or molecule. This inversion center removal may be accomplished through local asymmetric fields or as in the case of $PtCl_4^{2-}$ by an asymmetric vibration of the ion.

The Herzberg-Teller vibronic coupling model describes such introduction of asymmetry into the electronic states through molecular vibrations. This treatment is an application of first-order perturbation theory with the normal vibrational mode coordinates, Q_i, serving as the perturbation of the electronic wave function.

Under the Born-Oppenheimer approximation the total molecular wave function, Ψ, may be written as a product of an electronic wave function, ψ_e, and a nuclear wave function, Φ_N, or

$$\Psi(x,y,z, \ldots Q_i \ldots) = \psi_e(x,y,z, \ldots Q_i \ldots)$$
$$\Phi_N(\ldots Q_i \ldots) \qquad (33)$$

where Q_i is a normal vibration coordinate and x,y,z are the electronic coordinates. The total vibrational wave function, Φ_v, is defined as the product of all normal mode wave functions as

$$\Phi_v(.. Q_i ..) = \prod_{i=1}^{3N-6} \rho_{v,i}(Q_i) \qquad (34)$$

The transition moment integral can be written in the form

$$P(f_v \leftarrow oo) = |\int\int \psi_f \Phi_{v'} | \underline{d} | \psi_o$$
$$\Phi_o \, d\tau_{elec} \, d\tau_{vib} |^2 \qquad (35)$$

where the vibronic transition is occurring between a ground state electron wave function, ψ_o, and its associated vibration as the function, Φ_o, to an excited state, ψ_f, with vibration, $\Phi_{v'}$.

The Herzberg-Teller expansion of the electronic Hamiltonian in a Taylor series takes the form,

$$H_{el}(Q'') = H_{el}(0) + \sum_{i=1}^{3N-6} \left(\frac{\partial H_{el}}{\partial Q_i''}\right)_{Q=0} \cdot Q_i'' + \ldots \qquad (36)$$

This expansion applies around the equilibrium ground state geometry where Q''=0. The first term in this expansion is the Hamiltonian with no nuclear coordinate dependence and the second term permits a perturbative influence of the

normal coordinates. The Herzberg-Teller electronic wave function can be generated by using the electronic wave functions with equilibrium nuclear positions, $\psi(x,o)$, as a basis set. This wave function can be written as,

$$\psi_f(x,Q) = \psi_f(x,o) + \sum_{j \neq f} \left[\frac{\int \psi_j(x,o) |V| \psi_f(x,o) d\tau_{elec}}{E_f - E_j} \right] \psi_j(x,o) \quad (37)$$

where $V = \sum_{i=1}^{3N-6} \left(\frac{\partial H_{el}}{\partial Q_i} \right)_{Q=o} \cdot Q_i$. Note that the wave functions used as a basis set are independent of Q and are being used to generate a wave function with Q-dependence. It can also be seen that more than one normal vibration can be involved in a vibronic type of transition.

Insertion of the vibronic wave functions of equation (37) for both ground and excited states in equation (35) gives

$$\langle \psi_f(x,o) | \psi_o(x,o) \rangle \langle \Phi_{v'} | \Phi_o \rangle + \{ \sum_j \frac{\langle \psi_o | \frac{\partial H}{\partial Q} | \psi_j \rangle}{E_j - E_o}$$

$$\cdot \langle \psi_o | \underset{\sim}{d} | \psi_j \rangle + \sum_j \frac{\langle \psi_f | \frac{\partial H}{\partial Q} | \psi_j \rangle}{E_j - E_f} \langle \psi_f | \underset{\sim}{d} | \psi_j \rangle \} \langle \Phi_{v'} | Q | \Phi_o \rangle$$

+ higher order terms $\quad (38)$

The integrals in equation (38) will be nonzero only when the product of the irreducible representations of the electronic states, the vibrational wave functions, and the

electric dipole moment contain the totally symmetric representation. This relationship is written in terms of irreducible representations as,

$$\Gamma_f \; x \; \Gamma_v \; x \; \Gamma_d \; x \; \Gamma_o \; x \; \Gamma_{v_o} = \Gamma^A \qquad (39)$$

where Γ_f and Γ_o are the representations of the electronic states, Γ_v and Γ_{v_o} are representations of the vibrational states, and Γ_d is the representation of the dipole moment.

The occupation of the vibrational levels of molecules by molecules is temperature dependent; that is, as the temperature increases occupation of higher vibrational states increases. More energetic vibrations bring about greater asymmetries in the molecule and thus vibronic transition intensities are seen to increase as temperature increases. The temperature dependence of the band intensity can be exploited to obtain greater insight into the absorption spectra. The molecules will exist in the ground state of all vibrational modes when cooled to liquid helium temperatures (<15K). When crystals are cooled the spectra will show a narrowing of the absorption bands and vibronic transitions will show a reduction in intensity. The temperature dependence of a vibronic transition can be expressed as,

$$f(T) = f(T=o)\coth(h\nu_i/2kT) \qquad (40)$$

where ν_i is the frequency of the asymmetric vibration
(7).

A change in total electronic spin is normally forbidden
for electronic transitions. However, spin-orbit coupling
can result in the breakdown of this selection rule. The
spin-orbit coupling is particularly strong for a heavy
element such as platinum. Spin-orbit coupling is treated
as a perturbation in the Hamiltonian, i.e.,

$$H' = \underset{\sim}{L} \cdot \underset{\sim}{S} = \Sigma \; \xi(r_i) \; \underset{\sim}{\ell_i} \cdot \underset{\sim}{S_i} \qquad (41)$$

This operator effectively transforms a singlet spin wave
function into three triplet spin wave functions. Conse-
quently, under this perturbation a singlet wave function
interacts with a triplet wave function. Thus triplet and
singlet states are mixed and transitions, which are
primarily triplet←singlet, gain some allowed character and
appear in the spectra of platinum complexes as bands that
are 0.1 to 0.2 as intense as the bands of primarily spin-
allowed (singlet←singlet) transitions.

Crystalline solids with primitive unit cells are made
up of ions or molecules, which can interact with one
another. In other words the presence of an excitation in
one molecule is felt by others and this excitation can be
passed from one molecule to another. The crystal can be
considered to be a lattice arrangement of fixed molecules.

The simplest or unperturbed state for such a system would be for the collection of molecules to be noninteracting (2). In this case the electronic energy of a given molecule is described by the Schroedinger equation,

$$H_k \psi_k = E_k \psi_k \tag{42}$$

Summing this result over all the molecules in the collection making up the crystal gives,

$$(\sum_k H_k) \pi_k \psi_k = (\sum_k E_k) \pi_k \psi_k \tag{43}$$

The ground state of such a system is defined by,

$$\Psi^\circ = \pi_k \psi_k^\circ \tag{44}$$

and the excited state where the mth molecule is in an excited state would be,

$$\Psi'_m = \psi'_m \pi_{k \neq m} \psi_k^\circ \tag{45}$$

The interaction between molecules in a crystal is added on as a perturbation, $\sum_{m<n} V_{mn}$, to the unperturbed Hamiltonian in order to describe the energy levels. The summation for $\sum_{m<n} V_{mn}$ is such that m and n account for all possible intermolecular interactions in the crystal. This inter-action potential permits the excitation energy of one molecule to pass to another.

The interaction potential, $\sum_{m<n} V_{mn}$, has all the symmetry of the crystal lattice space group. Therefore, a valid wavefunction must belong to the totally symmetric representation of the space group. A good approximation to the excited state crystal wave functions for allowed transitions are those in which all the unit cells are in phase. This simplifies the consideration of symmetry properties to one unit cell.

In a particular unit cell there may be several sites, which are not related by a simple translation. A site has a group of symmetry operations associated with it. This group is known as the site group and consists of proper and improper rotations.

Molecules can be transformed between symmetry equivalent sites into each other by means of some of the symmetry operations, which constitute a group known as a factor group.

Crystal wave functions must be symmetry-adapted to incorporate the equivalent sites of a unit cell. A molecular wave function must now have an index for the unit cell and one for the site. An excitation wave function for the molecule on site, a, in cell, m, now appears as,

$$\Psi'_{ma} = \psi'_{ma} \, \pi' \psi_k^{\circ} \tag{46}$$

where the prime on π indicates that the product is over all sites except for the site, ma.

A wave function for excitation of an a-site molecule over the entire crystal is a summation over all the unit cells and is written as

$$\Phi'_a = \frac{1}{\sqrt{N}} \sum_m^N \Psi'_{ma} \qquad (47)$$

This equation is known as a one-site exciton and corresponds to excitation throughout the crystal, but localized to a set of equivalent sites within the crystal.

In the case of a crystal with two equivalent molecules per unit cell, two combinations can be formed from one-site excitons:

$$\Phi'_I = \frac{1}{\sqrt{2}} [\Phi'_1 + \Phi'_2] \qquad (48)$$

$$\Phi'_{II} = \frac{1}{\sqrt{2}} [\Phi'_1 - \Phi'_2] \qquad (49)$$

These two states originate from an excited molecular state and are the result of two translationally nonequivalent sites in the unit cell.

In the case where there is one molecule per primitive cell, the energy of the excited state above the ground state energy is given by the sum of three terms,

$$E_g^I = E^\circ + D + M^I \qquad (50)$$

where E° is the ground state energy of the molecule and where D and M^I can be expressed as the integrals shown

below,

$$D = \sum_m \int [\, |\psi_n'\psi_m^\circ|^2 - |\psi_n^\circ\psi_m^\circ|^2 \,] V_{n,m} d\tau \tag{51}$$

and

$$M^I = \sum_m \int (\psi_n'\psi_m^\circ)^* |V_{n,m}| \psi_n^\circ\psi_m' d\tau \tag{52}$$

Equation (52) is normally simplified to the form,

$$M^I = \sum_m I_{nm}' \tag{53}$$

where I_{nm} is just the integral in equation (52). The subscript, n, refers to the molecule of the nth unit cell and likewise for the mth subscript. The integral, $I_{n,m}'$, corresponds to exchange of excitation between the n and m molecules. The only terms, which contribute to M^I and result in band splitting, are those in which excitation is exchanged between translationally inequivalent molecules.

In the situation of two molecules in a primitive unit cell the energy of transitions from excitation exchange is expressed by

$$\left.\begin{array}{c} E^I \\ E^{II} \end{array}\right\} = E^\circ + D' \pm C \tag{54}$$

where D' is a band-displacement term and C is the sum of all exchange energies between translationally inequivalent molecules. In this case D' and C terms in Equation (54)

are defined by the integrals,

$$D' = \sum_m \int [|\psi'_{n2}\psi^o_{m1}|^2 - |\psi^o_{n2}\psi^o_{m1}|^2] V_{n2,m1} d\tau \qquad (55)$$

and

$$C = \sum_m \int (\psi'_{n2}\psi^o_{m1})^* |V_{n2,m1}| \psi^o_{n2}\psi'_{m1} d\tau \qquad (56)$$

where

$$I'_{nm} = \int (\psi'_{n2}\psi^o_{m1})^* |V_{n2,m1}| \psi^o_{n2}\psi'_{m1} d\tau \qquad (57)$$

The subscripts, n2, etc., refer to the molecule at site 2 of the nth unit cell. The indices, m and n, are for molecules which are translationally inequivalent. It is seen that the C term in equation (56) splits the energy of excitation exchange into two lines. These two levels each belong to a different linear combination of one-site excitons as seen in equations (48) and (49).

The interaction potential operator, $V_{n2,m1}$, as used in equations (55) and (56), is the sum of all pairwise interactions occurring between the electrons and nuclei of molecule n and those of molecule m. The number of matrix elements represented by $V_{n2,m1}$ is prohibitively great. Simplification is possible by assuming that only a limited set of electrons associated with each molecule may participate strongly in electronic excitation in the optical region. Also the summation over the crystal is terminated

after a small number of neighboring molecules have been included.

The electric dipole moment for the transition between the ground state and the excited state for the two linear combinations of one-site excitons is written as,

$$P_I = \int \Phi_I' \sum_i r_i \; \Phi^\circ \; d\tau \tag{58}$$

$$P_{II} = \int \Phi_{II}' \sum_i r_i \; \Phi^\circ \; d\tau \tag{59}$$

These integrals simplify to the electronic moment matrix elements for individual molecules at the sites in the unit cell written as,

$$P_I = p_1 + p_2$$

and $\hspace{11cm}$ (60)

$$P_{II} = p_1 - p_2$$

where p_1 and p_2 are the electric moment matrix elements for a molecule in one of the two sites of the unit cell.

Preliminary electronic absorption spectral studies of the square planar ion of platinum(II) involved the $PtCl_4^{2-}$ ion. One such study was that of Chatt, Gamlen, and Orgel (8), who proposed assignments for the various bands on an energy ordering of the d-orbitals in a study of the solution spectra of $PtCl_4^{2-}$ and a series of platinum(II) chloroamine complexes. An absorption spectrum (4) in the visible and

near ultraviolet of the aqueous solution of K_2PtCl_4 is shown

in Figure 2. Their scheme of ordering gave a d-orbital

energy ordering of $d_{z^2} < d_{xz} = d_{yz} < d_{xy} < d_{x^2-y^2}$ and is

shown in Figure 3.

In the solution spectra of $PtCl_4{}^{2-}$ the small peak at

21,000 cm^{-1} and a small shoulder at about 17,000 cm^{-1} were

assigned as spin-forbidden transitions. The next higher

energy features of the spectrum were two peaks at 25,400 cm^{-1}

and 30,300 cm^{-1}, respectively. These peaks were assigned as

the spin-allowed d←d transitions, $d^*_{x^2-y^2} \leftarrow d_{xy}$ ($^1A_{2g} \leftarrow {}^1A_{1g}$) and

$d^*_{x^2-y^2} \leftarrow d_{xz,yz}$ ($^1E_g \leftarrow {}^1A_{1g}$), respectively. A shoulder at

37,900 cm^{-1} was assigned as the d←d transition, $d^*_{x^2-y^2} \leftarrow d_{z^2}$

($^1B_{1g} \leftarrow {}^1A_{1g}$). Beyond 37,900 cm^{-1} the absorption rises

and a second more intense shoulder can be discerned at

43,400 cm^{-1}. This shoulder at 43,400 cm^{-1} was not reported

by Chatt et al. (8). Rather, they reported only the strong

band at 46,000 cm^{-1}, which is seen in Figure 2. The bands

at 43,400 cm^{-1} and 46,400 cm^{-1} must be dipole-allowed since

they possess such strong intensities. The transition

observed at 46,000 cm^{-1} was assigned by Chatt et al. (8) as

a p←d transition. Such a dipole-allowed transition would

have to be $p_z \leftarrow d_{xz,yz}$ ($^1A_{2u} \leftarrow {}^1A_{1g}$) from symmetry consider-

ations.

The assignments of the intense bands at 43,400 cm^{-1}

and 46,400 cm^{-1} have been a subject of some controversy.

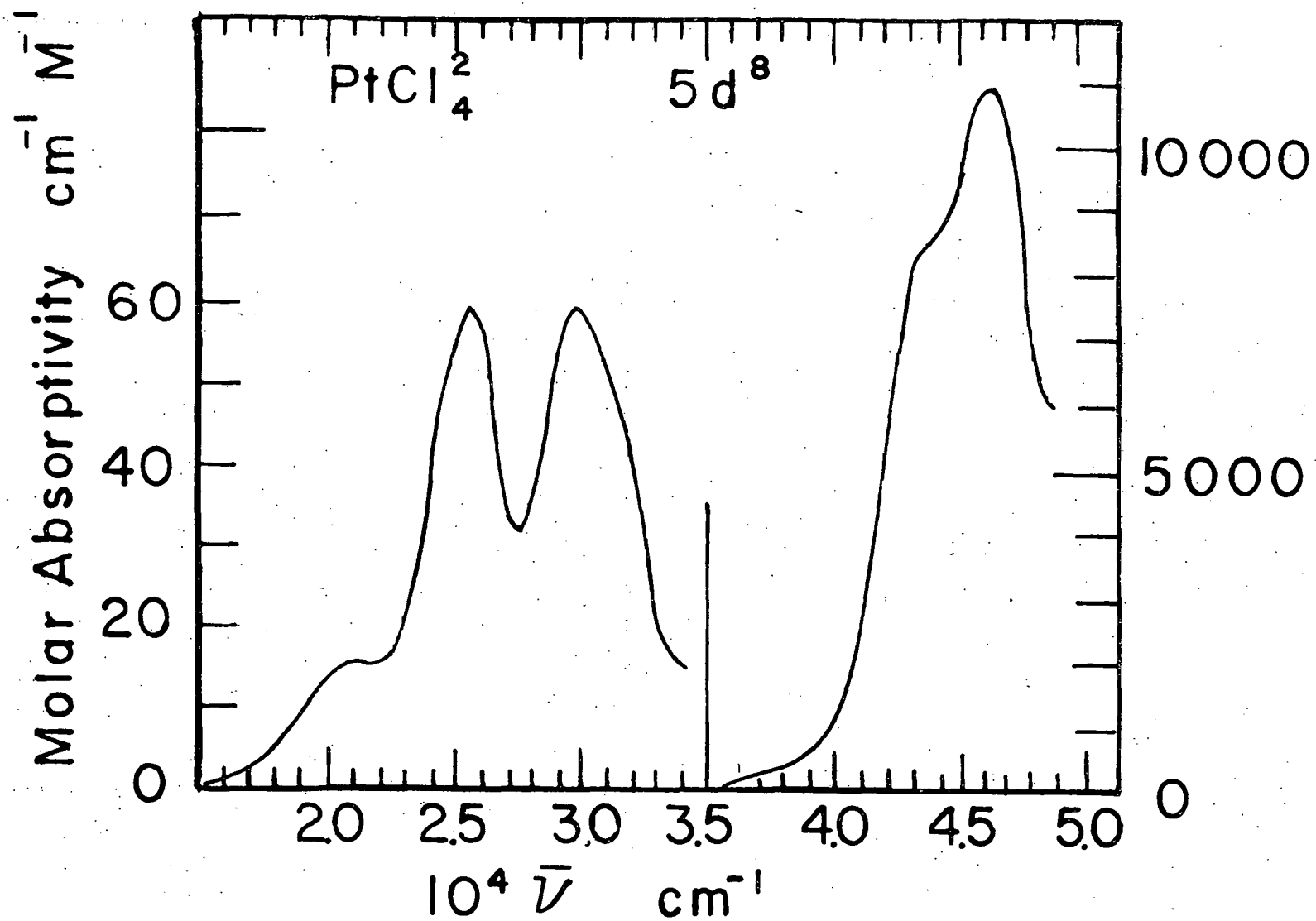Figure 2. Aqueous solution spectrum of K_2PtCl_4

Figure 3. Arrangement of energies for orbitals of
platinum(II) in D_{4h} symmetry relevant to
electronic absorption spectra

D_{4h}

a_{1g}^* (σ)

e_u^* (σ)

6p

a_{2u}

6s

b_{1g}^* (x^2-y^2)

b_{2g} (xy)

e_g (xz,yz)

5d

a_{1g} (z^2)

e_u

(π)

b_{2u}

a_{2u}

(σ)

e_u
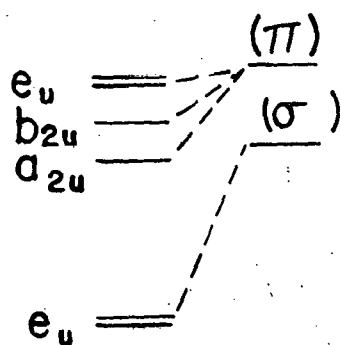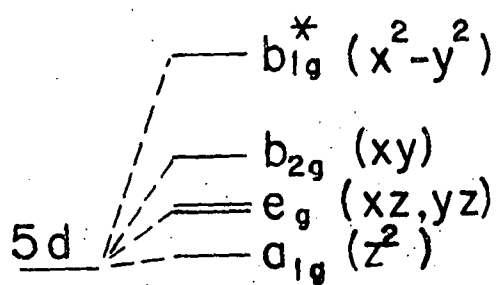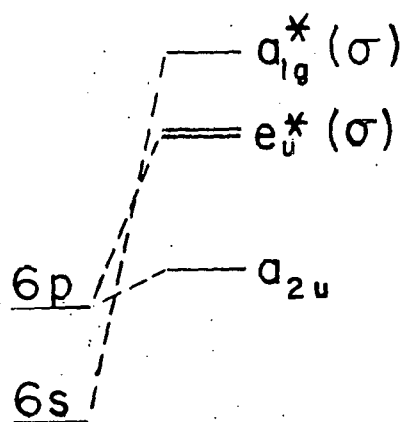
Metal   MO   Ligand

Jorgensen (9) proposed that the peak at 46,400 cm^{-1} was the charge-transfer transition, $d^{*}_{x^2-y^2} \leftarrow \pi$-Ligand ($^1A_{2u} \leftarrow {}^1A_{1g}$). This assignment was based on a comparison of the charge-transfer bands of the square planar cyanide complexes with those observed in the square planar chloride complexes for Pt(II) and Au(III). The first intense charge-transfer band is observed at lower energy for $AuCl_4^-$ than for $PtCl_4^{2-}$. This fact is given as evidence for a metal $\leftarrow$ Ligand charge-transfer since Au(III) is expected to be a better electron acceptor than the isoelectronic Pt(II). However, in the case of $Au(CN)_4^-$ the first intense transition occurs at higher energies than for $Pt(CN)_4^{2-}$. This was indicative of a charge-transfer of the Ligand $\leftarrow$ metal type. These arguments were supported by Gray and Ballhausen (10). The chloride ligand does not have any π^* (antibonding) orbitals of sufficiently low energy to be involved in any accessible spectroscopic transitions. On the other hand the cyanide ligand has available π^* orbitals, and in the case of cyanide complexes the strong charge-transfer transitions are apparently of the $\pi^* \leftarrow$ metal type. More recently, Basch and Gray (11) and Mason and Gray (12) also supported the charge-transfer assignment as metal (σ^*) $\leftarrow$ Ligand-π.

However, support for the $p \leftarrow d$ transition assignment of Chatt et al. (8) came from Cotton and Harris (13), who arrived at the same platinum d-orbital order through

calculations using semiempirical extended Hückel-type molecular orbital theory. McCaffery, Schatz, and Stephens (14) supported the p←d assignment on the basis of their magnetic circular dichoism (MCD) studies.

Other theoretical studies have been carried out for the $PtCl_4{}^{2-}$ anion because of its exemplary high D_{4h} symmetry. One such treatment by Fenske, Martin, and Ruedenberg (15) was a ligand field treatment. Electron-electron repulsions and spin-orbit coupling were included. The ordering of the d-orbitals under what seemed to be reasonable ligand field strengths was not consistent with that of Chatt et al. (8). Instead, an ordering of $d_{xz} = d_{yz} < d_{z^2} < d_{xy} < d_{x^2-y^2}$ was proposed. The inadequacy of a ligand field treatment became apparent when later experimental work was to confirm the ordering of the d-orbitals as presented in Figure 3. The theoretical approach of Gray and Ballhausen (10) employed linear combinations of atomic orbitals in a self-consistent field molecular orbital approach. The d-orbital ordering in this calculation was found to agree with that of Fenske et al. (15).

In spite of all the computation methods applied to the problem of d-orbital ordering in these square-planar complexes, theory alone could not be used to deduce spectroscopic assignments with impunity.

A number of spectroscopic studies of tetrachloro-
platinate(II) have been reported. There have also been a
number of transition assignments (16-22) based upon this
experimental research. The first spectroscopic examination
of K_2PtCl_4 crystals was the polarized crystal spectra
obtained by Yamada (16). Later work was to show that his
spectra in the region higher than 27,000 cm^{-1} was inaccurate
due to instrumental deficiencies. Martin and Lenhardt (18)
reported spectra up to 35,000 cm^{-1} at room temperature.
Subsequently, spectra at liquid helium temperatures were
recorded by Mortensen (19) and Martin, Tucker, and Kassman
(20). The latter work presented transition assignments that
supported those of Figure 3.

MCD studies of aqueous solutions of K_2PtCl_4 were
reported in 1966 by Martin, Foss, McCarville, Tucker, and
Kassman (23). Subsequent MCD studies were reported by
McCaffery, Schatz, and Stephens (14). All of these spectral
studies supported the original d-orbital ordering of Chatt
et. al. (8). Recently, polarized single-crystal reflection
spectra have been obtained by Anex and Takeudhi (24).
Absorption spectra were derived by means of a Kramers-Kronig
analyses of the reflectance results. Strong absorption in
both polarizations was noted in the region 40,000 to
50,000 cm^{-1}. The intensity of the band at 46,300 cm^{-1} was
found to be of much higher intensity in the c- or

z-polarization than that observed in the a- or x,y-
polarization. This observation supports the theory that
these intense transitions are due to the transition, $p_z \leftarrow d$.
Spectra at low temperatures for K_2PtCl_4 have been obtained
by Patterson, Godfrey, and Khan (25). Dilute solid solutions
of Cs_2PtCl_4 in host crystals of Cs_2ZrCl_6 were prepared.
These specially prepared crystals provided sharper resolution
of vibrational structure which appears on the absorption
bands. They also reported observing luminescence for one
transition band with vibrational fine structure for spectra
obtained at 4K. In a later publication Patterson, Harrison,
and Belair (26) reported the splittings observed in the
luminescence were due to the presence of ^{35}Cl and ^{37}Cl
isotopes in the $PtCl_4{}^{2-}$ ion.

A molecular orbital diagram based upon the experimental
and theoretical studies of $PtCl_4{}^{2-}$ ion is presented in
Figure 3. The dotted lines depicted in the diagram connect
the atomic orbital energy states of the platinum ion (+2)
to the molecular orbital energy states of $PtCl_4{}^{2-}$ ion. The
lowest unfilled orbital for a d^8 system such as platinum(II)
complexes in D_{4h} symmetry is the antibonding molecular
orbital $b_{1g}-\sigma^*$, formed around the $d_{x^2-y^2}$ atomic metal
orbital. The highest filled orbital is the b_{2g}, based on
the atomic orbital d_{xy} and considered to be π-antibonding
in character. The next lower lying molecular orbitals are

the degenerate e_g formed from the atomic orbitals, d_{xz} and d_{yz}, which are π-antibonding in character. The d_{z^2} atomic orbital is included in an a_{1g} molecular orbital, which has potential sigma bonding capability to the ligands. Atomic orbitals of the same symmetry have the potential to mix with one another in forming molecular orbitals. The p-orbitals of the ligands can engage in bonding interactions with metal orbitals through sigma and pi bonds. Twelve symmetry-adapted linear combinations of these ligand p-orbitals are possible. Only the ungerade combinations are included in Figure 3.

Crystals of anhydrous K_2PtBr_4 have a structure similar to K_2PtCl_4. Spectra for the aqueous solution as well as for single crystals at 300 and 15K have been reported by Kroening, Rush, Martin, and Clardy (27). The aqueous solution spectrum of K_2PtBr_4 is shown in Figure 4. The polarized absorption spectra of K_2PtBr_4 crystals (27) were recorded at both 300 and 15K over the region 15,000 – 37,000 cm^{-1} for both polarizations and are presented in Figure 5.

In the single-crystal spectra of K_2PtBr_4 the d←d transitions occur at 1,500 to 2,000 cm^{-1} lower energy than the equivalent transitions in the K_2PtCl_4 case. The intensity ratio of a- or x,y-polarization to c- or z-polarization is greater for K_2PtBr_4 than for K_2PtCl_4.
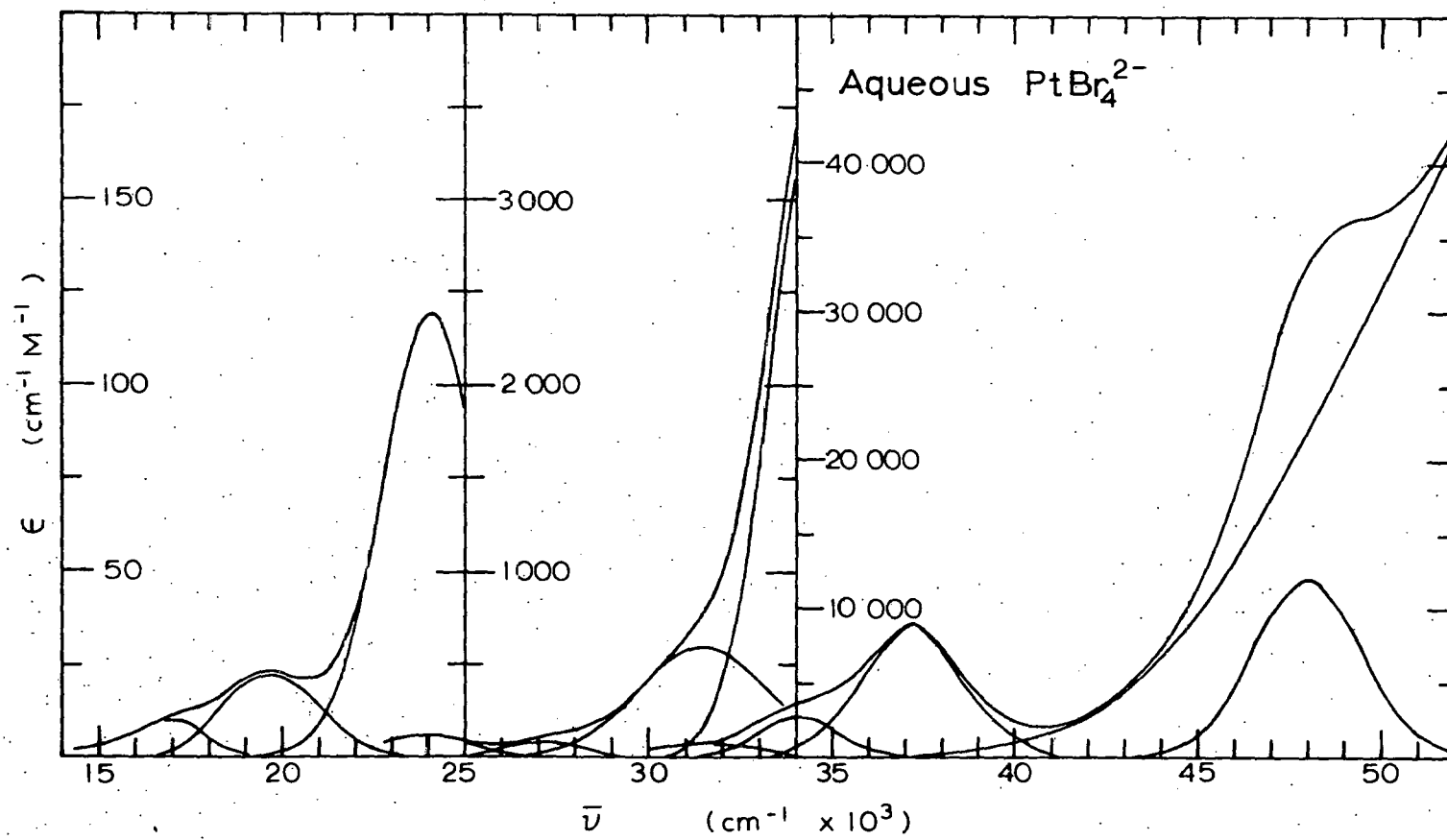
Figure 4. Aqueous solution spectrum of K_2PtBr_4

34
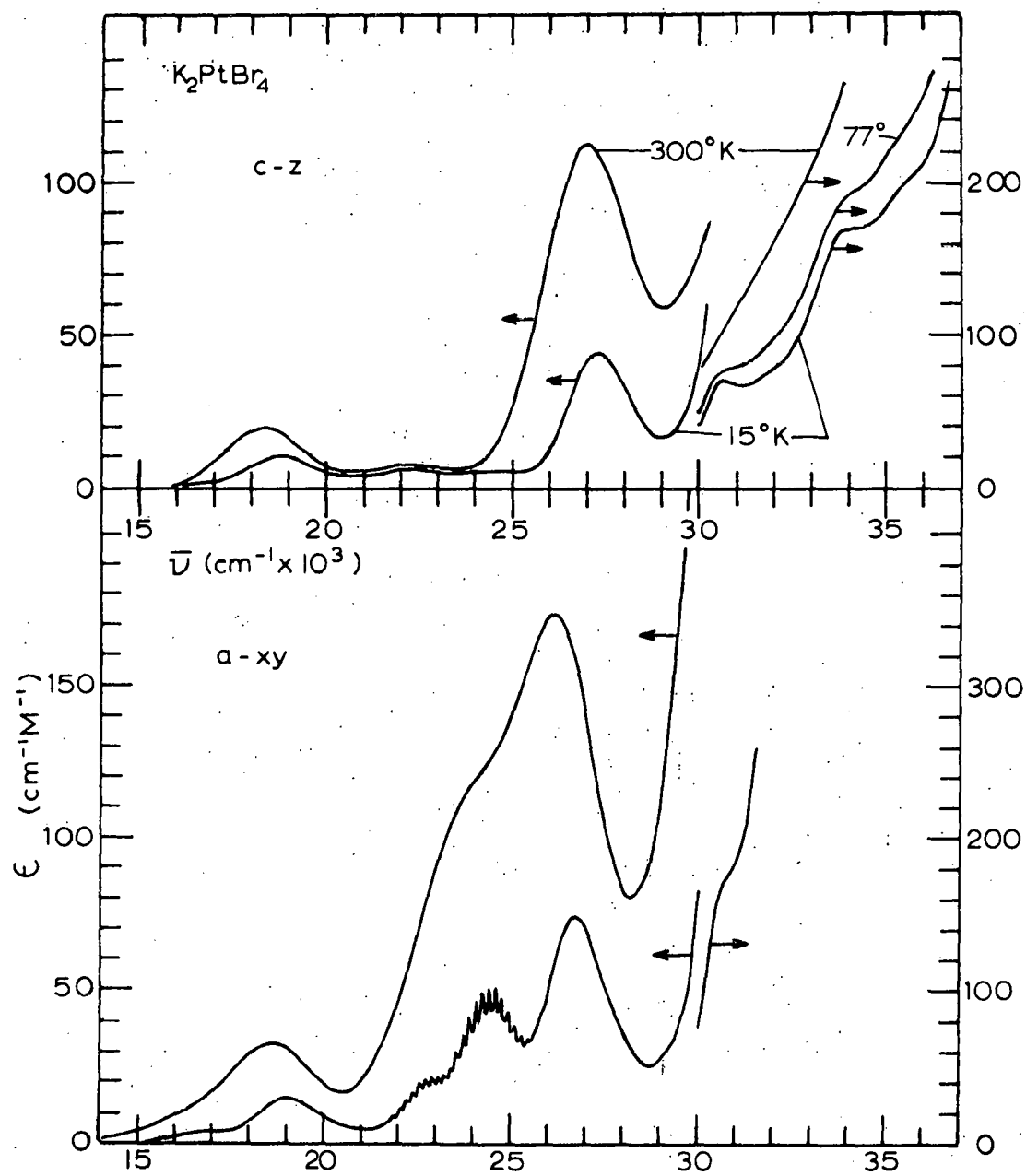
Figure 5. Polarized absorption spectra of K_2PtBr_4

Vibrational structure was observable at 15K for two of the d$\leftarrow$d bands as was the case with K_2PtCl_4.

In the solution spectrum two unsymmetrical peaks were observed at 17,000 cm^{-1} and 19,900 cm^{-1}. These peaks were assigned to the spin-forbidden transitions, σ^*-$d_{x^2-y^2}\leftarrow d_{xy}$ ($^3A_{2g}\leftarrow{}^1A_{1g}$) for the 17,000 cm^{-1} band and σ^*-$d_{x^2-y^2}\leftarrow d_{xz}, d_{yz}$ ($^3E_g\leftarrow{}^1A_{1g}$) for the band at 19,900 cm^{-1}. A distinctive peak at 24,000 cm^{-1} and a shoulder at 27,200 cm^{-1} in the solution spectrum were assigned as the spin-allowed, transitions, σ^*-$d_{x^2-y^2}\leftarrow d_{xy}$ ($^1A_{2g}\leftarrow{}^1A_{1g}$) and σ^*-$d_{x^2-y^2}\leftarrow d_{xz}, d_{yz}$ ($^1E_g\leftarrow{}^1A_{1g}$). Features in the solution spectrum above 32,000 cm^{-1} were so intense that they could not be due to d$\leftarrow$d transitions.

In the 300K $\underset{\sim}{a}$-(x,y) polarized crystal spectra of K_2PtBr_4 as shown in Figure 5, a shoulder is evident at 24,000 cm^{-1}. This shoulder resolved into a band at 15K that exhibits vibrational structure. In the $\underset{\sim}{c}$-z polarized spectrum this band is absent. Since this band occurred in only x,y polarization the transition was assigned as σ^*-$d_{x^2-y^2}\leftarrow d_{xy}$ ($^1A_{2g}\leftarrow{}^1A_{1g}$) and therefore must be vibronic in order to be allowed. This absorption band was assigned as the lowest possible energy for a spin-allowed transition. A peak, which appeared at 27,400 cm^{-1} in $\underset{\sim}{c}$-z polarization and at 26,800 cm^{-1} in the $\underset{\sim}{a}$-(x,y) polarization of K_2PtBr_4, was assigned as σ^*-$d_{x^2-y^2}\leftarrow d_{xz,yz}$ ($^1E_g\leftarrow{}^1A_{1g}$). This assignment was based upon similar structure in the K_2PtCl_4 spectrum

for which an A term in the MCD spectrum of the aqueous solution was reported by Martin et al. (23) and McCaffery et al. (14). Shoulders appearing at 16,900 cm^{-1} in the c-polarization and at 17,000 cm^{-1} in the a-polarization and bands at 18,800 cm^{-1} in the c-polarization and at 19,100 cm^{-1} in the a-polarization were assigned as spin-forbidden transitions. The final molecular states for these transitions would then be $^3A_{2g}$ and ^3E_g. A total of nine states are possible in the molecular states, $^3A_{2g}$ and ^3E_g. None of these states are distinctly observable even at 15K but rather are found merged into a peak and shoulder. A shoulder on the low energy side of the $^1A_{2u}$ band appears at 15K in the a-(x,y) polarization and exhibits vibrational structure. A slight hint of a band can be seen at 22,600 cm^{-1} at 15K for c-zpolarization. This shoulder has been assigned as $\sigma^*-d_{x^2-y^2} \leftarrow d_{z^2}$ ($^3B_{1g} \leftarrow ^1A_{1g}$). This assignment is in agreement with that made for the corresponding band of $PtCl_4^{2-}$ by Patterson et al. (25) in their study of the luminescence spectrum of Cs_2PtCl_4 in Cs_2ZrCl_6.

An enlarged view of the vibrational structure in the spectrum of a K_2PtBr_4 crystal at 15K is shown in Figure 6. This vibrational structure originates from the excitation to excited vibrational states for the totally symmetric vibrational mode, A_{1g}, of the excited electronic states. The energy separation between the vibrational peaks was 170 ± 10 cm^{-1}.
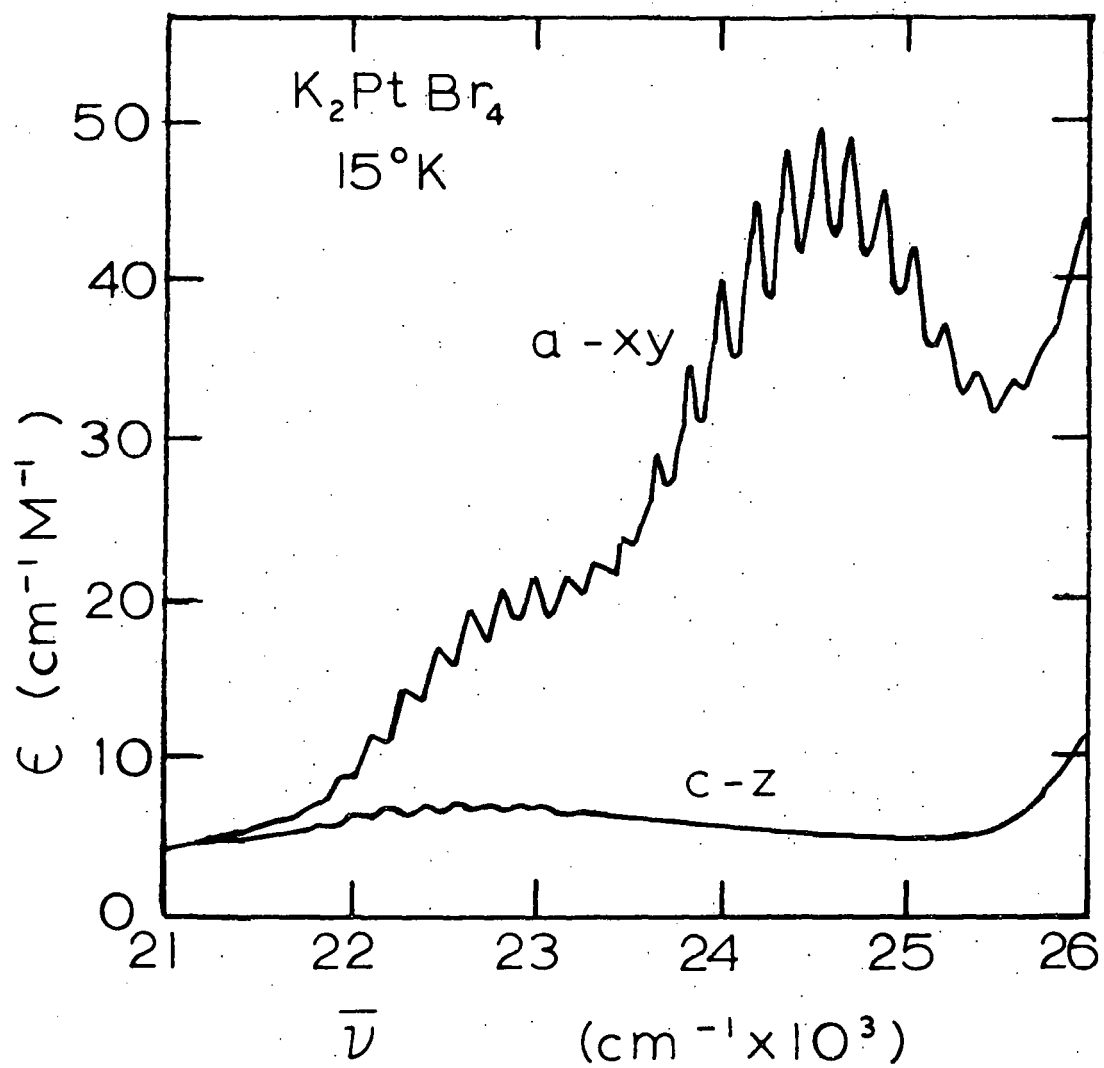
Figure 6. Vibrational structure of K_2PtBr_4 spectrum at 15K. The crystal was 26μ thick

A comparison of the transition assignments and the relative energies of them for the absorption spectra of K_2PtCl_4 and K_2PtBr_4 at 15K appears in Figure 7.

The trend appears that the bands of K_2PtBr_4 are between 1,500 to 2,200 cm^{-1} lower in energy than the corresponding bands of K_2PtCl_4. This holds for bands up to that of ^1E_g at around 30,000 cm^{-1}. Spectra of K_2PtCl_4 and K_2PtBr_4 show many of the same features and transitions that give rise to vibrational structure.

In accordance with the vibronic mechanism the spectra of each of these compounds exhibit a reduction of the oscillator strength upon cooling the crystal to lower temperatures. One difference between these two compounds is the relative intensities of the alternate polarizations. For example, transitions to the states ^3E_g and ^1E_g were more intense in $\underset{\sim}{c}$-z polarization than in $\underset{\sim}{a}$-(x,y) polarization, whereas just the opposite intensity ratios were noted for K_2PtBr_4. This observation implied that the ^1E_u transition from which the Laporte forbidden d←d transitions borrow intensity in the $\underset{\sim}{a}$-x,y polarization had moved to a lower energy relative to the $^1A_{2u}$ transition from which the $\underset{\sim}{c}$-z polarization borrows intensity (27).

In spectral studies reported previously for K_2PtCl_4 the spin-allowed transition to the $^1B_{1g}$ state, $\sigma^*-d_{x^2-y^2}\leftarrow d_{z^2}$ ($^1B_{1g}\leftarrow{}^1A_{1g}$), were not observed. This transition appears as
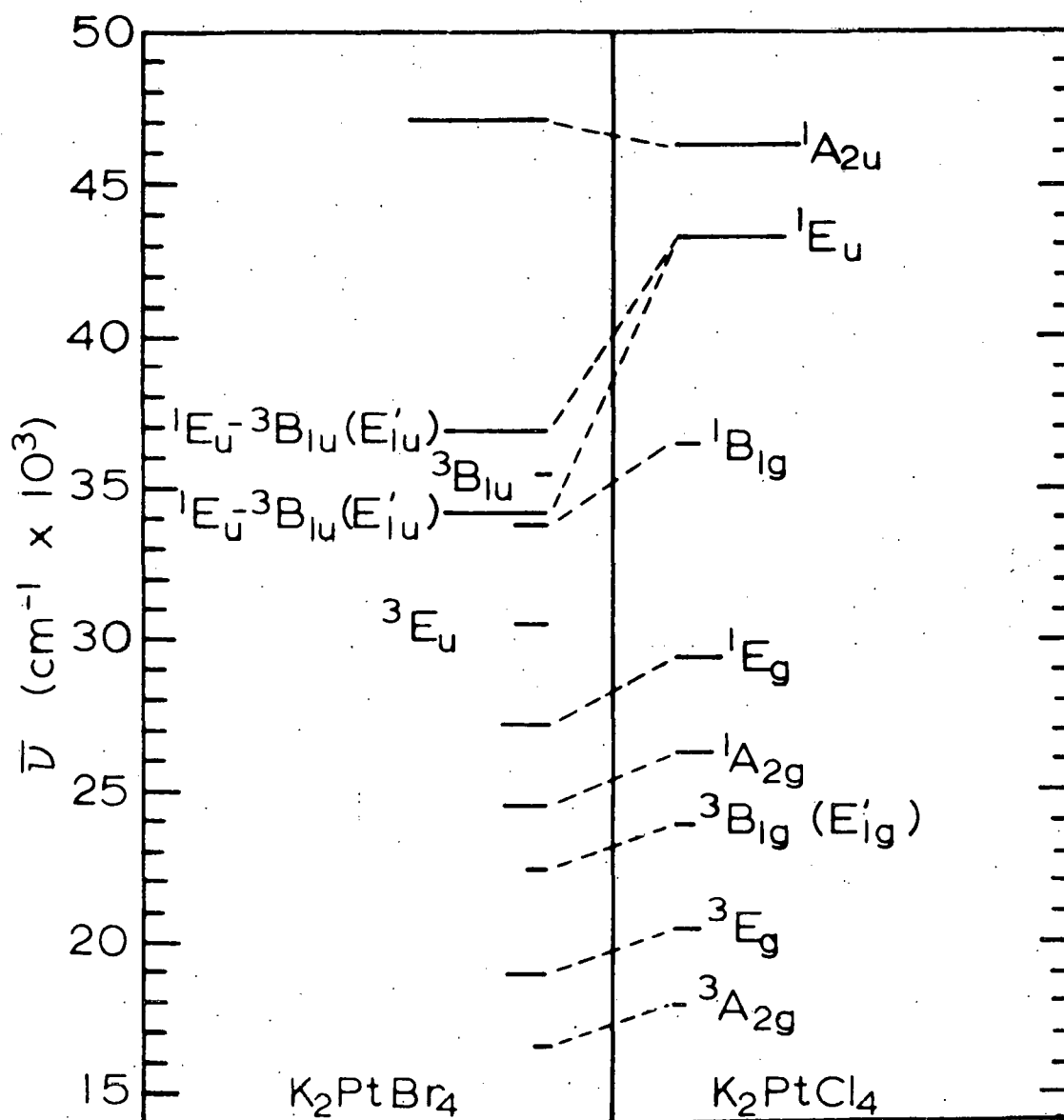
Figure 7. Comparison of excited states for K_2PtBr_4 and K_2PtCl_4. The length of line for each state is proportional to log ϵ_{max} (15K) for crystal transitions and log ϵ_{max} (soln) for the intense transitions

a shoulder on a rapidly rising absorption at almost 36,500 cm^{-1}. This transition is present in both polarizations of K_2PtCl_4 at 15K. The fact that this band occurs in a region of rapidly rising absorption prohibited the determination of the true temperature dependence of this transition.

The aqueous solution spectra of K_2PtBr_4, presented in Figure 4, showed the resolution of a band around 24,000 cm^{-1}, which appeared as a shoulder in the $\underset{\sim}{a}$-polarization spectrum at 300K. This transition was completely absent in the $\underset{\sim}{c}$-z polarization. This identifies the band as the vibronic transition, $\sigma^*-d_{x^2-y^2} \leftarrow d_{xy}$ ($^1A_{2g} \leftarrow ^1A_{1g}$), which according to the selection rules occurs only in $\underset{\sim}{a}$-(x,y) polarization. This transition has all the features associated with the analogous band in K_2PtCl_4.

The crystal spectra of K_2PtBr_4 yielded a deep valley for both $\underset{\sim}{a}$- and $\underset{\sim}{c}$-polarizations in the vicinity of 28,000 to 29,000 cm^{-1}. This minimum was not observed in the solution spectra (27). A transition with band maxima at 31,500 cm^{-1} is present in the solution spectrum but at most only very weak or totally absent in the crystal spectra. There is the possibility of impurities forming, as for example by the oxidation to species such as $PtBr_6^{2-}$, which then absorb in the region of 31,500 cm^{-1}.

Three distinct bands of increasing intensity at 34,200, 37,200, and 48,000 cm^{-1} are seen in the solution

spectrum of $PtBr_4^{2-}$. The crystal spectra of K_2PtBr_4 in Figure 5 in this region show that the a-polarized absorption has risen beyond the range of the technique by 32,000 cm^{-1} at 15K, whereas the c-polarized absorption spectrum at 15K could be followed to nearly 37,000 cm^{-1}. Three very weak transitions in c-polarization were observable between 30,000 and 36,000 cm^{-1}. It then follows that the two intense solution spectra peaks at 34,200 and 37,200 cm^{-1} must be polarized in the x,y-direction. From the work of McCaffery et al. (14) on the MCD spectrum of K_2PtCl_4 solutions, the absorption peak at 46,000 cm^{-1} was found to lack an A term and could therefore be assigned as $^1A_{2u}$. The peak at 48,000 cm^{-1} in the K_2PtBr_4 solution spectra can be assigned as the first $^1A_{2u}$ transition.

Crystals of $K_2PtBr_4 \cdot 2H_2O$ are quite similar in a number of spectral features to those of anhydrous K_2PtBr_4. $K_2PtBr_4 \cdot 2H_2O$ crystals were first reported in the literature by Biilman and Anderson (28). They characterized the crystals as dark brown to black orthorhombic crystals.

The spectra of $[N(C_2H_5)_4]_2Pt_2Br_6$ can be usefully compared to those of K_2PtBr_4. Each platinum atom in this dimeric molecule can be considered as lying in a square-planar arrangement of the bromide ligands. Stephenson (29) reported the crystal structure of $[N(C_2H_5)_4]_2Pt_2Br_6$ as triclinic $P\bar{1}$. The unit cell parameters were reported as

$a = 7.60$ Å, $b = 8.83$ Å, $c = 12.34$ Å, $\alpha = 105.6°$, $\beta = 84.0°$

and $\gamma = 112.8°$, with one molecule per unit cell. Day, Smith,

and Williams (30) reported polarized transmission spectra

for crystals of $[N(C_2H_5)_4]_2Pt_2Br_6$ at room temperature over

a very limited wavelength range. Recently, Cowman,

Thibeault, Ziolo, and Gray (31) reported the X-ray crystal

structure and electronic spectroscopic investigations of

$[N(CH_3)C_3]_2[Pt_2Cl_6]$ crystals, a closely related compound

incorporating basically the same platinum(II) dimeric

configuration in the molecule. They recorded crystal

absorption spectra of $[N(CH_3)C_3]_2[Pt_2Cl_6]$ at 300 and 15K

and assignments of the bands were made.

The existence of the quadruple bond has been known for

about ten years and was first proposed to exist in $Re_2Cl_8^{2-}$

by Cotton (32). Each rhenium in this dimer has available

four d-orbitals and four electrons. One of these d-orbitals

exhibits σ-character, while two other d-orbitals have

π-character, and the fourth d-orbital has δ-character. From

these orbitals it is then possible to form one σ, two π,

and one δ bonding orbitals and their corresponding anti-

bonding orbitals. The four pairs of electrons available

from the rhenium form the quadruple bond. A postulated

molecular orbital diagram is presented in Figure 8. As can

be seen from the diagram, d_{xy} orbitals are involved in the

δ-bond, d_{xz} and d_{yz} orbitals form the two π bonds, d_{z^2}

b_{2u} $L\text{-}\sigma^*, x^2\text{-}y^2$

b_{1g} $L\text{-}\sigma^*, x^2\text{-}y^2$

a_2 σ^* z^2

e_g $\pi^* xz, yz$

b_{1u} $\delta^* xy$

d   d

b_{2g} δ xy

e_u π xz, yz

a_{1g} σ z^2

b_{2u} $L\text{-}\sigma, x^2\text{-}y^2$

b_{1g} $L\text{-}\sigma, x^2\text{-}y^2$
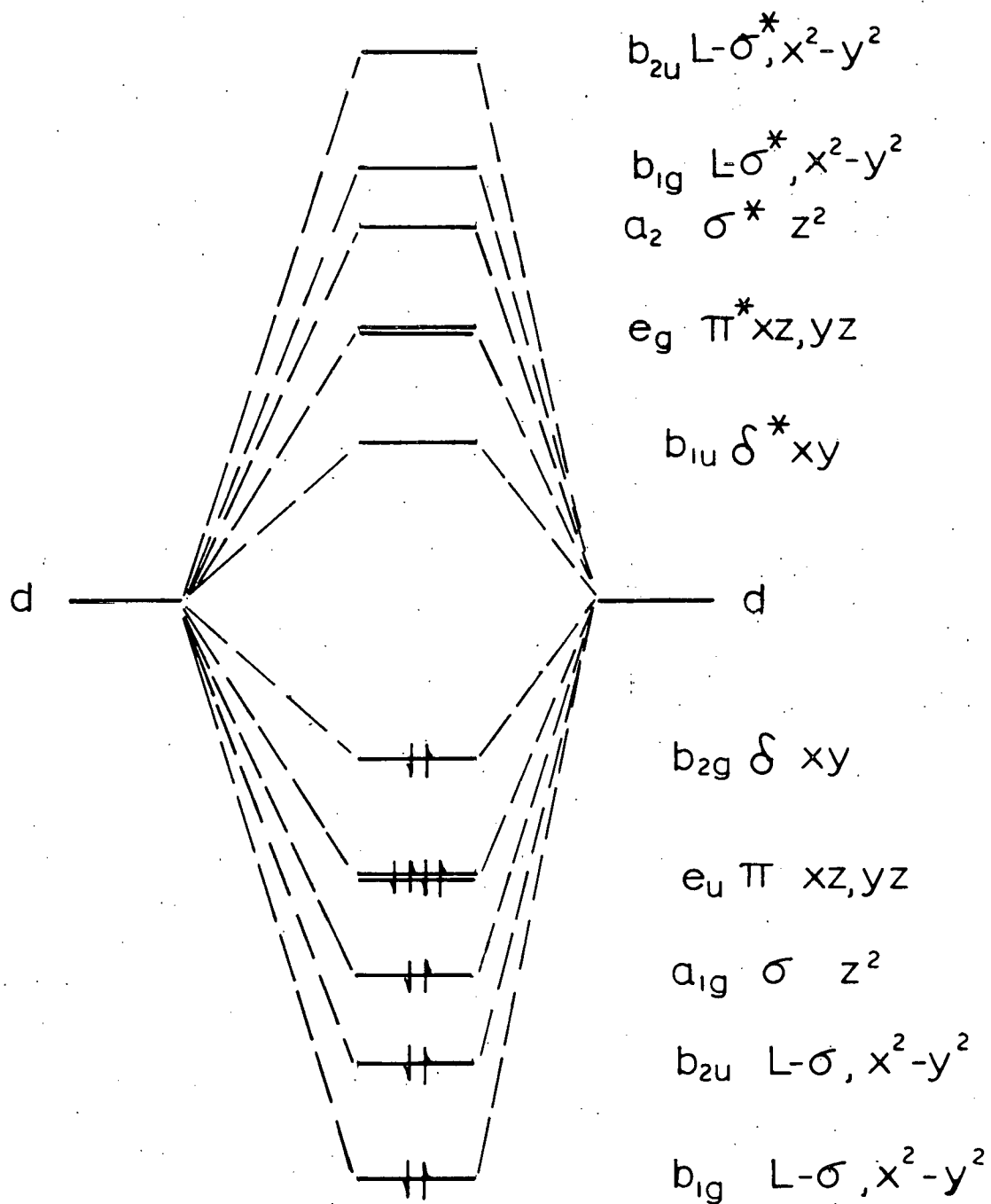
Figure 8. Molecular orbital diagram for quadruply bonded complex

orbitals are involved in σ bonds, and $d_{x^2-y^2}$ is a ligand σ bonding orbital.

Molybdenum carbonyl, $Mo(CO)_6$, was found to react with carboxylic acids to yield yellow crystalline compounds of the general formula, $Mo_2(OOCR)_4$. A depiction of the bonding present in these molybdenum carboxylates is presented in Figure 9. The short Mo-Mo distance of around 2.1 Å was indicative of a quadruple bond. The solution spectra of the molybdenum carboxylates were recorded by Dubicki and Martin (33) and Norman and Kolari (34).

Little work on the characterization of the quadruple bond through the interpretation of polarized absorption spectra has been carried out. Two such studies of quadruply bonded dirhenium compounds have been reported. Cowman and Gray (35) studied the electronic absorption spectra in crystals of $[N(C_4H_9)_4]_2Re_2Cl_8$ and $Re_2Cl_6[P(C_2H_5)_3]_2$ and assigned the low energy band to the $\delta^* \leftarrow \delta$ transition. In a later investigation of $[N(C_4H_9)_4]_2Re_2Cl_8$ Cotton et al. (36) reported a disordered crystal structure for the compound as well as an interpretation of the spectrum. The assignment of the low-energy band as a $\delta^* \leftarrow \delta$ transition was supported by this work.

A quadruple bond is known to exist between the two Mo atoms in the compound, $Mo_2(O_2CCH_2NH_3)_4(SO_4)_2 \cdot 4H_2O$. The crystal structure for this compound was reported by Cotton
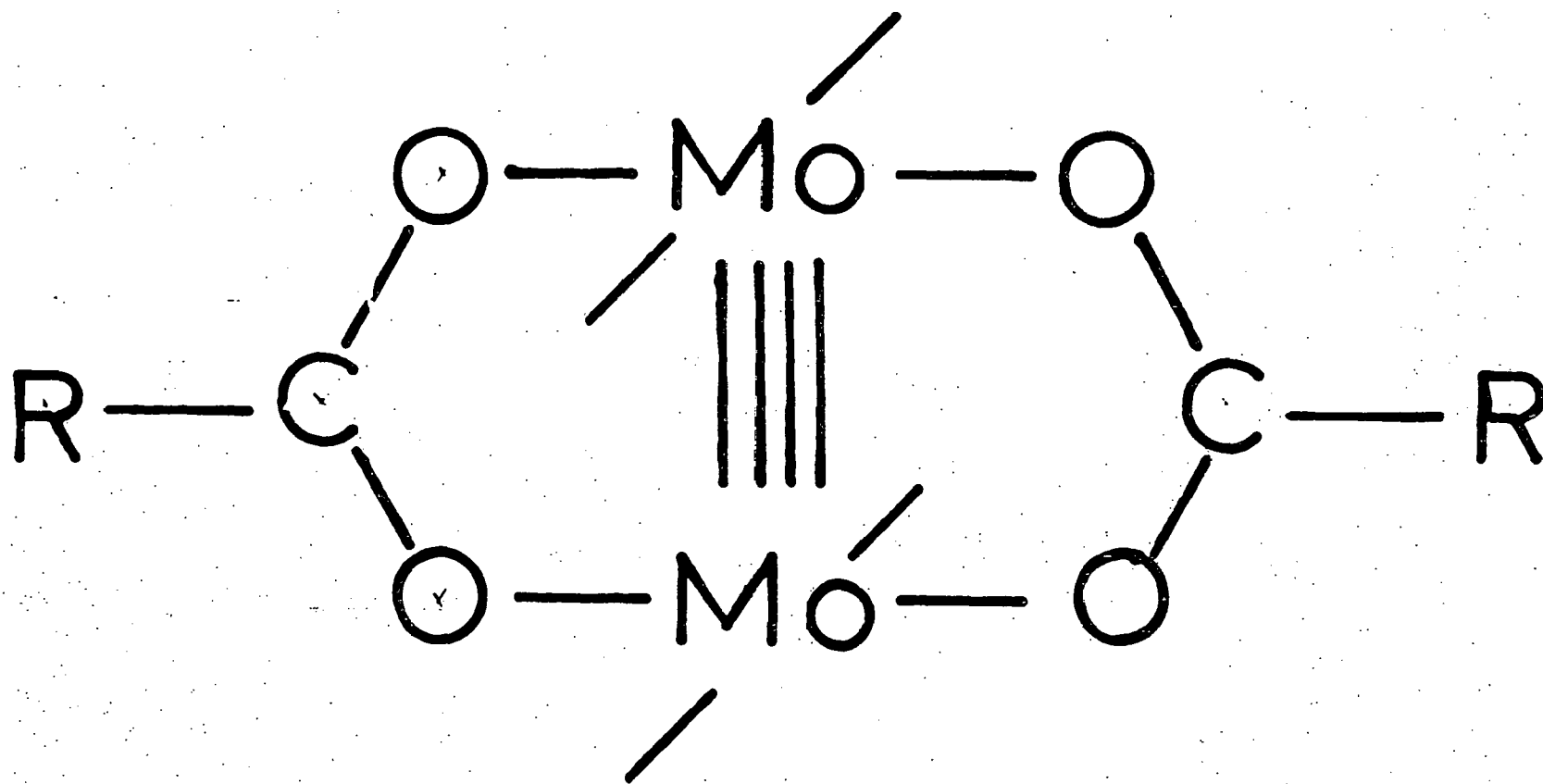
Figure 9. Schematic representation of a molecule of quadruply bonded Mo carboxylate

and Webb (37) and all the Mo_2^{4+} units were found to align themselves along the c-axis. This structure made the measurement and interpretation of the polarized spectra of crystals possible.

II. EXPERIMENTAL

K_2PtBr_4 was prepared by reduction of K_2PtBr_6. This reduction was accomplished by using either oxalate or a slow addition of a dilute hydrazine solution. K_2PtBr_6 crystals rapidly dissolve in water to give a red solution which slowly transformed to a reddish-brown color as the reduction to platinum(II) took place. The product, solid K_2PtBr_4, was obtained by evaporation of the solution at room temperature. The solution of K_2PtBr_4 is subject to slow auto-redox reactions to reform K_2PtBr_6 and platinum black. A thermogravimetric analysis (27) was performed on a batch of K_2PtBr_4, which yielded weight loss to 650°C as Br_2 of 25.6%, a weight loss to 900°C as KBr of 42.6%, and a platinum black residue of 31.7%. The calculated percentage weight loss values were: Br_2, 27.0%; KBr, 40.1%; Pt, 32.9%. Crystals of $K_2PtBr_4 \cdot 2H_2O$ were obtainable from the evaporation of K_2PtBr_4 solutions. These crystals would undergo a crystal transformation upon exposure to the laboratory atmosphere to an opaque powdered block of the anhydrous compound, which retained the original crystal shape. If the dehydration was accomplished at a sufficiently slow rate, crystals would form which were stable to the atmosphere. X-ray diffraction studies revealed these crystals to be the tetragonal crystals of anhydrous K_2PtBr_4. Crystals of $K_2PtBr_4 \cdot 2H_2O$ were prepared for spectral studies by

sandwiching a drop of the concentrated solution of K_2PtBr_4 between fused quartz plates. Crystals of $K_2PtBr_4 \cdot 2H_2O$ would slowly form, usually in about one day in contact with the mother liquor. Anhydrous K_2PtBr_4 crystals would occasionally form from these solutions. The sensitivity of $K_2PtBr_4 \cdot 2H_2O$ crystals to the loss of water of hydration made it imperative to leave the crystal sandwiched between the quartz plates in direct contact with the mother liquor. A selected area of the crystal was isolated for spectral examination by means of a pinhole prepared from annealed spring brass sheet metal. The pinhole was positioned over the crystal and was attached to the quartz plate by means of varnish. This assembly could be mounted into a cryostat and spectra could be recorded at room and liquid helium temperature (<15K). The 15K spectra of $K_2PtBr_4 \cdot 2H_2O$ were of usually poorer quality than those obtained at room temperature. The separation of the quartz plates upon cooling through freezing contraction of the solution was most likely the primary reason for the difference in quality. About half of the spectra obtained for $K_2PtBr_4 \cdot 2H_2O$ were not usable due to interference effects and light leaks. The spectra reported here were reproducibly repeated for several different crystals.

Another interesting feature of $K_2PtBr_4 \cdot 2H_2O$ crystals was the presence of strongly polarized red sections, which

formed in some crystals surrounded by normal crystal sections.
It was possible to obtain the absorption spectra from these
red areas. It was noted that the red sections were more
predominate in crystals of K_2PtBr_4 grown from older solutions.

Crystals of $[N(C_2H_5)_4]_2Pt_2Br_6$ were available from a
synthesis. These crystals were prepared following the
procedure outlined by Harris, Livingstone and Stephenson
(38). The starting material, K_2PtCl_4, was dissolved in
water with sodium bromide and tetraethylammonium bromide
and heated on a steam-bath for three hours. The product
was filtered off and washed with cold water after which it
was recrystallized from acetone. The recrystallization
process yielded thin crystal plates with a micaceous
cleavage. Crystals for spectroscopy were washed on a
microscope slide with an ethanol-water solution prior to
mounting over a pinhole in a platinum plate.

Crystals of $[N(C_2H_5)_4]_2Pt_2Br_6$ were pale-yellow when
white-light was polarized in the direction of the extinction
for the high refractive index. Under white-light polarized
in the low extinction direction, the crystal was essentially
colorless. Thicker crystals of $[N(C_2H_5)_4]_2Pt_2Br_6$ grown
from nitrobenzene appeared brown in light polarized with the
high extinction and faintly pink in the low extinction.

The Becke line method (39) was employed to determine
the index of refraction. The low extinction refractive

index, n_D^{25}, was measured to be 1.5803. The high extinction refractive index was found to be beyond the range of the refractometer being used to measure the index of refraction of the immersion fluids. However, this refractive index was noted to be below 1.74 (CH_2I_2). Birefringence methods were used to estimate the index of refraction for the high extinction as 1.69.

The molar concentration of these crystals is rather low, only 2.38 M ($Pt_2Br_6^{2-}$). This is due in part to the presence of the bulky cation in the crystal. Thin crystals for spectroscopic work were readily available, which allowed studies of absorptions with molar absorptivity up to 4000 $cm^{-1}M^{-1}$ ($Pt_2Br_6^{2-}$). An interference method (40) was used to obtain an estimate of crystal thickness. The interference is the result of multiple internal reflections occurring within the crystal. A crystal was found which exhibited interference in the region between 434.5 and 598.4 nm for the low-extinction polarization. The positions of the maxima and minima in the absorbance were noted and recorded. The actual crystal thickness, L, can be obtained from the relation,

$$L = N/(2\bar{\nu}_N \, n_N) \tag{61a}$$

where N is an integer, $\bar{\nu}_N$ is the absorption minimum in cm^{-1}, and n_N is the refractive index of the crystal at $\bar{\nu}_N$. An

expression relating successive maxima and minima in wave-numbers can be written as

$$n_m \, \overline{\nu}_m / n_N \, \overline{\nu}_N = 1 + m/N \tag{61b}$$

where n_m is the refractive index of a maximum or minimum at $\overline{\nu}_m$ and m is a successive half-integral number for maxima and integral for minima. From equation (61b) the limiting expression can be derived as,

$$\lim_{m \to o} m\overline{\nu}_N / (\overline{\nu}_m - \overline{\nu}_N) = N + N(dn/d\overline{\nu})_N \, \overline{\nu}_N / n_N \tag{62}$$

This expression permits a determination of the wavelengths of the maxima and minima in the recorded spectra, which can be determined with an uncertainty of 0.1 - 0.2 nm. A linear least-squares fit of $m\overline{\nu}_m / (\overline{\nu}_m - \overline{\nu}_N)$ versus $\overline{\nu}$ gives a precise value of this quantity in the limit as $m \to o$. According to equation (62) the first term gives an approximate value for N, and the last term provides a correction factor, which must be included. The variation in the refractive index with wavenumber or dispersion is included in the correction term as $dn/d\overline{\nu}$. This correction term may not be negligible. The crystal of $[N(C_2H_5)_4]_2Pt_2Br_6$, which showed interference, gave a $\lim_{m \to o} m\overline{\nu}_m / (\overline{\nu}_m - \overline{\nu}_N)$ of 27.83 for $\overline{\nu}_N = 18730 \text{ cm}^{-1}$. The maximum value for N would be 27 since any larger N value would given an unexpected negative dispersion. A reasonable dispersion of 2.6×10^{-6}

cm was computed for N = 27 indicating that it was the most probable value for N. The crystal thickness calculated from equation (61a) was $4.6 \pm 0.2 \mu$ for an N = 27. This crystal was used as a standard for determining crystal thickness through a comparison of absorbances at suitable wavelengths with other crystals.

Crystals of $Mo_2(O_2CCH_2NH_3)_4(SO_4)_2 \cdot 4H_2O$ were available from a synthesis (37). $Mo_2(O_2CCH_2NH_3)_4(SO_4)_2 \cdot 4H_2O$ was prepared by the addition of $K_4Mo_2Cl_8$ to a solution made up of glycine in a 0.8 $\underline{M}$ HCl solution kept under nitrogen. The product, $Mo_2(O_2CCH_2NH_3)_4Cl_4 \cdot xH_2O$, was mixed into a solution of glycine in 0.5 $\underline{M}$ H_2SO_4. Yellow, needle-like crystals of $Mo_2(O_2CCH_2NH_3)_4(SO_4)_2 \cdot 4H_2O$ formed and were filtered off.

The refractive indices (Na D) for this crystal was determined by the Becke line method. Some commercially available immersion fluids were used in the determination, and the refractive indices were found to be n_o = 1.604 and n_E = 1.620. Crystal thickness was estimated from the birefringence.

A Cary 14 spectrophotometer equipped with Glan calcite polarizers in both the reference and sample beams was used for recording polarized crystal spectra. The polarizer in the reference beam served to eliminate polarizer effects caused by calcite absorption or systematic polarization inherent in the instrument. A high intensity tungsten

filament light source was used in the spectral region, 650 nm to around 280 nm. A hydrogen arc lamp was employed as a radiation source in the ultraviolet region from 300 to 200 nm.

In the recording of a spectrum of a crystal mounted over a small pinhole it becomes necessary to insert the proper screen or pinhole into the reference beam to maintain the absorbance recording within the operating limits of the instrument. This was particularly true of regions where the crystals absorbed strongly and smaller pinholes could be placed in the reference beam. Wavelength overlap was included between adjacent segments of the spectra recorded with different reference pinholes. A baseline was prepared by using a pinhole of the approximate size as that used in mounting the crystal. This pinhole was then placed in the sample beam and the appropriate pinhole is placed in the reference and the results recorded. The spectral and baseline data were recorded by a Cary-Datex digitalized system on punched computer cards. A PL/1 program was used to match the segments of data in both the spectra and baselines and then subtract out the baseline from the appropriate spectrum. The results were then scaled and plotted by the Simplotter.

A cryostat was used for low temperature spectra of crystals. A platinum pinhole plate was mounted in the cryostat directly against the copper block, which formed

the bottom of the vacuum insulated can. The cryostat with its crystal were cooled with the addition of liquid nitrogen to 77K and the polarized spectra were normally recorded at this temperature. The liquid nitrogen in thermal contact with the crystal was then replaced with liquid helium and the crystal was then cooled to the nominal temperature of 15°K by the use of liquid helium.

A device was available by which the platinum pinhole could be mounted in a holder, which was attached to a rotating microscope stage. The crystal could then be rotated in the beam to a known angle. This rotation feature was useful in the collection of interference wave data.

III. RESULTS AND DISCUSSION

A spectroscopic study of $K_2PtBr_4 \cdot 2H_2O$ requires a
knowledge of the spatial orientation of the molecules in the
crystal. X-ray data were collected on a crystal of
$K_2PtBr_4 \cdot 2H_2O$.

Crystals of $K_2PtBr_4 \cdot 2H_2O$ were extremely difficult to
retain in the laboratory atmosphere due to the loss of
waters of hydration. Capillary mounting of crystals in the
presence of a concentrated solution of K_2PtBr_4 was
unsuccessfully attempted. A method of mounting these
unstable crystals had to be devised to protect them from
dehydration. It was found that by placing a small droplet
of K_2PtBr_4 solution in liquid methyl cellulose, crystals
would form and grow in the liquid vacuole. The methyl
cellulose was originally placed on a sheet of polyethylene,
which provided a surface to which the cellulose solution
would not strongly adhere to as it dried. After a suitable
crystal had grown inside of the cellulose, a sharp razor
blade was used to cut into the cellulose surrounding the
liquid vacuole with its crystal. This piece of cellulose
with its vacuole was mounted on a glass fiber and then
fixed onto a goniometer. This technique permitted the
crystal to be in direct contact with the solution from
which it originated. This method sometimes yielded multiple
crystals inside these small vacuoles, so care had to be

exercised in making certain only a single crystal was forming in the vacuole. Collection of X-ray data on approximately twenty crystals was attempted, only one of which was suitable for data collection.

The unit cell parameters for $K_2PtBr_4 \cdot 2H_2O$ were $\alpha = \beta = \gamma = 90°$; $a = 8.31(2)$ Å, $b = 13.73(3)$ Å, $c = 4.84(1)$ Å with two molecules per unit cell. The crystal was mounted in contact with solution and was noted to be growing during the collection of the X-ray data. Apparently, water was able to diffuse from the plastic vacuole resulting in a slow increase in the concentration of the K_2PtBr_4 solution within the vacuole, which in turn caused the observed crystal growth. The final crystal size was measured microscopically to be 0.40 x 0.36 x 0.036 mm^3.

X-ray intensity data were collected on a four-circle diffractometer, which was interfaced with a PDP-15 computer. A molybdenum K_α (.7107 Å) radiation source was used with a graphite monochromator and scintillation counter. Data were collected for the hkℓ and hkℓ̄ octants and were within a 2θ sphere of 50°. Three standard noncoplanar reflections were chosen to monitor changes in peak intensity as a consequence of any crystal decomposition or crystal movement. However, the intensities of two of the three standard reflections showed a considerable increase with the passage of time. This increased intensity was most likely due to the

increase in mosiac character of the crystal during the collection of the intensity data.

A total of 1200 reflections of X-ray intensity data were collected by means of the step scan technique (41) to give integrated intensities. These reflections constituted two complete octants of data. The attenuation of the X-ray beam through absorption was found to be large as indicated by a linear absorption coefficient (42) of 300.08 cm^{-1}. Absorption corrections on the X-ray data were attempted by two different programs, OR ABS (43) and TALABS (44). In each case the data set created by the absorption correction program was found to give structures which would not refine as well as that of uncorrected data. Lorentz-polarization corrections were made during data reduction by means of the equation,

$$(LP)^{-1} = \sin2\theta[(1 + \cos^2 2\theta_m)/(\cos^2 2\theta + \cos^2 2\theta_m)] \tag{63}$$

where θ_m is the glancing angle of the monochromator, 6.1°. The standard deviations (σ_I) in the intensities have been calculated from the total count (TC) and the background count (BC) values by the expression:

$$(\sigma_I)^2 = TC + BC + (0.03TC)^2 + (0.03BG)^2 + (0.03I)^2 \tag{64}$$

The nonstatistical errors in TC, BG, and I were estimated from the last terms in the above expression. The standard deviation in the structure factor (σ_F) was calculated by the finite difference method (45).

Equivalent reflections from the different octants were averaged and reflections were eliminated when $||F_o|-|F_A||/|F_A| > 30\%$, where F_o is the observed structure factor and F_A is the averaged structure factor. This averaging procedure gave a total of 470 unique reflections and eliminated 65 reflections due to poor agreement with the average structure factor.

The growth of standard reflection intensities was corrected by an adjustment program. The adjustment was based upon the linear growth of intensity for the standards. A least-squares fit was used to obtain the slope and intercept of these reflection intensity growth lines. Growth of intensity was assumed to be linear with respect to the reflection number. Adjustment of the intensity of a reflection could then be made based on hkℓ values and reflection number. This particular correction to the data was successful and permitted further refinement of the structure.

Two orthorhombic space groups (P_{ba2}, C_{2v}^8, No. 32 and P_{bam}, D_{2h}^9, No. 55) were found to fit the extinction conditions of the reflection data. The two space groups

differ only in that space group No. 55 has an inversion center. A Howells, Phillips and Rogers (H.P.R.) plot was made to determine whether an inversion center was indicated in a cumulative distribution curve for the reflection intensities [46]. The H.P.R. plots were not conclusive for the presence or absence of an inversion center. Refinement of the data in the two possible space groups did not reveal any distinction between them since they refined to the same level. Therefore, the results are given for the structure refined in space group No. 55.

A three-dimensional Patterson [47] map was obtained from the reflection data and atom positions were determined from this map. There were five unique atoms in the structure of $K_2PtBr_4 \cdot 2H_2O$. The platinum atom was fixed at the origin. Two unique bromine atom positions, one potassium and one oxygen position were input and the structure was refined using a full-matrix least-squares in a local modification of OR FLS [48]. The real and imaginary parts of anomalous dispersion were obtained from the relativistic Hartree-Fock scattering factors of Doyle and Turner [49].

In the refinement of the structure in space group No. 55, the anisotropic temperature factors were restricted by symmetry conditions. All the atoms in this structure were in special positions as can be concluded from the position coordinates seen in Table 1. The temperature

Table 1. Positional parameters for $K_2PtBr_4 \cdot 2H_2O$

Atom	x	y	z
Pt	0	0	0
Br	0.2907	0.0266	0
Br	0.4591	0.3246	0
K	0.2547	0.1926	0.5
O	0.6188	0.1399	0.5

factors were then restricted to the following conditions, $\beta_{11} \neq \beta_{22} \neq \beta_{33} \neq \beta_{12}$, $\beta_{13} = \beta_{23} = 0$. The general form of the temperature factor expression is,

$$\exp(-\{h^2\beta_{11} + k^2\beta_{22} + \ell^2\beta_{33} + 2hk\beta_{12} + 2h\ell\beta_{13} + 2k\ell\beta_{23}\}) \tag{65}$$

In the actual refinement of the structure, temperature factors cannot reliably be reported due to the failure to correct for absorption of the X-ray beam. Also, the quality of the data limits any consideration of the temperature factors.

The refinement of the structure was carried out on F_o. The function minimized in this refinement was $\Sigma w(|F_o|-|F_c|)^2$ where w serves as a weighting coefficient defined by $1/\sigma_F^2$. The degree of the refinement was measurable by a discrepancy factor defined by,

$$R = \Sigma \left| |F_o|-|F_c| \right| / \Sigma |F_o| \qquad (66)$$

and also by a weighted discrepancy factor,

$$wR = [\Sigma w(|F_o|-|F_c|)^2/\Sigma w|F_o|^2]^{1/2} \qquad (67)$$

A reduced, averaged, and corrected for standard reflection increase data set refined to an R of 0.180 and a wR of 0.229. A listing of the reflections and their F_o and F_c values are presented in Table 2. The positional parameters of the five unique atoms are presented in Table 1. A depiction of a space-filling model of the unit cell for $K_2PtBr_4 \cdot 2H_2O$ projected into the a,b face is shown in Figure 10. The dotted circles in Figure 8 represent the potassium and oxygen atom positions and are at $z = \frac{1}{2}$ positions in the unit cell. The position of the oxygen atom did not settle out and the position parameters as reported in Table 1 for oxygen are uncertain to a degree.

The crystal spectra for $K_2PtBr_4 \cdot 2H_2O$ were recorded in the region 14,000 to 32,000 cm^{-1}. In the related anhydrous K_2PtBr_4 this is the spectral region where the d←d transitions

Table 2. Observed and calculated structure factors for $K_2PtBr_4 \cdot 2H_2O$

L = 0

H	K	FO	FC
0	2	87	135
0	4	109	176
0	6	196	311
0	8	32	31
0	10	69	105
0	12	102	120
0	14	7	-5
0	16	57	51
1	1	145	166
1	2	45	-60
1	3	30	9
1	4	50	-37
1	5	169	186
1	6	101	-108
1	7	83	113
1	8	35	-52
1	9	26	32
1	10	38	-69
1	11	135	156
1	12	58	-55
1	13	61	72
1	14	19	-7
1	15	29	33
1	16	32	-31
2	0	103	79
2	1	68	67
2	2	28	25
2	3	9	16
2	4	3	21
2	5	13	0
2	6	86	133
2	7	80	93
2	8	75	63
2	10	66	74
2	11	15	13
2	12	124	150
2	13	43	45
2	14	44	56
2	16	70	86
3	1	201	243
3	2	164	119
3	3	146	112
3	4	107	-68
3	5	234	217
3	6	70	103
3	7	175	134
3	8	82	73
3	9	34	51
3	10	11	-16
3	11	129	116
3	12	69	74
3	13	41	49
3	14	14	14
3	15	19	25
4	0	204	265
4	1	57	54
4	2	131	105
4	3	79	-48
4	4	135	140
4	5	123	-102
4	6	101	183
4	8	30	46
4	9	54	-76
4	10	124	103
4	11	75	-64
4	12	79	81
4	13	16	14
4	14	18	27
5	1	62	38
5	2	49	33
5	3	22	21
5	4	78	-53
5	5	84	64
5	6	29	-18
5	7	63	73
5	8	5	25
5	9	42	66
5	10	72	-61
5	11	103	99
5	12	4	3
5	13	75	87
6	0	77	72
6	1	106	81
6	2	135	116
6	3	24	21
6	4	98	89
6	5	5	1
6	6	92	78
6	7	85	116
6	8	69	100
6	9	16	21
6	10	61	61
6	11	28	20
6	12	72	75
7	1	167	149
7	2	67	54
7	3	156	153
7	4	98	-83
7	5	103	118
7	6	28	22
7	7	72	95
7	9	60	86
7	10	65	-58
7	11	48	51
8	0	62	50
8	1	32	29
9	2	62	60
8	3	32	-28
8	4	80	70
8	5	77	-63
8	6	45	51
8	8	38	-70
8	9	34	-49
9	1	32	25
9	2	17	27
9	3	64	76
9	5	5	27
9	6	13	22

L = 1

H	K	FO	FC
0	0	301	298
0	2	126	234
0	4	121	194
0	6	173	220
0	8	89	76
0	10	87	72
0	12	135	120
0	16	40	38
1	1	156	168
1	2	3	29
1	4	157	-143
1	6	11	-30
1	7	133	119
1	8	91	-67
1	9	38	29
1	10	108	-89
1	11	149	142
1	12	23	-14
1	13	73	72
1	14	50	-39
1	15	48	43
2	0	180	189
2	1	90	55
2	2	43	-59
2	3	15	17
2	4	44	35
2	5	8	1
2	6	194	168
2	7	88	75
2	9	30	16
2	10	137	119
2	11	16	10
2	12	129	128
2	13	44	43
2	14	35	44
3	1	206	225
3	2	27	48
3	4	14	22
3	6	64	37
3	7	180	131
3	8	110	86
3	10	0	5
3	11	131	109
3	12	41	35
3	13	51	50
3	14	48	42
3	15	20	22
4	0	176	168
4	1	74	59
4	2	162	160
4	4	78	124
4	6	197	141
4	7	0	9
4	8	124	95
4	9	102	-78
4	10	78	62
4	11	58	-59
4	12	78	92
4	14	33	34
5	1	30	40
5	2	71	74
5	3	6	13
5	4	100	-111
5	5	94	69
5	7	57	66
5	9	56	63
5	10	78	-74
5	11	109	99
5	12	23	31
5	13	59	59
6	0	135	123
6	1	63	69
6	2	59	72
6	3	18	24
6	4	70	93
6	5	3	3
6	6	122	99
6	8	56	60
6	10	95	87
6	12	50	62
7	1	120	141
7	2	25	27
7	3	152	154
7	4	33	-40
7	5	105	106
7	6	7	-8
7	7	106	96
7	8	17	21
7	9	87	83
7	10	39	-44
7	11	43	46
8	0	16	15
8	1	32	35
8	2	70	83
8	3	36	-31
8	4	59	63
8	5	54	-62
8	6	37	34
8	7	2	5
8	8	85	93
8	9	59	-52
9	1	15	27
9	2	36	44
9	3	35	67
9	4	22	-23
9	5	19	32
9	6	32	41

L = 2

H	K	FO	FC
0	0	388	391
0	4	126	141
0	6	191	250
0	8	37	28
0	10	112	89
0	12	48	85
0	14	9	-3
1	1	177	128
1	2	46	-44
1	3	34	12
1	4	38	-30
1	5	170	148
1	6	102	-86
1	7	103	93
1	8	48	-44
1	9	35	28
1	10	67	-58
1	11	149	133
1	12	63	-47
1	13	67	63
1	14	16	-6
1	15	37	35
2	0	94	64
2	1	53	50
2	2	37	23
2	3	8	12
2	4	25	20
2	6	136	106
2	7	82	68
2	8	64	54
2	10	75	63
2	11	12	11
2	12	130	129
2	13	48	38
2	14	50	50
3	1	207	194
3	2	143	92
3	3	140	90
3	4	86	-52
3	5	217	173
3	6	96	84
3	7	144	112
3	8	81	61
3	9	65	45
3	11	123	99
3	12	67	63
3	13	46	43
3	14	12	11

H	K	FO	FC		H	K	FO	FC		H	K	FO	FC
4	0	209	216		1	11	108	104		1	2	20	-25
4	1	40	43		1	13	54	55		1	7	60	58
4	2	116	89		2	1	45	34		1	8	22	-28
4	3	55	-39		2	2	30	-32		1	9	27	22
4	4	173	117		2	4	57	26		1	11	81	65
4	5	98	-84		2	5	11	2		2	2	40	15
4	6	186	154		2	6	128	115		2	3	2	8
4	7	8	2		2	7	52	52		2	5	5	1
4	8	54	41		2	9	15	13		2	6	81	63
4	9	85	-64		2	10	96	88		2	7	33	41
4	10	113	89		2	12	93	95		2	8	40	38
4	11	65	-55		2	13	28	31		2	9	8	8
4	12	78	70		3	1	181	152		2	10	46	41
5	1	49	32		3	2	25	32		2	11	0	8
5	2	31	26		3	3	106	81		3	1	129	117
5	4	55	-44		3	5	134	135		3	2	67	53
5	5	68	54		3	6	38	26		3	3	82	60
5	6	25	-15		3	7	108	95		3	4	37	-29
5	7	80	63		3	8	59	61		3	5	133	106
5	8	12	20		3	9	55	39		3	6	46	52
5	9	61	58		3	10	0	6		3	7	80	72
5	10	59	-51		3	11	93	80		3	8	32	37
5	11	86	86		3	12	25	25		3	9	41	31
5	12	6	2		3	13	40	39		3	10	10	-6
6	0	57	61		4	0	125	118		4	0	127	131
6	1	71	67		4	1	48	39		4	1	18	23
6	2	105	99		4	2	145	113		4	2	77	57
6	4	93	77		4	3	34	-34		4	3	23	-24
6	5	8	2		4	4	118	89		4	4	101	75
6	6	75	67		4	5	92	-69		4	5	46	-51
6	7	103	99		4	6	134	101		4	6	107	97
6	8	89	87		4	7	4	4		4	8	33	28
6	9	13	19		4	8	87	72		4	9	37	-40
6	10	61	53		4	9	59	-57		5	1	37	20
6	11	19	18		4	10	58	45		5	2	14	14
7	1	134	129		4	11	40	-43		5	3	20	13
7	2	46	49		4	12	64	69		5	4	26	-25
7	3	128	131		5	1	38	29		5	5	47	35
7	4	75	-71		5	2	48	51		5	6	11	-11
7	5	117	102		5	3	14	10		5	7	51	42
7	6	23	19		5	4	94	-78		5	8	0	12
7	7	93	83		5	5	58	50		6	0	40	49
7	8	5	11		5	7	50	50		6	1	34	41
7	9	78	75		5	9	51	48		6	2	70	65
7	10	51	-50		5	10	57	-54		6	3	0	12
8	0	44	44		5	11	79	75		6	4	58	50
8	1	17	24		6	0	91	90		6	6	47	44
8	2	44	51		6	1	41	48		7	1	81	85
8	3	23	-24		6	2	55	53		7	2	22	30
8	4	61	61		6	3	18	18					
8	5	56	-54		6	4	68	69			L = 5		
8	6	45	46		6	5	4	4		H	K	FO	FC
8	7	6	0		6	6	89	74		0	0	116	97
9	1	10	23		6	7	68	77		0	2	89	84
9	3	46	66		6	8	46	45		1	1	84	56
					7	1	99	106		1	2	6	7
	L = 3				7	3	119	115		1	3	21	5
H	K	FO	FC		7	4	25	-28		1	6	6	-12
0	0	254	188		7	5	85	80		2	2	11	-15
0	2	165	151		7	7	72	74		2	5	5	2
0	8	63	57		8	1	17	25		3	3	56	48
0	10	62	54		8	2	55	63		3	5	74	74
0	12	93	89		8	3	22	-23		3	6	11	13
1	1	149	107		8	4	45	48		4	2	67	65
1	3	13	5							4	4	54	51
1	5	92	116			L = 4							
1	7	91	84		H	K	FO	FC					
1	8	46	-48		0	0	242	217					
1	9	32	24		0	2	93	69					
1	10	68	-64		0	10	62	57					
					1	1	113	73					

a

b

$K_2PtBr_4 \cdot 2H_2O$
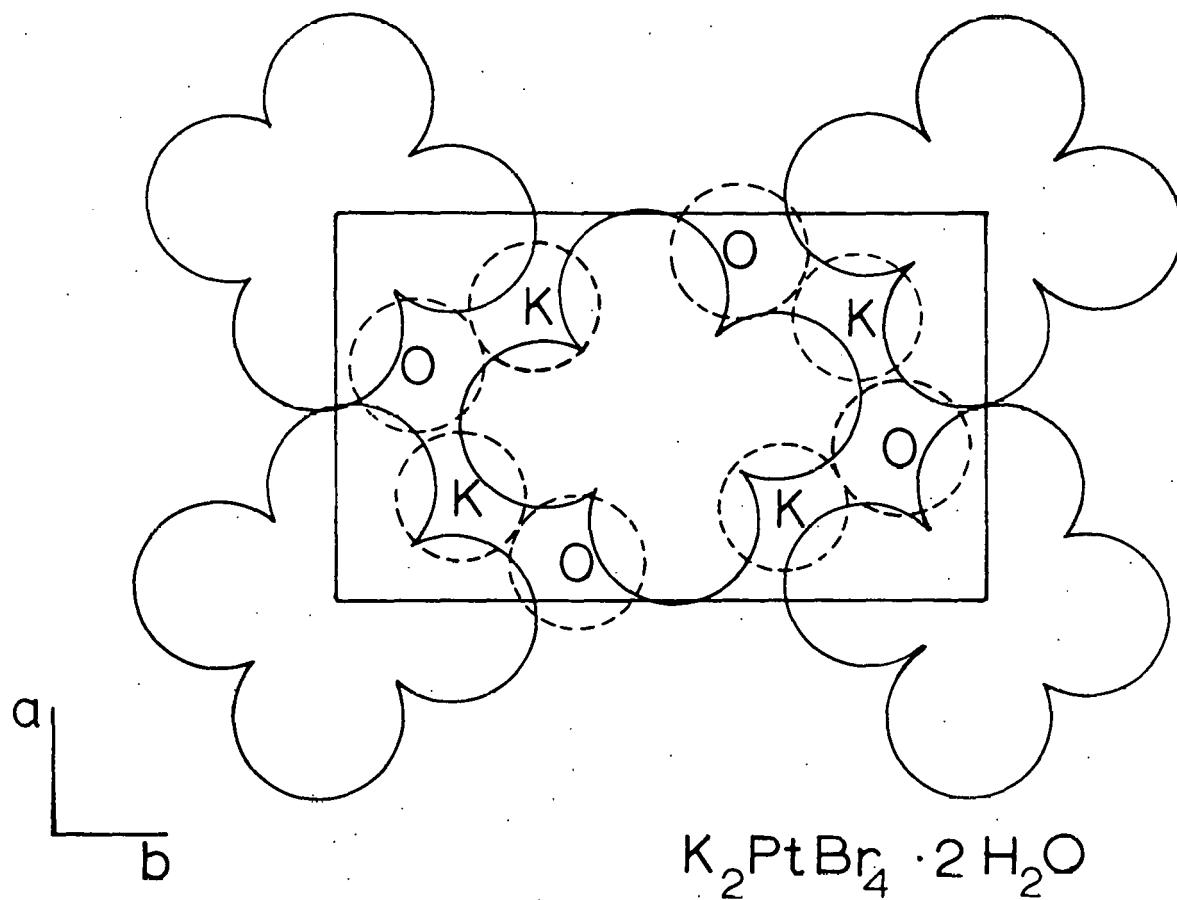
Figure 10. Unit cell of $K_2PtBr_4 \cdot 2H_2O$, dashed atoms are
at $z = \frac{1}{2}$

were observed. In particular, it is the region where the transisions from the $^1A_{1g}$ ground state to the $^{1,3}A_{2g}$ ($d_{x^2-y^2} \leftarrow d_{xy}$) and $^{1,3}E_g$ ($d_{x^2-y^2} \leftarrow d_{xz,yz}$) excited states occur for the D_{4h} $PtBr_4^{2-}$ ion. However, in the hydrated crystal with space group, P_{bam}, the $PtBr_4^{2-}$ ion occurs in a site of much lower symmetry than the D_{4h} site in the space group, $P_{4/mmm}$, of the anhydrous crystal. Therefore, the possible effects of the lower symmetry in the hydrated crystal as well as other crystal effects will be considered.

For an orthorhombic crystal such as $K_2PtBr_4 \cdot 2H_2O$ the principal axes of the real and imaginary parts of the optical indicatrix for each wavelength coincide with the crystallographic axes. For the crystal with light entering a face parallel to at least one of the crystallographic axes, the extinction directions, therefore, will be along such an axis and perpendicular to it. For $K_2PtBr_4 \cdot 2H_2O$ the spectra recorded for the 001 face provided the a- and b-polarizations whereas an 010 face provided the c-polarization. It was possible, therefore, to obtain spectra polarized along each of the crystallographic axes. The three sets of polarized crystal spectra at both 300K and 15K are shown in Figure 11.

The crystal thickness of $K_2PtBr_4 \cdot 2H_2O$ was determined from a study of the interference resulting from the air gap between the two quartz plates, which was adjacent to the crystal. The positions of the recorded maxima and minima
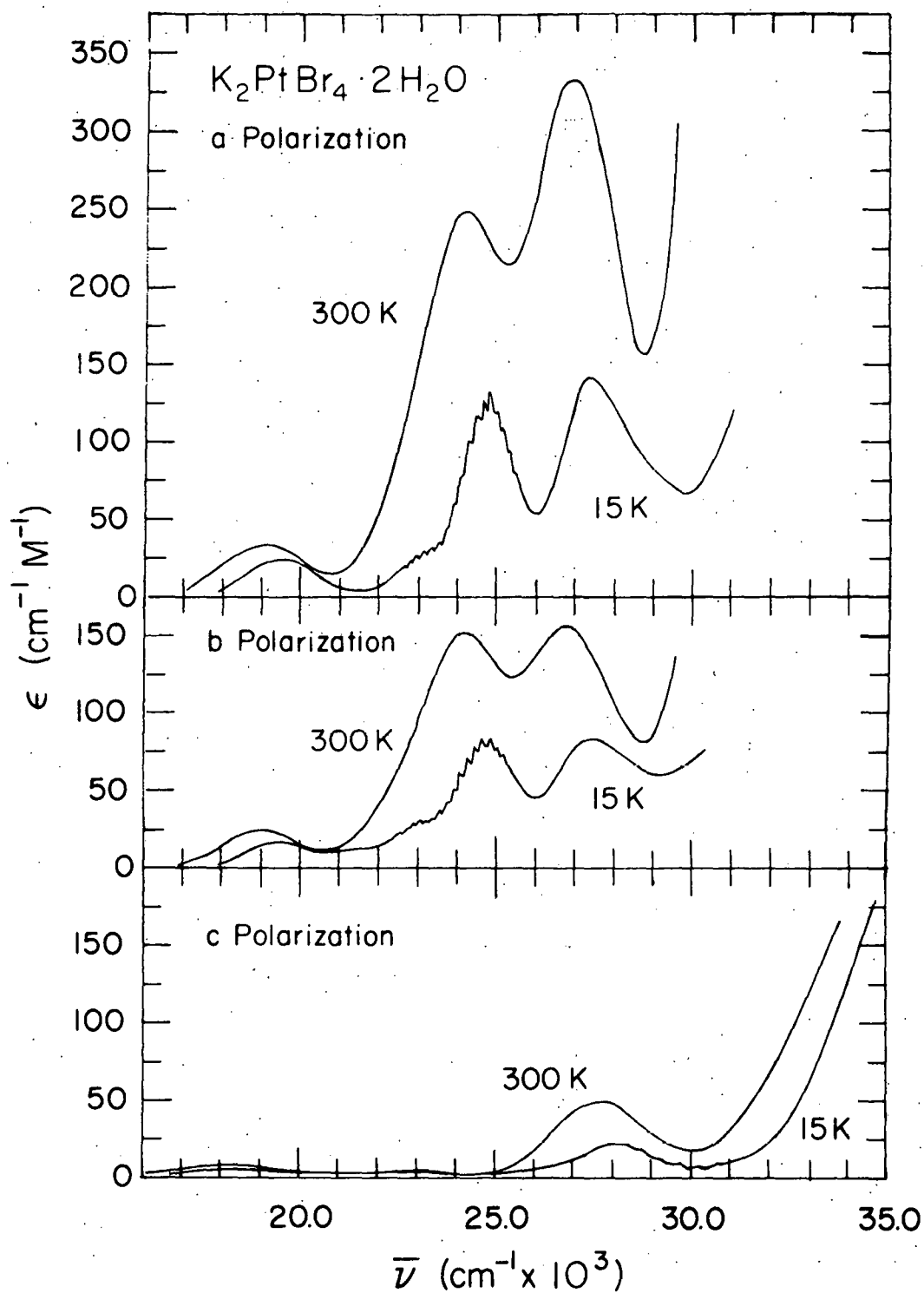
Figure 11. Polarized absorption spectra of $K_2PtBr_4 \cdot 2H_2O$ at 300 and 15K

in the absorbance were tabulated and substituted into
equations (61a) and (62) for computation of the crystal
thickness. Since the medium between the plates was air, a
value of 1.00 was used for the index of refraction.

The crystals of the hydrate for white light polarized
in the a- or b-directions were tan colored. However, the
color was much darker for the a-polarization. With light
polarized in the c-direction, pure sections of the crystals
appeared pink. Red sections in the crystal were occasionally
observable for white light polarized in the c-direction.
These sections would form as the crystal grew from solution.
The spectrum was obtained of these sections and appears in
Figure 12. A fuller discussion of the red sections and
their origin will be presented later.

The X-ray study of $K_2PtBr_4 \cdot 2H_2O$ revealed that the
planar $PtBr_4^{2-}$ ions were stacked directly over one another
along the c-axis. The c-axis spectrum therefore corresponds
to the molecular z-axis and should be comparable to the
c-polarized spectrum of the anhydrous K_2PtBr_4 (27). The
a-spectrum of K_2PtBr_4 is very similar to the a- and b-
polarized spectra of $K_2PtBr_4 \cdot 2H_2O$.

In the case of $K_2PtBr_4 \cdot 2H_2O$ the a- and b-polarized
spectra are similar in many of their features. The pre-
dominant features at room temperature are the two absorption
bands at 24,700 cm^{-1} and 27,500 cm^{-1}. In K_2PtBr_4 spectra

RED SECTION - K_2PtBr_4 HYDRATE CRYSTAL
"z"-c Polarization

15°K

300°K

15°K

$\overline{\nu}$ (cm^{-1} ×10^3)

"y"- b Polarization

300°K

15°K
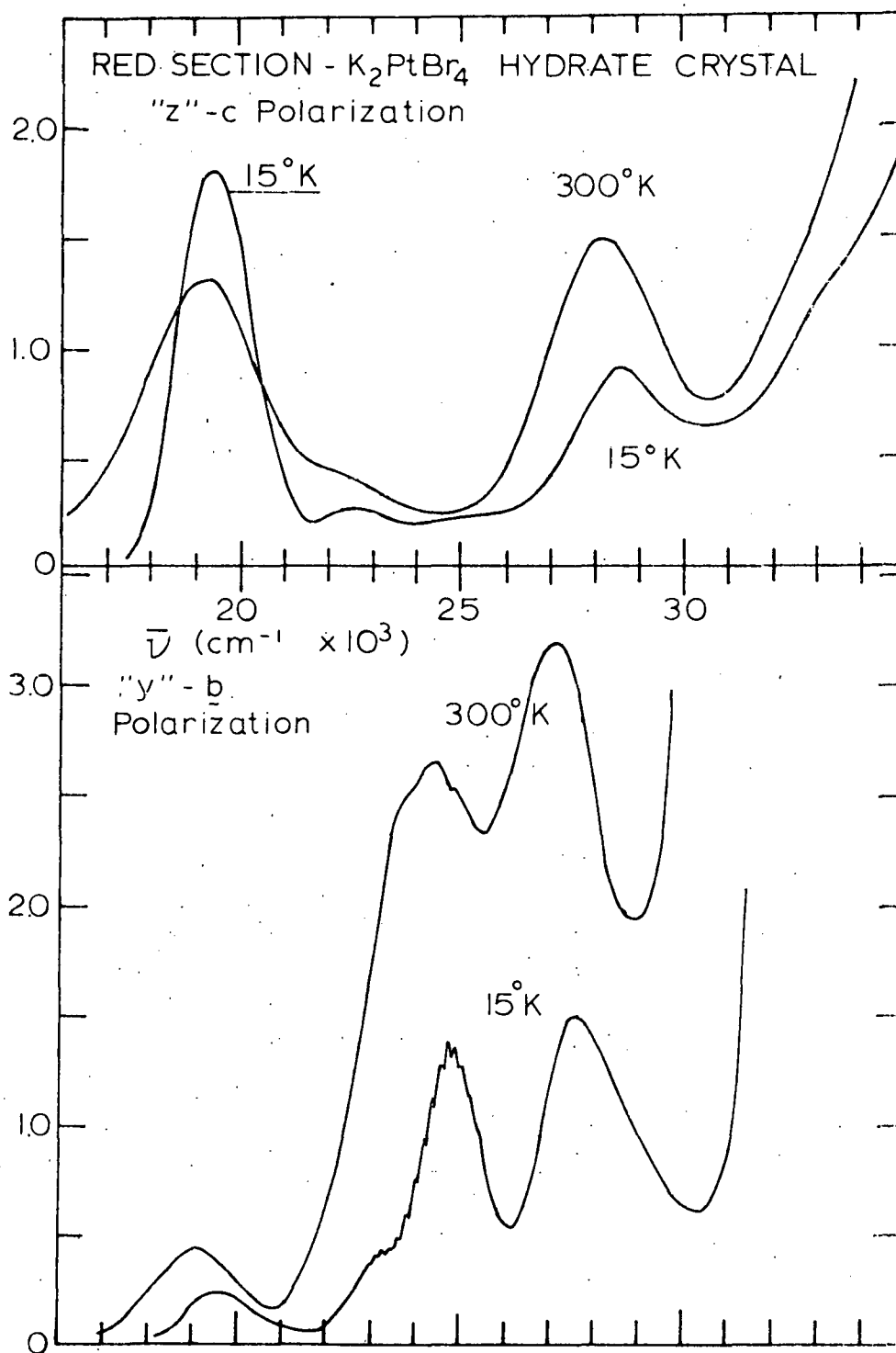
Figure 12. Polarized absorption spectra of red section in $K_2PtBr_4 \cdot 2H_2O$

these two peaks at room temperature were not as clearly
resolved, but appeared as a peak with a shoulder on the low
energy side. In $K_2PtBr_4 \cdot 2H_2O$ these two bands in the a-
polarized spectra were almost twice the intensity as they
are in the b-polarized spectra. Also, the band at
27,500 cm^{-1} was noted to be somewhat larger in absorbance
than the band at 24,700 cm^{-1} for the a-polarization while
these two bands were of approximately equal intensity in
the case of the b-polarized spectra. Upon cooling to 15K
these two bands in both a- and b-polarization showed a
decrease in intensity characteristic of a vibronic
transition.

The $PtBr_4^{2-}$ ion possesses 9 normal vibrations, which
are bases under D_{4h} for the irreducible representations:
A_{1g}, A_{2u}, B_{1g}, B_{2u}, and 2 sets with E_u. The asymmetric
vibrations by mixing with the electronic states by a
vibronic mechanism will permit transitions which would
otherwise be forbidden.

As was developed earlier, the vibronic selection rules
require that for a D_{4h} ion, the product of $\psi^\circ \psi' Q_i$ must
contain a basis for A_{1g}. Therefore, if $\psi^\circ \psi' Q_i$ contains a
basis for A_{2u}, the transition will appear in z-polarization
and if it contains E_u the transition will appear in x,y-
polarization. For the spin-allowed one electron excitations
of $PtBr_4^{2-}$, the following possible polarizations are

permitted from the set of molecular vibrations. For $^1A_{2g}\leftarrow$ $^1A_{1g}$ ($d_{x^2-y^2}\leftarrow d_{xy}$): forbidden in z, allowed x,y. For $^1E_g\leftarrow{^1A_{1g}}$ ($d_{x^2-y^2}\leftarrow d_{xz,yz}$): allowed in x, y, z. For $^1B_{1g}\leftarrow{^1A_{1g}}$ ($d_{x^2-y^2}\leftarrow d_{z^2}$): allowed in x, y, z. The spin-forbidden singlet to triplet transitions associated with the above set of spin-allowed transitions must be considered in the double group D_4'. These transitions can occur with appreciable intensity because of the appreciable spin-orbit coupling of the heavy platinum atom. A treatment under this double group indicates that there will be components in each set of the transitions $^3A_{2g}\leftarrow{^1A_{1g}}$, $^3E_g\leftarrow{^1A_{1g}}$, and $^3B_{1g}\leftarrow{^1A_{1g}}$, which will be allowed in each of x-, y-, and z-polarizations.

In each polarization for $K_2PtBr_4\cdot 2H_2O$ there is a band with a maximum at about 27,500 cm^{-1} which is very close to the peak in anhydrous K_2PtBr_4, which had been assigned as $^1E_g\leftarrow{^1A_{1g}}$ ($d_{x^2-y^2}\leftarrow d_{xz,yz}$) largely on the basis of the A-terms in the MCD spectrum of the aqueous solution. A similar arrangement appears appropriate for the hydrate. It is to be noted that the bands for this transition give no evidence for resolution of vibrational structure.

The band seen at 24,700 cm^{-1} for the a- and b-polarizations at room temperature is completely absent in the c-polarized spectra. At 15K this peak at 24,700 cm^{-1} resolves into a band at 24,700 cm^{-1} and a shoulder at 23,100 cm^{-1}. This band and shoulder exhibit vibrational

structure which can be seen in Figure 13. The fact that the band at 24,700 cm^{-1} was absent in c-polarization identified this transition as $^1A_{2g} \leftarrow ^1A_{1g}$ ($\sigma^*(b_{1g}) \leftarrow b_{2g}$ (d_{xy})). For this electronic transition the selection rules of equation (39) indicate that it is allowed with x,y-polarization but forbidden in z since there is no A_{1u} molecular vibration. In the anhydrous K_2PtBr_4 the analogous band occurs at 24,400 cm^{-1} in the 15K spectrum and is absent in the c-z polarization as well.

Weaker bands are seen in the room temperature spectra at 18,900 cm^{-1} (a), 18,100 cm^{-1} (b), and 18,400 cm^{-1} (c). These transitions are apparently due to spin-forbidden transitions to the $^3A_{2g}$ and ^3E_g states. There are 3 possible states for $^3A_{2g}$ and 6 for ^3E_g, but only a single peak could be resolved in this region of the spectra even for 15K. A band with a weak shoulder occurred in the anhydrous K_2PtBr_4 spectra and these were given a similar assignment.

A shoulder at 23,000 cm^{-1} becomes evident for a- and b-polarizations on the low energy side of the $^1A_{2g}$ band at 15K. This particular transition appears very weakly in the c-z polarization as well. This transition has been assigned as $^3B_{1g} \leftarrow ^1A_{1g}$ ($\sigma^*(b_{1g}) \leftarrow a_{1g}$ (d_{z^2})). This assignment was supported by the work of Patterson et al. (25) based upon the analogous band in $PtCl_4^{2-}$ which was studied by luminescence of crystals of Cs_2ZrCl_6 doped with Cs_2PtCl_4.
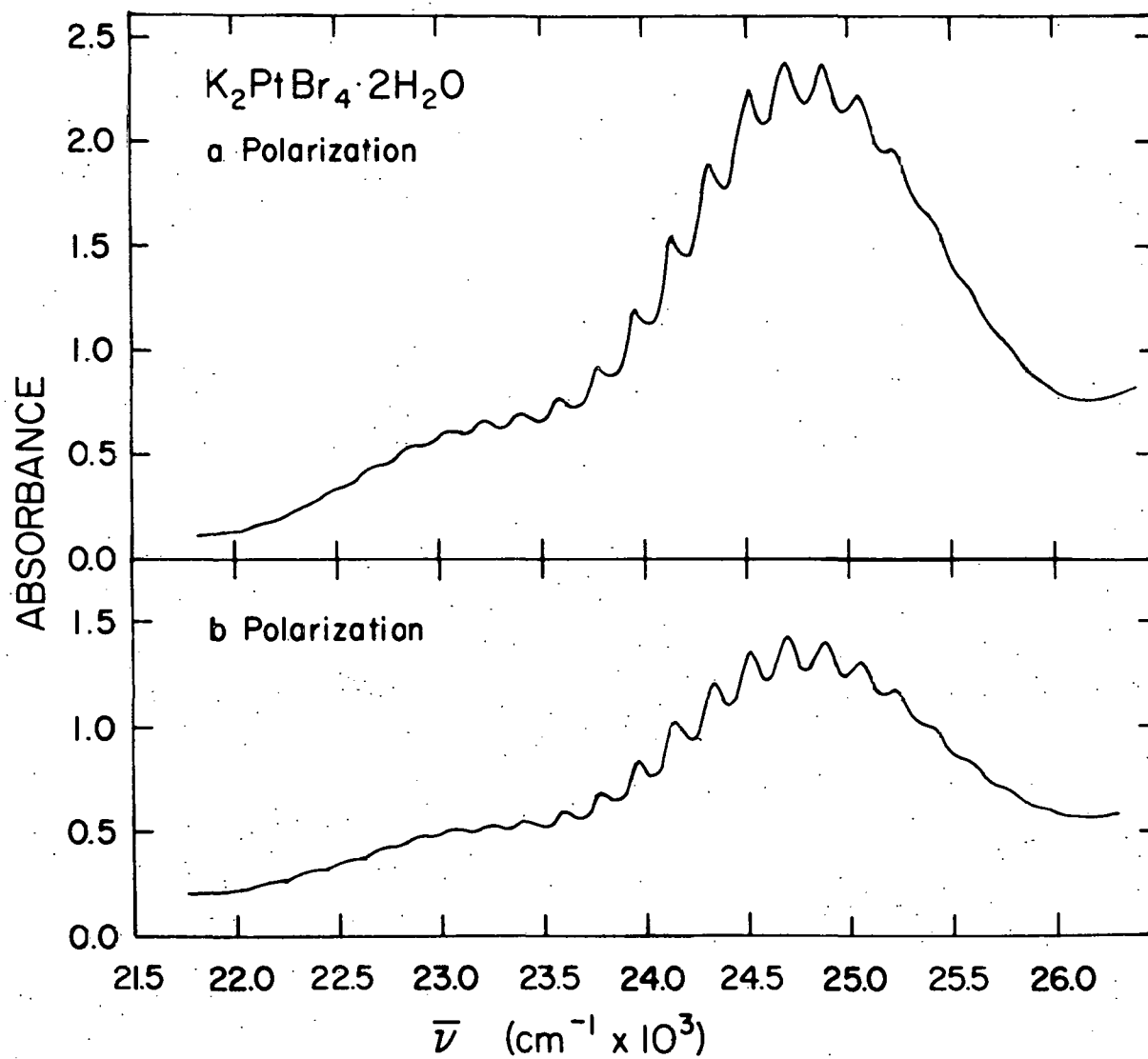
Figure 13. Vibrational structure in crystal spectrum of $K_2PtBr_4 \cdot 2H_2O$

The vibrational structure, observed in these spectra at 15K, was the result of excitation to excited vibrational states for the totally symmetric (A_{1g}) vibration of the excited electronic states. The portion of the spectrum exhibiting this vibrational structure for $K_2PtBr_4 \cdot 2H_2O$ is shown in Figure 13. The peak positions in wavenumbers of these vibrational components are tabulated in Table 3 over the two bands, $^3B_{1g}$ and $^1A_{2g}$, for all polarizations.

The vibrational structure observed in c-polarization was quite weak and was not resolved in most of the available spectra for this polarization. The average separation of these peaks was 180 ± 10 cm^{-1} for crystals of $K_2PtBr_4 \cdot 2H_2O$. The separation of this structure was greater than that measured for anhydrous K_2PtBr_4 at 170 ± 10 cm^{-1}. It was found that this difference in energy spacing of the vibrational structure could serve as a means of distinguishing a hydrated K_2PtBr_4 crystal from that of an anhydrous K_2PtBr_4 crystal. The probable explanation for this increased energy of the vibrational structure spacing was that in the case of the hydrate the $PtBr_4^{2-}$ units are situated so that the stretching vibrational modes bring the bromine atoms into stronger repulsive interaction with the bromines associated with adjacent $PtBr_4^{2-}$ units.

Raman studies by Hendra (50) on K_2PtBr_4 indicated that the vibrational energy of the A_{1g} vibration in the ground

Table 3. Vibrational structure observed at 15K for
          $K_2PtBr_4 \cdot 2H_2O$

a-polarization $\bar{\nu}$ (cm^{-1})	b-polarization $\bar{\nu}$ (cm^{-1})	c-polarization $\bar{\nu}$ (cm^{-1})
22,090		22,180
22,300	22,330	22,350
22,480	22,510	22,550
22,660	22,710	22,750
22,850	22,890	
23,030	23,060	
23,220	23,260	
23,400	23,410	
23,580	23,590	
23,760	23,780	
23,950	23,970	
24,140	24,140	
24,330	24,330	
24,510	24,520	
24,690	24,690	
24,880	24,880	
25,050	25,050	
25,220	25,240	
25,390	25,420	
25,580	25,590	
	25,770	

electronic state was 205 cm^{-1}. This energy was higher than that computed from the vibrational structure. The energy spacing was expected to be smaller in the electronic spectra because an electron had been promoted into an antibonding orbital; in effect relaxing the bonds and lowering the vibrational frequency.

The vibronic mechanism allows an E_u asymmetric vibrational mode to mix in and give an E_u excited state. This E_u state gives rise to two possible transitions. Under D_{4h} point group symmetry the transitions to the E_u states are degenerate and the transition moments lie in the plane and are 90° apart. The C_{2h} site symmetry of $K_2PtBr_4 \cdot 2H_2O$ splits the energy of these transitions and it may also serve to alter the magnitude and the orientation of these two transition moments. This splitting should be evident in the vibrational structure of the $K_2PtBr_4 \cdot 2H_2O$ spectra as a shoulder or peak near each of the peaks of the progression. No such effect was ever observed in this vibrational structure.

In anhydrous K_2PtBr_4 the $PtBr_4^{2-}$ ions occupy sites of full D_{4h} symmetry with four-fold symmetry of the molecule. The absorption of an in-plane polarization (perpendicular to z) is independent of the angle of rotation of the polarization vector about the z-axis, that is, the absorption is independent of the polarization angle, φ.

These molecules also lie exactly along the c-direction of
the unit cell. However, unlike anhydrous K_2PtBr_4, the ions
in $K_2PtBr_4 \cdot 2H_2O$ occupy sites of only C_{2h} point group
symmetry. A possible effect of this lower site symmetry
is the splitting of the ^1E_g degenerate states of D_{4h}. In
$K_2PtBr_4 \cdot 2H_2O$ there are two molecules per primitive unit
cell which are symmetry related to one another by the screw
and glide elements of the space group. It is then
necessary to consider the Davydov crystal states which are
linear combinations of one-site excitons as seen in
equations (48) and (49). If a 2-fold screw operation of
the space group is used to transform one molecule at a
given site into the molecule located at the remaining site
then the z-axis of the original molecule will be in the
opposite direction. Because of this the transition moment
integral for a z-polarized transition includes for the two
crystal states the terms

$$< \Phi_1'(z) \, + \, (- \, \Phi_2'(z)) \, | \, z \, | \, \Phi_o > \, = \, 0 \qquad (68)$$

and

$$< \Phi_1'(z) \, - \, (- \Phi_2'(z)) \, | \, z \, | \, \Phi_o > \, \neq \, 0 \qquad (69)$$

Thus, only one of the two possible Davydov crystal states
gives a nonzero transition moment integral.

On the other hand, the effect of the screw operation on a transition moment in the molecular x-direction results in two states which will be associated with different crystal ($\underline{a}$ or $\underline{b}$) polarizations. Likewise, a transition moment in the y-direction will give two Davydov states as well.

For a D_{4h} molecule the x and y components for the vibronic transition, $^1A_{2g} \leftarrow ^1A_{1g}$, will be normal to one another. They will also correspond to degenerate transitions. The lower site symmetry of $K_2PtBr_4 \cdot 2H_2O$ has the capability of splitting the degeneracy and offers the possibility of providing two transitions in each of the $\underline{a}$- and $\underline{b}$-polarizations. The breaking of the degeneracy also removes the restrictions that the absorptions have the same intensities in the $\underline{a}$- and $\underline{b}$-polarizations.

The spectra for the red sections in crystals grown from aged solutions of K_2PtBr_4 is shown in Figure 12. There is an intense band, apparently polarized completely in the $\underline{c}$-direction with a maximum at $19,400$ cm^{-1}, since the $\underline{b}$-polarized spectrum in Figure 12 appears normal. Also a crystal which exhibited the red sections would appear completely homogeneous when viewed under $\underline{a}$- or $\underline{b}$-polarization. Frequently, the red sections were surrounded by areas of the normal crystals. It can be seen from Figure 12 that when the crystal was cooled the peak height

of this absorption band increased as the width narrowed. This behavior is characteristic of a dipole allowed transition.

Somewhat similar red sections were reported for the red Cossa's salt (51), $KPt(NH_3)Cl_3 \cdot H_2O$, where red sections were shown to be due to the platinum(IV) ion, $Pt(NH_3)Cl_5^-$, which served as an impurity defect. Accordingly, the red sections in $K_2PtBr_4 \cdot 2H_2O$ are believed to be due to $PtBr_6^{2-}$, which replaces $PtBr_4^{2-}$ ions as an impurity defect. The $PtBr_6^{2-}$ ions will fit into a stack of the $PtBr_4^{2-}$ ions as shown in Figure 14. The $PtBr_6^{2-}$ ion is rather crowded and its axial bromides must be rather close to the platinum in $PtBr_4^{2-}$. For example, if the $PtBr_6^{2-}$ ion with a Pt-Br bond distance of 2.43 Å (52) fits into an undistorted unit cell, the bromide ligand would only be 2.41 Å from the platinum(II) atom. This appears short enough to provide for considerable orbital overlap between the bromide and the platinum(II) atom. The absorption band can therefore be attributed to a Pt(IV)←Pt(II) electron transfer.

A molecular orbital diagram in Figure 15 shows the orbitals which might be involved in such a mixed valence charge transfer. A transition which would be dipole allowed in the c-direction, is shown in the figure. It involves an electron transfer, $d_{z^2}(IV) \leftarrow d_{z^2}(II)$ and would be a $\sigma^* \leftarrow \sigma$ type. It would certainly involve the p_z-orbital
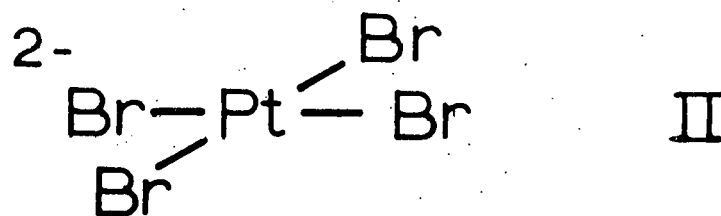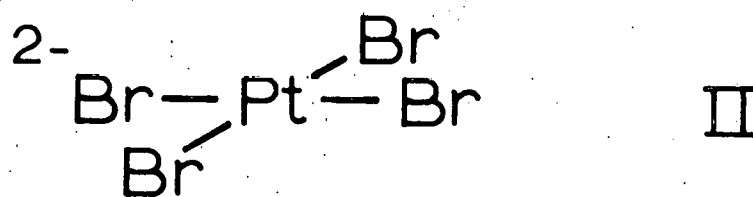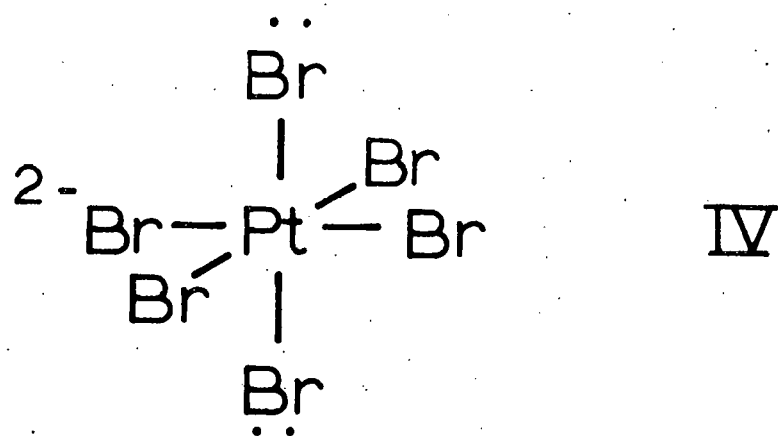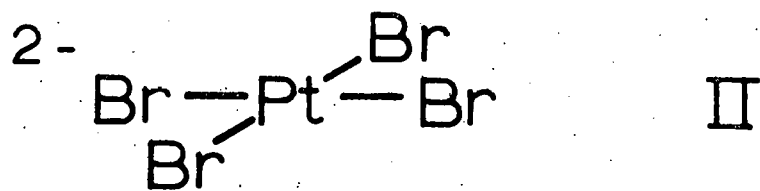
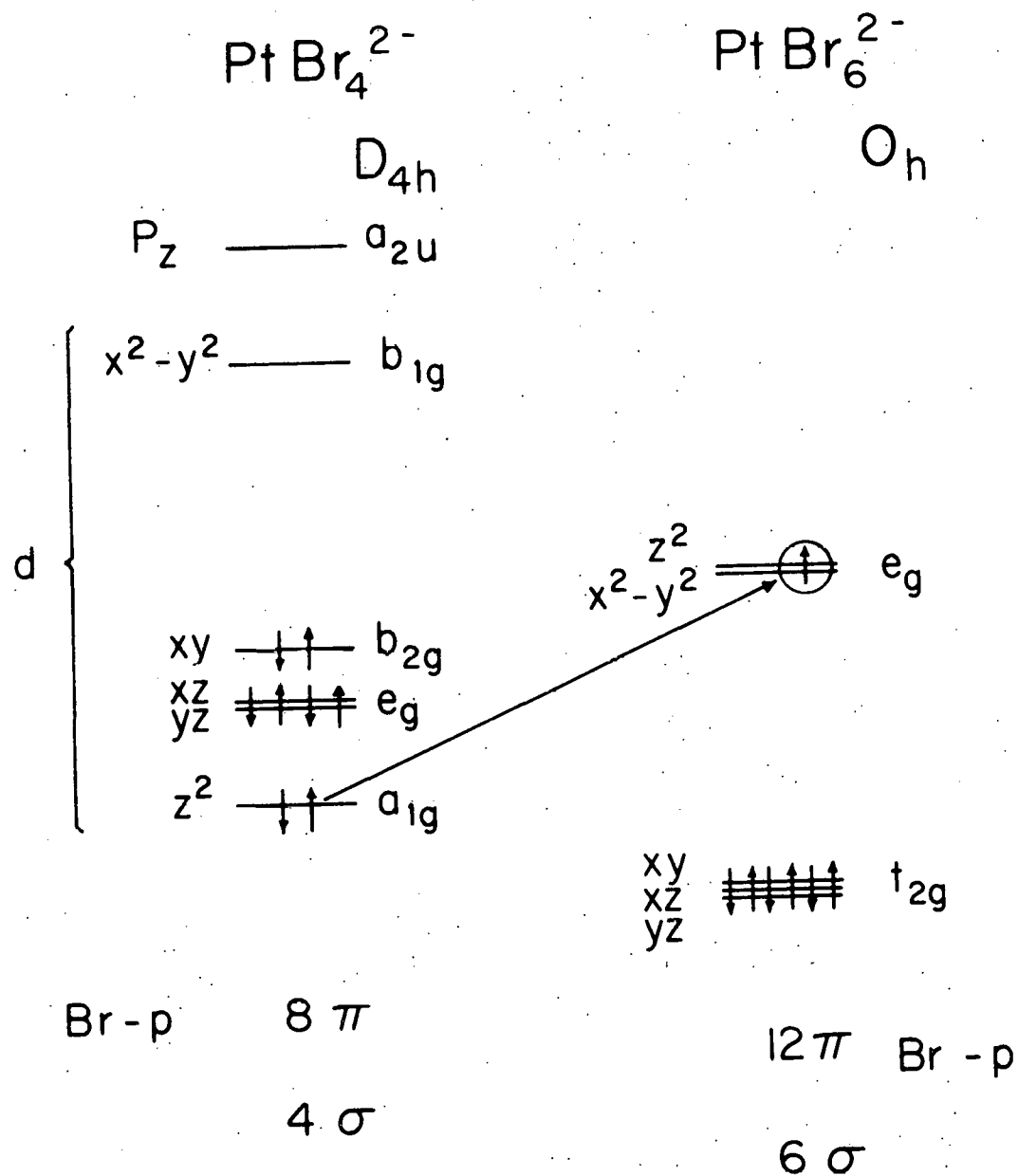Figure 14. Stacking of PtBr$_4^{2-}$ and PtBr$_6^{2-}$

Figure 15. Molecular orbital diagram for the electron transfer from $PtBr_4^{2-}$ to $PtBr_6^{2-}$.

of the bromide ligand to provide the overlap as shown in Figure 16. Since the impurity defect is believed to be quite small, the order of a few percent at most, the transition on a molecular basis is probably quite intense.

Electron transfer transitions from the b_{2g} orbital of $PtBr_4^{2-}$ into the available orbitals of $PtBr_6^{2-}$ would be forbidden because there would be zero overlap for an electron transfer to the d_{z^2} or the $d_{x^2-y^2}$ orbitals of $PtBr_6^{2-}$. The e_g d-orbitals of d_{xz} and d_{yz} associated with $PtBr_4^{2-}$ are of π-symmetry and there exists some potential overlap of these orbitals via the bromide π-orbitals with those of the $PtBr_6^{2-}$. Apparently, this overlap is so small that this electron transfer, which would be polarized normal to the stacking axis, is not seen.

The observed transitions in the region from 16,000 to 27,500 cm^{-1} for anhydrous K_2PtBr_4 are summarized in Table 4. The transition observed for $K_2PtBr_4 \cdot 2H_2O$ crystal spectra at 300 and 15K are tabulated with their corresponding assignments in Table 5.

The crystal structure of $[N(C_2H_5)_4]_2Pt_2Br_6$ reported by Stephenson (29) reveals that the $Pt_2Br_6^{2-}$ ion is essentially planar with point group symmetry of D_{2h}. The projection of the $Pt_2Br_6^{2-}$ anion onto the 001 cleavage face gives an orientation of the anion as seen in Figure 17. The space group for the crystal structure, $P\bar{1}$, requires
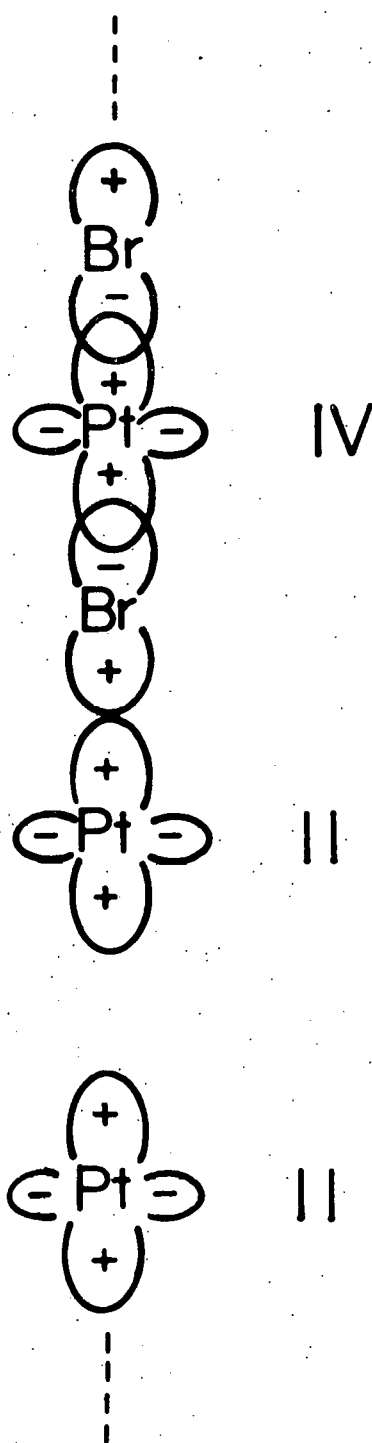
Figure 16. Overlap of the d_{z^2} orbitals of Pt(II) and Pt(IV) with the p_z orbital of bromide ligand

Table 4. Observed transitions in anhydrous K_2PtBr_4 spectra[a]

c-z polarization			a-xy polarization			Excited state: transition assignment
$\bar{\nu}$	ε_{max}	Osc. str.	$\bar{\nu}$	ε_{max}	Osc. str.	
(cm^{-1})	$(cm^{-1}M^{-1})$	$f \times 10^4$	(cm^{-1})	$(cm^{-1}M^{-1})$	$f \times 10^4$	
16,900	1 (5)	0.05 (0.75)	17,000	4 (9)	0.4 (1.5)	$^3A_{2g}$: $\sigma^*-b_{1g}(d_{x^2-y^2}) \leftarrow b_{2g}(d_{xy})$
18,800	12 (21)	1.1 (2.2)	19,100	15 (28)	1.3 (3.4)	^3E_g: $\sigma^*-b_{1g}(d_{x^2-y^2}) \leftarrow e_g(d_{xz,yz})$
22,600	3 (8)	0.2 (1.7)	22,700	13 (32)	0.9 (3.4)	$^3B_{1g}$: $\sigma^*-b_{1g}(d_{x^2-y^2}) \leftarrow a_{1g}(d_{z^2})$
Absent	---	---	24,400	46 (83)	3.5 (8.8)	$^1A_{2g}$: $\sigma^*-b_{1g}(d_{x^2-y^2}) \leftarrow b_{2g}(d_{xy})$
27,400	44 (110)	4.2 (13)	26,800	73 (160)	7.0 (21)	^1E_g: $\sigma^*-b_{1g}(d_{x^2-y^2}) \leftarrow e_g(d_{xz,yz})$

[a]Values of ε and f without parentheses are for 15K. Values in parentheses are for 300K. Data obtained from reference (27).

Table 5. Observed transitions and assignments for $K_2PtBr_4 \cdot 2H_2O^a$

a-polarization			b-polarization		
$\bar{\nu}$ (cm^{-1})	ε_{max} (cm^{-1}M^{-1})	Osc. Str. $f \times 10^4$	$\bar{\nu}$ (cm^{-1})	ε_{max} (cm^{-1}M^{-1})	Osc. Str. $f \times 10^4$
19,600	23	1.7	19,400	22	1.7
	(37)	(4.0)		(20)	(1.9)
23,100	20	1.2	23,000	20	1.5
	(34)	(2.2)		(27)	(2.1)
24,700	122	8.5	24,700	77	5.9
	(224)	(22)		(129)	(13)
27,500	136	12.1	27,500	82	8.4
	(314)	(37)		(143)	(19)

[a]Values of ε and f without parentheses are for 15K. Values in parentheses are for 300K.

$\bar{\nu}$ (cm^{-1})	c-polarization ε_{max} $(cm^{-1}M-1)$	Osc. Str. $f \times 10^4$	Excited state: Transition assignment
18,400	5	0.4	$^3A_{2g}$: $\sigma^*-g_{1g}(d_{x^2-y^2}) \leftarrow b_{2g}(d_{xy})$
	(10)	(0.9)	^3E_g: $\sigma^*-b_{1g}(d_{x^2-y^2}) \leftarrow eg(d_{xz,yz})$
23,100	4	0.2	$^3B_{1g}$: $\sigma^*-b_{1g}(d_{x^2-y^2}) \leftarrow a_{1g}(d_{z^2})$
	(4)	(0.2)	
absent			$^1A_{2g}$: $\sigma^*-b_{1g}(d_{x^2-y^2}) \leftarrow b_{2g}(d_{xy})$
28,200	20	1.8	^1E_g: $\sigma^*-b_{1g}(d_{x^2-y^2}) \leftarrow eg(d_{xz,yz})$
	(47)	(5.6)	

$$[N(C_2H_5)_4]_2[Pt_2Br_6]$$
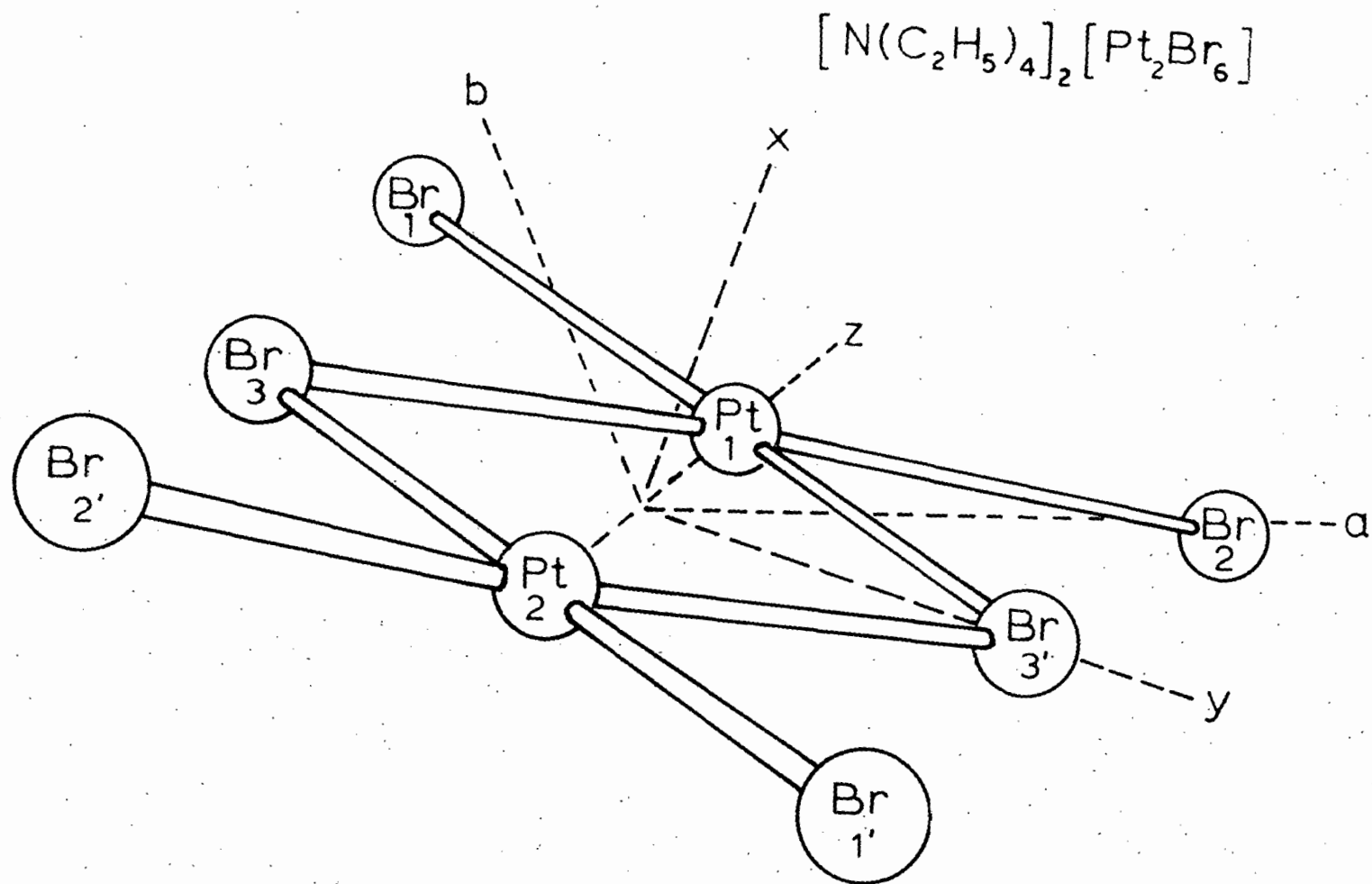
Figure 17.   Projection of $Pt_2Br_6{}^{2-}$ ion onto the ool cleavage face

that the $Pt_2Br_6^{2-}$ anion have an inversion center symmetry element. The two platinum atoms and the two bridging bromines all lie in a plane. The z-axis is taken as lying along the Pt-Pt distance and thus is the long molecular axis of the anion. The x-axis of the molecule is defined as being normal to the Pt-bridging bromine plane. The y-axis is taken as perpendicular to the x- and y-axes and thus forms a right-handed molecular coordinate system as depicted in Figure 17. The selected y-axis was found to pass within 0.02 Å of the position of the bridging bromines, Br(3) and Br(3'). Study of the orientation of the molecule in the crystal revealed that the light wave front enters the $Pt_2Br_6^{2-}$ ion from a nearly end on approach. The z-axis formed an angle of 16.23° with this wave normal.

For a thin crystal of $[N(C_2H_5)_4]_2Pt_2Br_6$ mounted on the X-ray diffractometer, the axes and angles reported by Stephenson were confirmed. The face of the crystal was identified as the 001 face and the location of the unit cell axes in the face were established for comparison with the observed extinction direction axes. From these studies the high extinction direction was found to be 18±1° from the a-axis and was coincident with the projection of the y-axis on the 001 face. The y-axis was 18.35° from the a-axis and formed an angle of 8.60° with the projection onto the 001 face. The absorption was calculated for the

high or yellow extinction to be: y = 98%; z = 2%; x ∿ 0.1%.
The high extinction was then effectively the y-transition
moment. The low or white extinction seen on the 001 face
is 13.7° from the x-axis and 76.3° from the z-axis. The
contributions to absorption for the low extinction were
calculated to be: x = 94%; z = 6%; y = 0. This extinction
contains predominantly x-polarized absorption.

The spectra of the high and low extinctions are shown
in Figure 18. The absorption for the high extinction
spectrum is much stronger than that of the low extinction
spectrum at all wavelengths. The high extinction spectrum
shows two strong peaks. The peak at 23,800 cm^{-1} has an
ε_{max} of 800 cm^{-1}M^{-1} at room temperature, and upon cooling
to 15K the ε_{max} increases to 1,400 cm^{-1}M^{-1}. The higher
energy peak seen at 29,200 cm^{-1} has an ε_{max} that also
increases from 3,300 to 3,700 in the process of cooling to
15K. The increased peak height at cooling is diagnostic
of a nonzero static transition dipole.

Day et al. (30) incorrectly identified the developed
face on crystals of $[N(C_2H_5)_4]_2Pt_2Br_6$ as the 100 face on the
basis of measured angles between crystal edges.

In a comparison of the spectra of the $Pt_2Br_6^{2-}$ ion with
those of K_2PtBr_4 in the region of 24,000 - 30,000 cm^{-1}, the
ε's of $Pt_2Br_6^{2-}$ are at least ten-fold higher than those
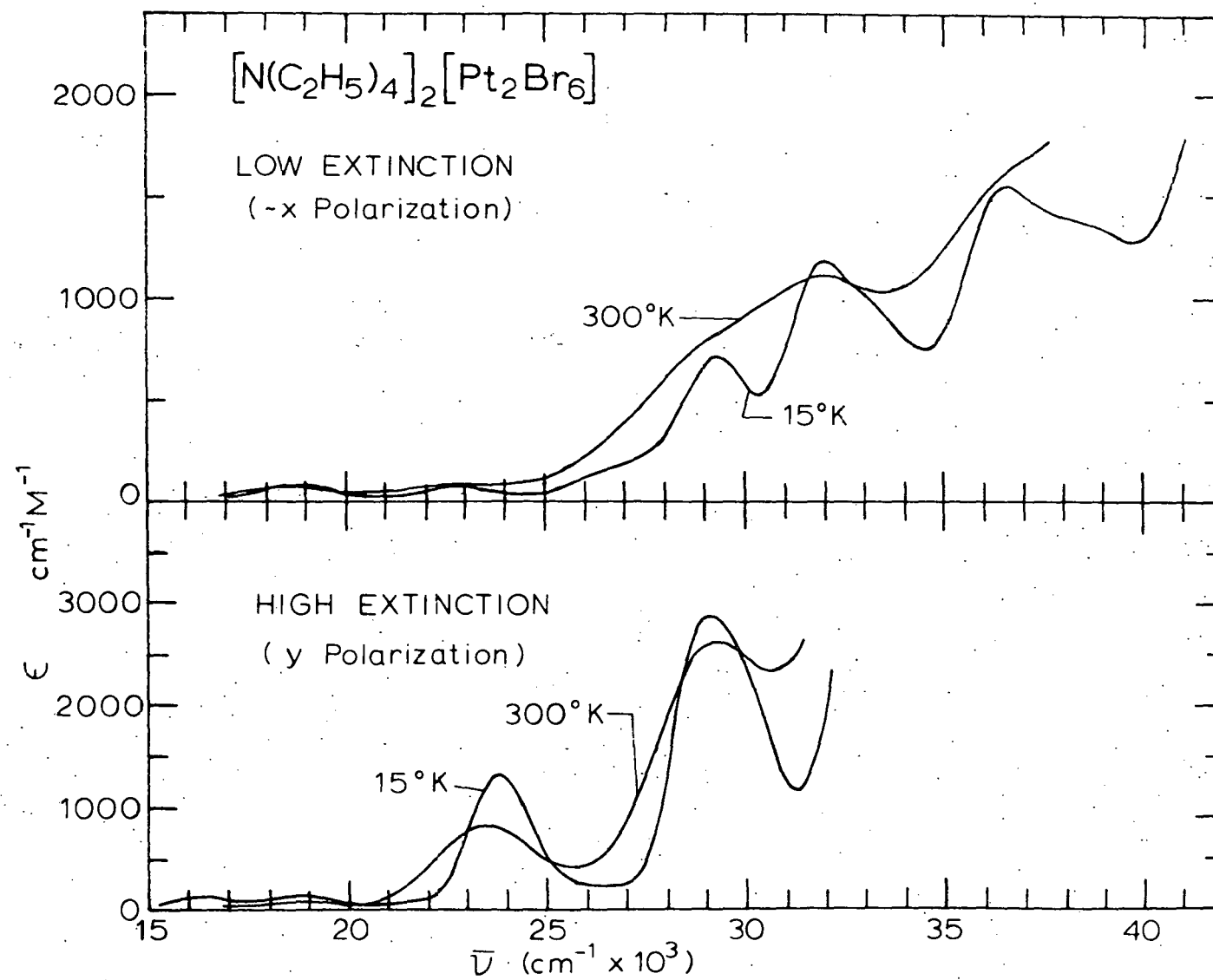observed for K_2PtBr_4 when compared on a per platinum atom

basis. In the case of K_2PtBr_4 the transitions seen in this region are d←d and are allowed only as a result of vibronic perturbations.

The distinctly different spectra of the high and low extinction directions of Figure 18 demonstrate the isolation of y-axis absorptions in the high extinction direction. For example, at 23,800 cm^{-1} there was no evidence for the presence of a peak in the low extinction whereas the high extinction had an $\varepsilon = 1,300$ $cm^{-1}M^{-1}$.

The room temperature spectrum of the low extinction shows a gradual increase in absorption from 20,000 to 38,000 cm^{-1}. Little structure is seen in this spectrum with the exception to a shoulder at 32,000 cm^{-1}. On cooling the crystal to 15K the spectrum of the low extinction showed a number of moderately strong peaks appearing. These peaks appear to be superimposed on a broad general absorption that is occurring in this region of the spectrum. Three peaks at 29,000, 32,000, and 36,500 cm^{-1} have ε's of 300 or greater. These peaks appear to have the temperature dependence which would label them as dipole-allowed transitions.

Spectra of the low extinction were recorded with a crystal rotated in the light beam about the high extinction axis. Such a rotation results in an angle change between the wave front normal of the light and the z-molecular axis.

Figure 18. Polarized spectra of the high and low extinctions

of $[N(C_2H_5)_4]_2Pt_2Br_6$

$[N(C_2H_5)_4]_2[Pt_2Br_6]$

LOW EXTINCTION
(~x Polarization)

300°K

15°K

HIGH EXTINCTION
(y Polarization)

300°K

15°K

ϵ $cm^{-1}M^{-1}$

$\bar{\nu}$ $(cm^{-1} \times 10^3)$

Two spectra of different tilt angles are shown in Figure 19.
The spectrum of crystal tilt = -17° shows a peak at
31,500 cm^{-1}, that is a dominant feature while the spectrum
at tilt = +22° shows little of this peak. From this
result it was concluded that the band seen at 31,500 cm^{-1}
was z-polarized.

A thick crystal of $[N(C_2H_5)_4]_2Pt_2Br_6$ was selected to
observe the low energy region of 15,000 - 24,000 cm^{-1}. These
spectra in both polarizations at 300 and 15K are shown in
Figure 20. This low energy region occurs where spin-
forbidden d←d transitions are seen for K_2PtBr_4. At low
temperature bands in the spectra are seen at 16,300 and
18,800 cm^{-1} in the high extinction polarization and appear
to be dipole-allowed transitions. In the case of the low
extinction, dipole-allowed transitions appear at 18,900 and
21,700 cm^{-1}. The region of 17,500 cm^{-1} showed a temperature
dependence for the low extinction polarization indicative of
a vibronic transition.

If the platinum atoms in this dimer were noninteracting
with one another, then the d-orbitals associated with each
platinum could be ordered as for a D_{4h} square planar ion.
In this case the energies and intensities for the transitions
would be expected to be similar to those of $PtBr_4^{2-}$. This
was not the case.

Figure 19. Low extinction spectra at 15K which have been tilted
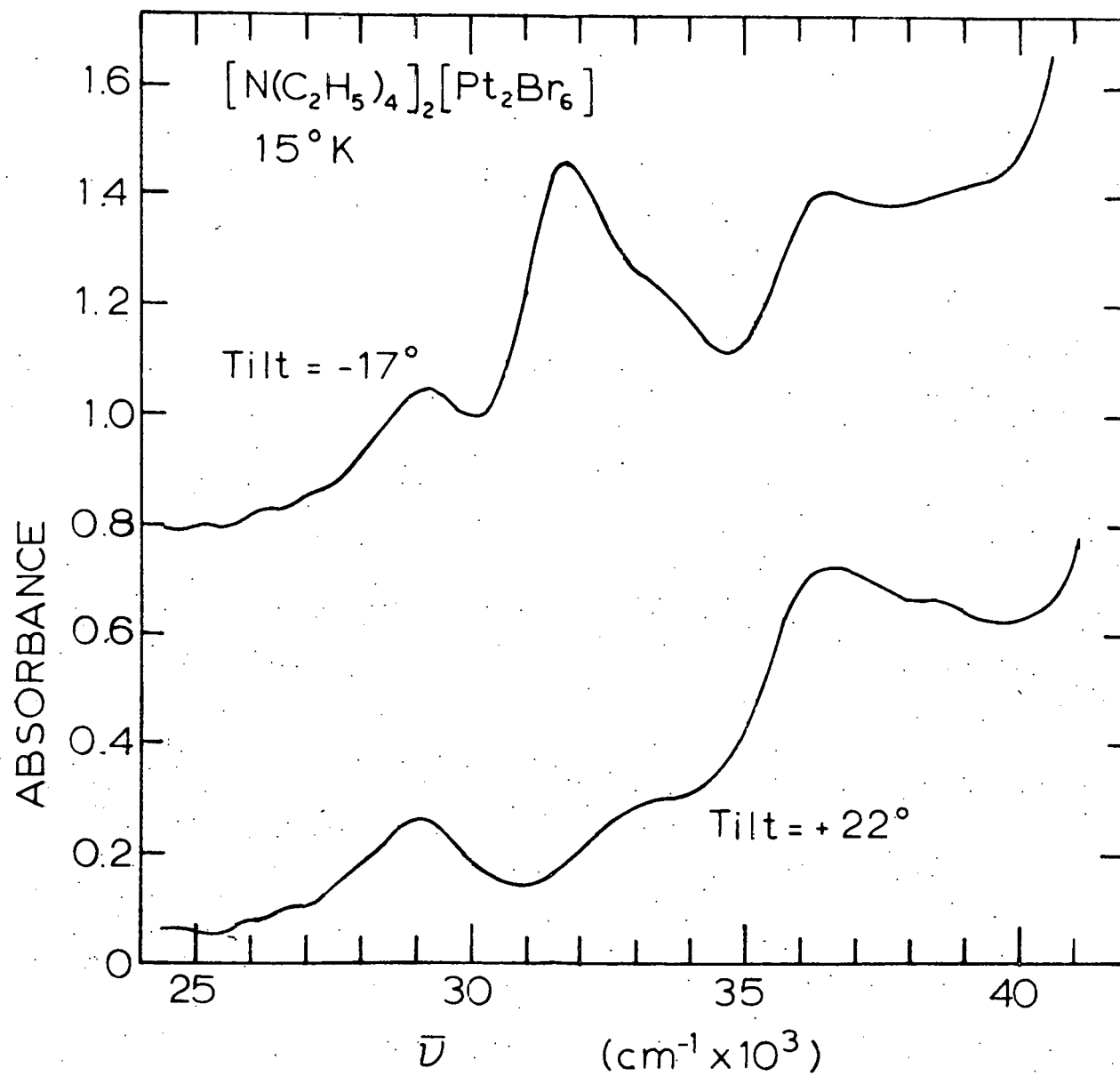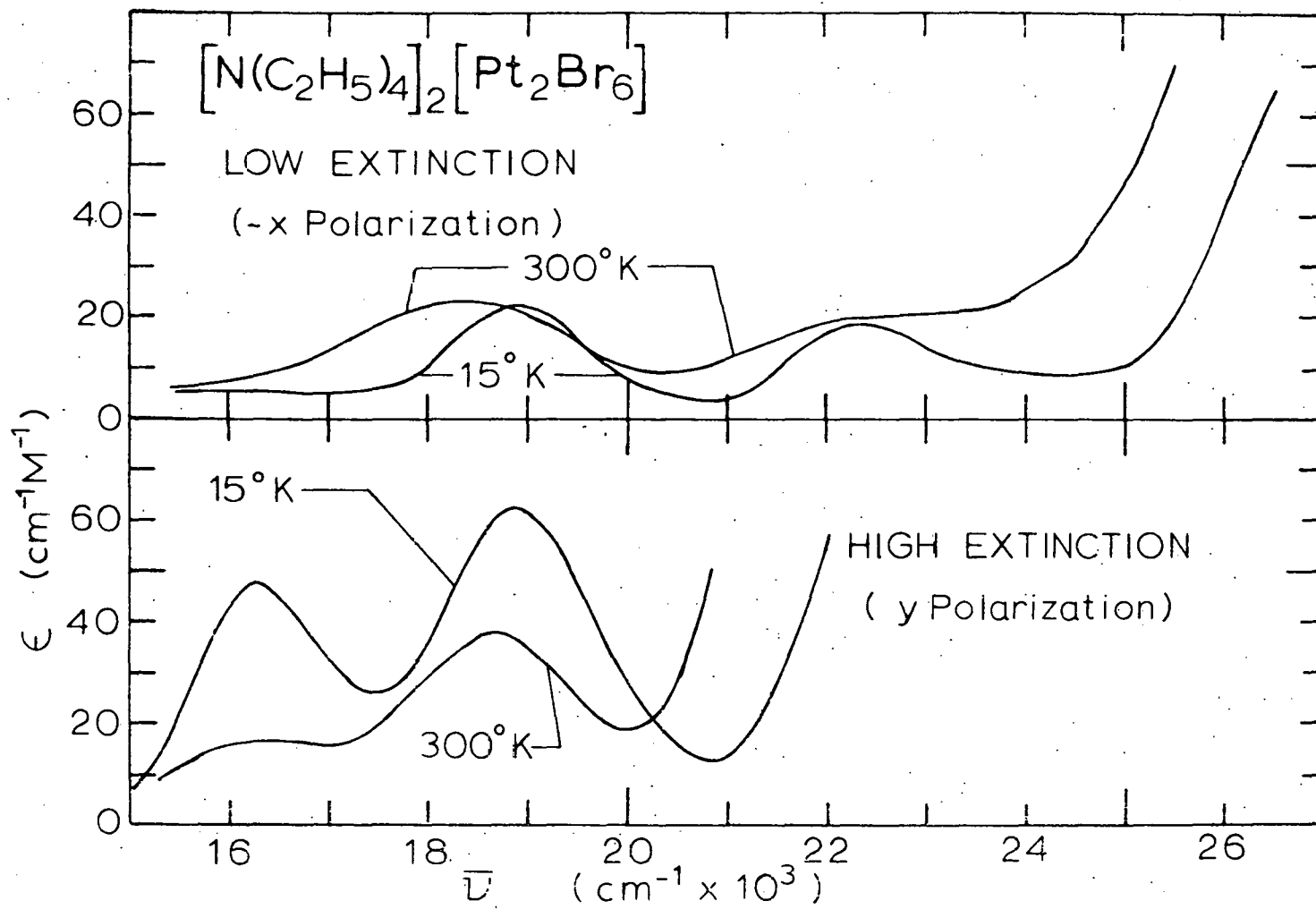in the light beam about the high extinction axis

Figure 20. Polarized crystal spectra for a thick crystal

(77 μ) of $[N(C_2H_5)_4]_2Pt_2Br_6$

At the opposite extreme electrons could be held in
delocalized molecular orbitals which could be formed from
linear combinations of equivalent orbitals. In this case
the two lowest unfilled orbitals would be the combinations
of $(d_{yz,1} + d_{yz,2})/2^{\frac{1}{2}}$ with b_{3g} symmetry and $(d_{yz,1} -
d_{yz,2})/2^{\frac{1}{2}}$ with b_{2u} symmetry under D_{2h} symmetry. Interaction
of these two orbitals with ligand p-orbitals give a pair
of antibonding orbitals. The two molecular orbitals formed
by these linear combinations are shown in Figure 21. Also
included in Figure 21 are the two highest filled orbitals
formed from the linear combinations of $d_{y^2-z^2}$ orbitals to
give b_{1u} and a_g symmetry. Then for each d←d transition for
the monomeric ions there will be four possible transitions
in the case of the dimer. Two of these four transitions
are u←g and might therefore be dipole allowed. For a
molecule of D_{2h} symmetry the possible final states attained
by dipole-allowed transitions with the indicated polari-
zations have the symmetry $B_{1u(z)}$, $B_{2u(y)}$, and $B_{3u(x)}$.

A representation of the energies of molecular orbitals
formed through the linear combination of atomic orbitals in
$Pt_2Br_6^{2-}$ is shown in Figure 22. The relative energy ordering
of the 5d orbitals of platinum under D_{4h} symmetry are shown
to be split by the D_{2h} symmetry of $Pt_2Br_6^{2-}$ through these
linear combinations of the atomic orbitals. Also shown in
Figure 20 are the symmetry of the spin-allowed u←g, d←d
states under D_{2h} point group symmetry as well as the

Figure 21. Molecular orbitals formed on the basis of
combinations of the d_{yz} and $d_{y^2-z^2}$ orbitals
of platinum and the bromide p-orbitals.
Also shown are the dipole-allowed d←d
transitions

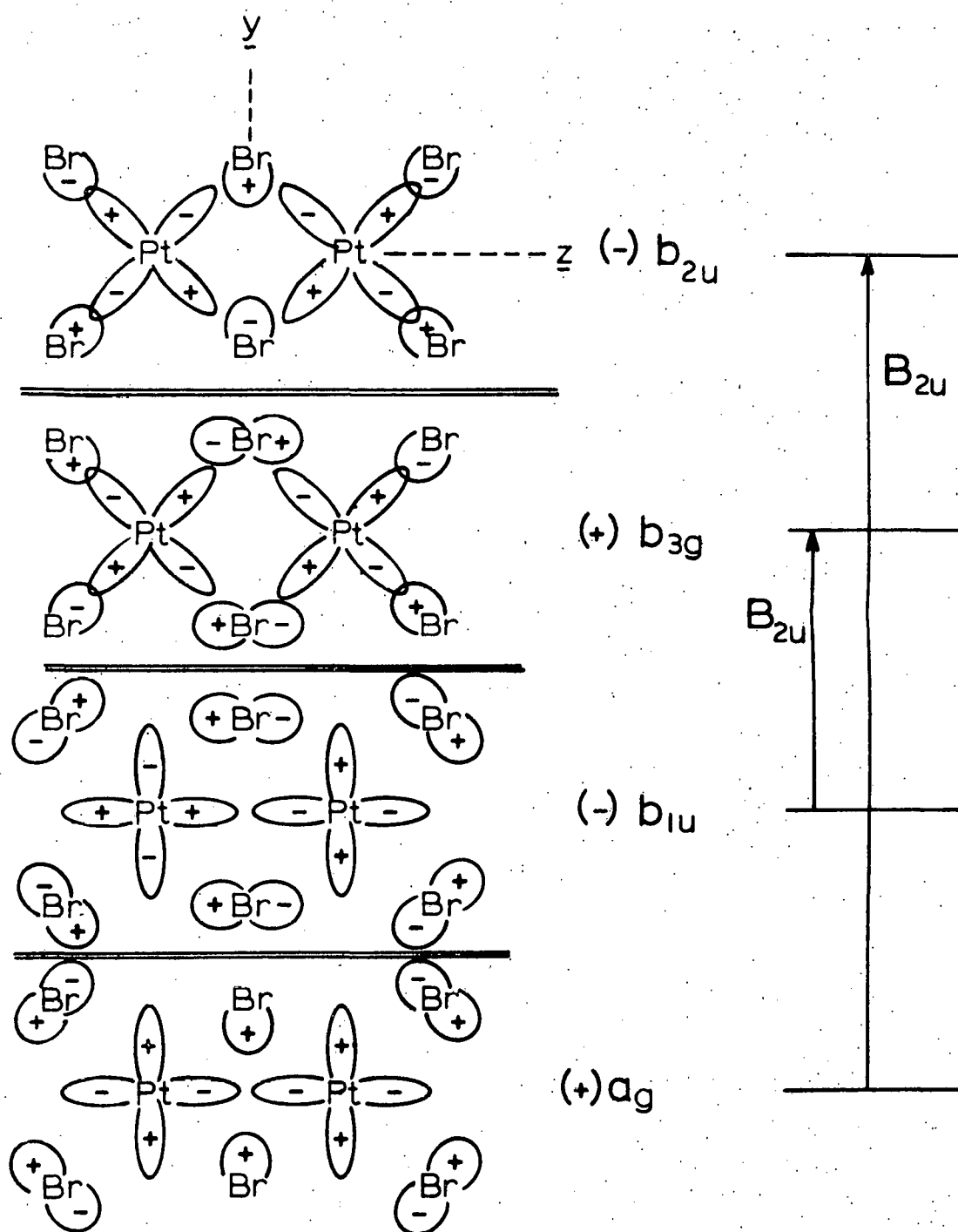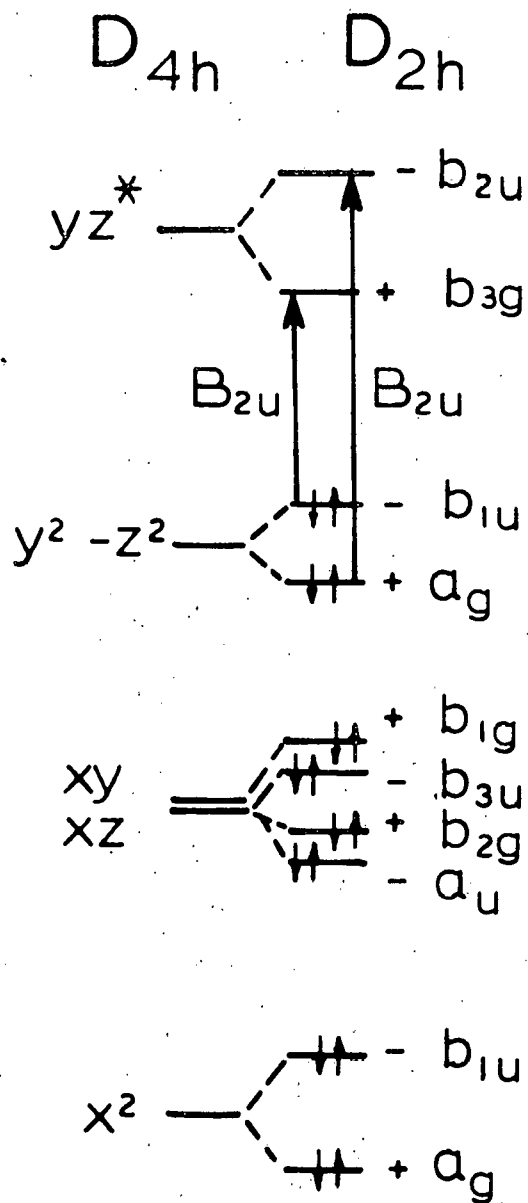Figure 22. Symmetry of the LCAO-MO's in $Pt_2Br_6^{2-}$

under D_{2h} point group formed from the Pt

5d orbitals under D_{4h} point group. Also

shown is the symmetry for the spin-allowed

u←g, d←d states under D_{2h} and polarization

of dipole-allowed transitions

polarization of these dipole-allowed transitions. The orbitals $d_{y^2-z^2}$ and d_{x^2} have the same symmetry and have the potential of mixing with one another. The lowest spin-allowed pair of transitions should occur with y-polarization. In the next high group of transitions the electrons are excited from the next lower energy lying molecular orbitals, which are formed from the degenerate orbitals of the $PtBr_4^{2-}$ ion. From these orbitals four ungerade excited states are possible. Two states are of ^1A_u symmetry and are dipole-forbidden. The two remaining states are $^1B_{3u}$ states for the $d_{yz} \leftarrow d_{xy}$ transitions and are polarized in the x-direction. The highest pair of d←d transitions will be allowed in y-polarization. This particular ordering predicts no dipole-allowed, spin-allowed d←d transitions with z-polarization.

The energy separation of molecular orbitals in $Pt_2Br_6^{2-}$ will be dependent upon the extent of overlap in the LCAO-MO. This overlap also determines the energy separation of transitions as well as the intensity of the allowed transitions. A great deal of overlap between orbitals might involve the bridging ligand p-orbitals.

In the case where the overlap between orbitals is not large, then the electronic interaction between the two platinums would be intermediate between the situation where the platinum atoms are isolated and where there is significant

overlap of orbitals. In this intermediate case the platinum
atoms in the dimer could be considered to be coupled chromo-
phores. There would be zero overlap between the orbitals
of these chromophores. The coupling between the chromophores
would occur as a result of crystal effects. The ground-
state molecular wave function for such a system would be
written as,

$$\Phi = \varphi_1^o \varphi_2^o \tag{70}$$

where φ_1^o and φ_2^o are ground-state wave functions for the
platinum chromophores. Excitation of this chromophore system
would result in two excited states, one for each chromophore,
and expressed as,

$$\phi_1' = \varphi_1'\varphi_2^o; \qquad \phi_2' = \varphi_1^o\varphi_2' \tag{71}$$

where φ_1' would correspond to one of the platinum chromo-
phores in the excited state as a result of an electronic
excitation in the molecular orbitals associated with it.
Two linear combinations of the excitation wave function
for the transitions are possible and are given by

$$\Phi_+' = (\phi_1' + \phi_2')/2^{\frac{1}{2}} \tag{72}$$

and

$$\Phi_-' = (\phi_1' - \phi_2')/2^{\frac{1}{2}} \tag{73}$$

The d←d transitions of the individual chromophores such as $\varphi_1' \leftarrow \varphi_1^o$ are dipole forbidden. The dipole-dipole interaction between the two chromophores does not allow enhancement of transition intensities. The increased number of d←d transitions in the platinum chromophore model are due to mixing in of dipole-allowed transitions via the electronic field at the local sites. Consideration of one of the platinum ions reveals that the molecular field has C_{2v} site symmetry. The mixing in of dipole-allowed transitions can be considered by application of perturbation theory as

$$\varphi_1' = \varphi_1'(d \leftarrow d) + a\, \varphi_1'' \tag{74}$$

where the coefficient, a, is given by

$$a = (\textstyle\int \rho_1'(d \leftarrow d) |V_1(C_{2v})| \rho_1''\, d\tau)/(E' - E'') \tag{75}$$

It is to be noted that $\rho_1'' \leftarrow \rho_1^o$ is a dipole allowed transition.

As a result of the perturbation of mixing in allowed transitions a d←d transition from the ground state to either Φ_+' or Φ_-' becomes allowed. However, due to the presence of an inversion center, if the transition $\Phi_+' \leftarrow \Phi^o$ is dipole allowed then the transition $\Phi_-' \leftarrow \Phi^o$ is forbidden and <u>vice versa</u>. Under the C_{2v} site symmetry the ground state will be $^1A_1$ and the d←d transitions will give the following states: $^1B_2$, $d_{yz} \leftarrow d_{y^2-z^2}$ (y polarization); $^1B_1$, $d_{yz} \leftarrow d_{xy}$

(x-polarization); $^1A_2$, $d_{yz} \leftarrow d_{xz}$ (forbidden); B_2, $d_{xz} \leftarrow d_{x^2}$ (y-polarization). The same polarizations for the dipole allowed transitions result as in the case of the delocalized MO model with the difference being that there is only a single transition for each d←d state rather than two. One drawback to the coupled chromophore model is the treatment of charge transfer transitions whereby an electron is transferred from a bridging ligand to platinum.

Two intense bands for $Pt_2Br_6^{2-}$ under y-polarization in the region where only spin-allowed d←d transitions occur in K_2PtBr_4 spectra. The positions of these bands are at 23,800 and 29,200 cm^{-1}. The crystal spectra of K_2PtBr_4 has two spin-allowed transitions at 24,000 cm^{-1} and 33,800 cm^{-1}. The low energy peak in the vicinity of 24,000 cm^{-1} shows a close correspondence in the spectra between $PtBr_4^{2-}$ and $Pt_2Br_6^{2-}$. The band seen at 29,200 cm^{-1} of $Pt_2Br_6^{2-}$ could not be as easily attributed to the high energy $d_{yz} \leftarrow d_{y^2-z^2}$ transition as in $PtBr_4^{2-}$. The band seen at 31,500 cm^{-1} in z-polarization of $Pt_2Br_6^{2-}$ must be a ligand to metal charge transfer. In one of the previously presented models two transitions are possible to the orbitals formed from the $\sigma^*(d_{yz})$ orbitals. Only one strong transition band is discernible over the energy range. It was therefore concluded that the splitting of the transition was so small as not to be resolved in the band. This result

agrees with the single transition associated with each d←d
state of the coupled chromophore model. However, the band
at 23,800 cm^{-1} is strong and such a large amount of intensity
borrowing would be required and would be unlikely as well.
With these findings in mind it appears that orbital overlap
and electron delocalization may need to be invoked in order
to account for the intensities.

The band seen in y-polarization at 23,800 cm^{-1} has been
assigned as $^1B_{2u} \leftarrow {}^1A_g$ ($d_{yz} \leftarrow d_{y^2-z^2}$). The intensity of this
band was found to be 37 times greater than in the equivalent
transition of K_2PtBr_4 at 24,000 cm^{-1}. This transition can
be considered to be $\pi_z \leftarrow \sigma_z$.

The band at 29,200 cm^{-1} has an $\epsilon = 2,800$ cm^{-1}M^{-1} in
comparison to the ϵ of 1,300 cm^{-1}M^{-1} for the band at
23,800 cm^{-1}. This band can possibly be assigned as
$^1B_{2u} \leftarrow {}^1A_g$ ($d_{yz} \leftarrow d_{x^2}$). However, this transition appears with
much larger intensity than the 33,800 cm^{-1} band in the case
of K_2PtBr_4. This assignment would mean that the band occurs
4,300 cm^{-1} below the analogous band in K_2PtBr_4. The
possibility exists that the 29,200 cm^{-1} band is a Pt←Br
charge transfer.

In the x-polarized spectrum a shoulder is weakly
apparent at 26,500 cm^{-1} with $\epsilon \approx 100$ cm^{-1}M^{-1}. This band
was assigned as $^1B_{3u} \leftarrow {}^1A_g$ ($d_{yz} \leftarrow d_{xy}$). This particular band
under the chromophore model derives its intensity by the

mixing in of x-polarized allowed transitions. This is
supported by the fact that there are transitions up to
42,000 cm^{-1} which are all rather weak from which the inten-
sity would be borrowed. The molecular orbital delocalization
model also favors low intensity since the electron would
be promoted from an orbital with δ_z symmetry into one of π_z
symmetry. The noted overall intensity decreases with temper-
ature lowering in the x-polarized spectrum is indicative
of the presence of some vibronic transitions in the region.

For spin-forbidden d←d transitions the electronic wave
function including spin must be considered in the D_2' double
rotational point group. The singlet spin wave function is
A' and B_1', B_2', and B_3' are triplet spin functions. As a
result of spin-orbit coupling, if there is a dipole allowed
transition to a singlet state in one polarization, then
transitions to two primarily triplet states will be dipole
allowed in the other polarizations. The transition to the
third and remaining triplet state will be dipole-forbidden
but is vibronically allowed. Transitions to the ^3A_u states
will be dipole allowed in all three polarizations. Since
the transitions in y-polarization are more intense than
those in the x-polarization, the y-polarized spin-forbidden
bands are more intense and exceed in intensity the spin-
allowed d←d transitions of K_2PtBr_4. The $^3B_{2u}$ transitions
are dipole forbidden in y polarization. Two transitions

seen at 16,300 cm^{-1} and 18,800 cm^{-1} are apparently dipole-allowed in y polarization and are thought to be components of $^3B_{3u}$ and $^3A_u \leftarrow ^1A_g$, $d_{yz} \leftarrow d_{xy}$ and d_{xz}. In the x-polarized spectrum, because the $^1B_{2u}$ transition occurs at 23,800 cm^{-1}, the $^3B_{2u}$ transition must be associated with the lower energy 18,900 cm^{-1} dipole-allowed band. The band seen at 22,300 cm^{-1} may be a $^3B_{2u}$ with the associated singlet at 29,200 cm^{-1}. In the region of 17,500 cm^{-1} the absorption appears to be dipole-forbidden but vibronically allowed and might be due to a component of one of the g←g transitions. These spin-forbidden band assignments are speculative at best and more mixing may be involved in the states.

Ligand to metal (M←L) charge-transfers occur in all three molecular polarizations. Some of these transitions are dipole allowed. The terminal and bridging bromide ligands in $Pt_2Br_6^{2-}$ must be considered separately in a discussion of charge-transfer transitions. In essence, the charge-transfer transitions involve the transfer of an electron from a bromide ligand p orbital into one of the two σ^* orbitals based on the metal d_{yz} orbitals. The x, y, and z axes of each ligand were taken parallel to the molecular axes. Linear combinations of the p_z and p_y orbitals of the terminal bromides are used to construct σ_t and in-plane $\pi_{t,h}$ orbitals. The p_x orbitals form out-of-plane $\pi_{t,x}$ orbitals. The irreducible representations of 12

symmetry-adapted LCAO of orbitals originating from the
terminal bromides are presented in Table 6. Under the D_{2h}
point group the linear combinations of σ_t and $\pi_{t,h}$ orbitals
serve as functions for identical sets of irreducible
representations. The energy of interaction for the σ and π
bonds would be expected to produce an energy separation
between these two bonding types. In the case of K_2PtBr_4
the energy separation of the charge transfer bands, $\sigma^*\leftarrow L\pi$
and $\sigma^*\leftarrow L\sigma$, was around 11,000 cm^{-1}. The symmetries of
possible singlet, ungerade excited states for electrons
transferred from these molecular orbitals are also presented
in Table 6.

The bridging bromine p orbitals, $p_{b,y}$ and $p_{b,z}$, cannot
be combined to form separate σ and π type orbitals. The
LCAO's of these four orbitals are strongly involved in
Pt-Br σ-bonds. The $p_{b,x}$ orbitals give LCAO's which have
pure π character. The symmetry of the LCAO's as well as
the symmetry designation of the singlet ungerade states are
also presented in Table 6.

In PtBr$_4{}^{2-}$ an intense band occurs at 37,000 cm^{-1} which
was assigned as $\sigma^*\leftarrow L\pi$. The next higher band in this salt
occurs at 48,000 cm^{-1}. The assignment of this particular
band was questionable and could be $\sigma^*\leftarrow L\sigma$ or $p\leftarrow d$. However,
this is the lowest possible energy for the $\sigma^*\leftarrow L\pi$. The
crystal spectra of K_2PtBr_4 indicate that the intense $\sigma^*\leftarrow L\pi$

Table 6. Symmetry of the LCAO's formed by the bromide ligand p-orbitals

Type of Bromide	Orbital type	LCAO	Singlet ungerade excited states (polarization)
Terminal	$\pi_{t,x}$	b_{1g}, b_{2g}, a_u, b_{3u}	$2\ ^1A_u$, $2\ ^1B_{3u}(x)$
	$\pi_{t,h}$	a_g, b_{3g}, b_{1u}, b_{2u}	$2\ ^1B_{1u}(z)$, $2\ ^1B_{2u}(y)$
	σ_t	a_g, b_{3g}, b_{1u}, b_{2u}	$2\ ^1B_{1u}(z)$, $2\ ^1B_{2u}(y)$
Bridging	$\pi_{b,x}$	b_{3u}, b_{1g}	^1A_u, $^1B_{3u}(x)$
	$\rho_{b,y}$	a_g, b_{2u}	$^1B_{1u}(z)$, $^1B_{2u}(y)$
	$\rho_{b,z}$	b_{3g}, b_{1u}	$^1B_{1u}(z)$, $^1B_{2u}(y)$

transitions originate from an electron transferred from in-plane π orbitals. A dipole-allowed $\sigma^* \leftarrow L\pi$ transition from an out-of-plane ligand π orbital in the region of 37,000 cm^{-1} is relatively weak with an ϵ of less than 1,000 cm^{-1}M^{-1}. These conclusions on the spectral assignments of K$_2$PtBr$_4$ appear to be pertinent to Pt$_2$Br$_6^{2-}$ since the x-polarized spectrum was recorded to 41,000 cm^{-1}. All the dipole-allowed transitions for the x-polarization originate from electrons transferred from out-of-plane p$_x$ orbitals on the bromides.

The spectra of salts of dimeric palladium(II) ions in glasses at 77K were recorded by Mason and Gray (12). They reported the intense transitions in the energy region of the $\sigma^* \leftarrow L\pi$ and $\sigma^* \leftarrow L\sigma$ transitions for the monomeric ions. Intense transitions were noted at lower energies than the $\sigma^* \leftarrow L\pi$ transition as well. Mason and Gray (12) proposed that the low energy charge transfer transitions occurring in the region, 29,000 - 31,000 cm^{-1}, arose from electron transfer from the bridging bromide ligands, i.e., M$\leftarrow\pi_b$. The bridging bromide in-plane p orbitals are all involved in the σ bonding but the p$_x$, out-of-plane, orbitals are of pure π-symmetry with respect to the Pt-Br bonds. Charge-transfer from the p$_x$-orbitals would be polarized in the x-direction. However, the intense transitions in the 29,000 - 31,000 cm^{-1} region for Pt$_2$Br$_6^{2-}$ occurs in the z-

and y-polarization, whereas the transitions are comparatively
weak in the x-polarized spectrum. Therefore, bridging
bromide $M \leftarrow \pi_b$ transitions do not contribute to the intense
bands in this region. Rather, they must be attributed to
$M \leftarrow \pi_z$.

The band seen at 31,500 cm^{-1} for z-polarization in
$Pt_2Br_6{}^{2-}$ is similar to the lowest energy intense band in
the Pd(II) dimer. This band corresponds to an electron
transfer from a ligand π orbital and is assigned as
${}^1B_{1u} \leftarrow {}^1A_{1g}$ $(\sigma^* \leftarrow \pi_{t,h})$.

The assignment of a $\sigma^* \leftarrow \pi_{t,h}$ band at such a low energy
suggests that the band seen at 29,400 cm^{-1} in the y-polarized
spectrum may be a $\sigma^* \leftarrow \pi_{t,h}$ transition to the pair of ${}^1B_{2u}$
states. Additional intense absorption in y-polarization is
seen in the spectrum in the vicinity of 37,000 cm^{-1}. These
observations suggest a mixing of $d \leftarrow d$ and $\sigma^* \leftarrow L\pi$ character
in two strong y-polarized bands at 29,400 cm^{-1} and at
around 36,000 cm^{-1}. Note that the y-polarized spectrum was
rising rapidly at 21,000 cm^{-1} and the absorption was too
intense to scan over this higher peak.

Two bands at 29,000 and 36,500 cm^{-1} in the x-polarized
spectra were assigned as electron transfers from $\pi_{t,x}$ and
$\pi_{b,x}$ to σ^*'s.

The bridging bromide ligands linking the two platinums
in $Pt_2Br_6{}^{2-}$ donate charge to the platinum. The terminal

bromide ligands donate more charge to the platinum atoms than do the bridging ligands. The net result is that both bridging bromides and platinums are more positive than in $PtBr_4^{2-}$. The $M\sigma^*\leftarrow L\pi_b$ transition in $Pt_2Br_6^{2-}$ can reasonably be expected to occur at nearly the same energy as the $M\leftarrow L\pi$ bands in $PtBr_4^{2-}$ and the $M\sigma^*\leftarrow L\pi_t$ transitions of $Pt_2Br_6^{2-}$ should occur at lower energies. Very weak bands at 33,000 and 39,000 cm^{-1} are apparent and are likely due to spin-forbidden charge-transfer bands.

Cowman et al. (31) reported the crystal spectra of crystals containing the ion $Pt_2Cl_6^{2-}$. They reported observing d$\leftarrow$d transitions with enhanced intensities and also two bands in the y-polarized spectrum with a separation of 1,650 cm^{-1} which would be assigned as $^1B_{2u}\leftarrow ^1A_g$ ($d_{yz}\leftarrow d_{y^2-z^2}$). Apparently, the smaller Pt-Pt bond distance of 3.42 Å provided a larger band separation.

The vibrational structure observed at 15K for crystals of K_2PtBr_4 at 22,700 cm^{-1} and 24,400 cm^{-1} was completely absent in $Pt_2Br_6^{2-}$ spectra. The vibrational structure results from the Franck-Condon effect which allows transitions to vibrational states of the totally symmetric vibrations in the excited electronic states. The $PtBr_4^{2-}$ possesses only one totally symmetric (A_{1g}) vibration and the $Pt_2Br_6^{2-}$ ion possesses four A_g vibrations. In $Pt_2Br_6^{2-}$ there is the doubling of the electronic states. This brings

about eight different vibrational progressions and obscures any resolution of this structure.

A component at 31,500 cm^{-1} in the aqueous spectrum of $PtBr_4^{2-}$ is absent in the crystal spectra of K_2PtBr_4. It is possible that this band is due to a small amount of $Pt_2Br_6^{2-}$ forming in equilibrium with $PtBr_4^{2-}$. This transition would correspond to $^1B_{1u} \leftarrow {}^1A_g$ ($\varepsilon \sim 9000$ $cm^{-1}M^{-1}$) in the crystal spectra of $Pt_2Br_6^{2-}$.

A summary of observed transitions and their assignments for the crystal spectra of $[N(C_2H_5)_4]Pt_2Br_6$ is presented in Table 7.

The polarized single crystal spectra of $Mo_2(O_2CCH_2NH_3)_4(SO_4)_2 \cdot 4H_2O$ were recorded for the absorption band in the region of 20,000 to 25,000 cm^{-1} (53). The spectra of this compound at 15K exhibited very detailed vibrational-electronic absorptions. The solution spectra of $Mo_2(O_2CCH_2NH_3)_4^{4+}$ was recorded in aqueous solution of 0.25 $\underline{M}$ HCl with some dissolved glycine and is shown in Figure 23. The room temperature spectra of crystals of $[Mo_2(O_2CCH_2NH_3)_4](SO_4)_2 \cdot 4H_2O$ are shown in Figure 24. A hint of some of the structure on the band is present in the c-polarized spectrum at room temperature. The spectra of a(x,y)- and c(z)-polarization at 15K are presented in Figure 25. Striking vibrational structure was clearly resolved in both polarizations.

Table 7. Observed transitions and assignments for $[N(C_2H_5)_4]_2Pt_2Br_6$ crystal spectra at 15K.

$\bar{\nu}(cm^{-1})$	$\varepsilon_{max}(cm^{-1}M^{-1})$	Polarization	Osc. Str. $fx10^4$	Excited state: Transition assignment
16,300	50	y	4	^3A_u: $d_{yz} \leftarrow d_{xz}$
17,500	(vibronic)	x		$g \leftarrow g$
18,800	60	y	6	$^3B_{3u}$: $d_{yz} \leftarrow d_{xy}$
18,900	20	x	2	$^3B_{2u}$: $d_{yz} \leftarrow d_{y^2-z^2}$
22,300	20	x	2	$^3B_{2u}$: $d_{yz} \leftarrow d_{x^2}$
23,800	1300	y	150	$^1B_{2u}$: $d_{yz} \leftarrow d_{y^2-z^2}$
26,500	100	x	10	$^1B_{3u}$: $d_{yz} \leftarrow d_{xy}$
29,000	300	x	35	$^1B_{3u}$: $d_{yz} \leftarrow L\pi_{t,x}$
29,200	2800	y	320	$^1B_{2u}$: $d_{yz} \leftarrow d_{x^2}$ or $L\pi_t$
31,500	9000	z	1000	$^1B_{1u}$: $d_{yz} \leftarrow L\pi_t$
33,000	100	x		spin-forbidden charge transfer
36,560	400	x	46	$^1B_{3u}$: $d_{yz} \leftarrow L\pi_{b,x}$
38,000	100	x	7	spin-forbidden charge transfer
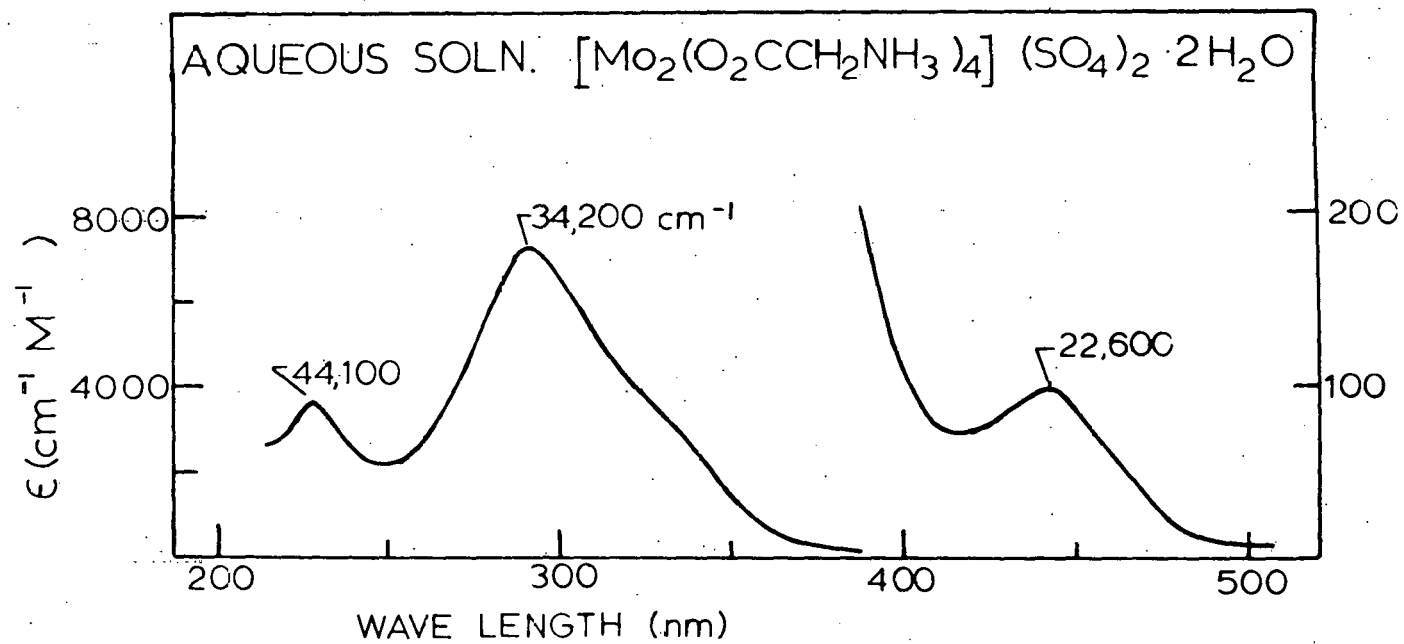
Figure 23. Aqueous solution spectra of $Mo_2(O_2CCH_2NH_3)_4(SO_4)_2 \cdot 4H_2O$

Figure 24. Polarized absorption spectra of

$Mo_2(O_2CCH_2NH_3)_4(SO_4)_2 \cdot 4H_2O$ at 300K

300°K

$[Mo_2(O_2CCH_2NH_3)_4](SO_4)_2 \cdot 2H_2O$
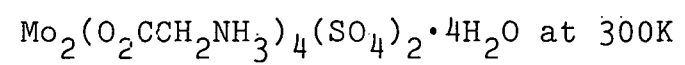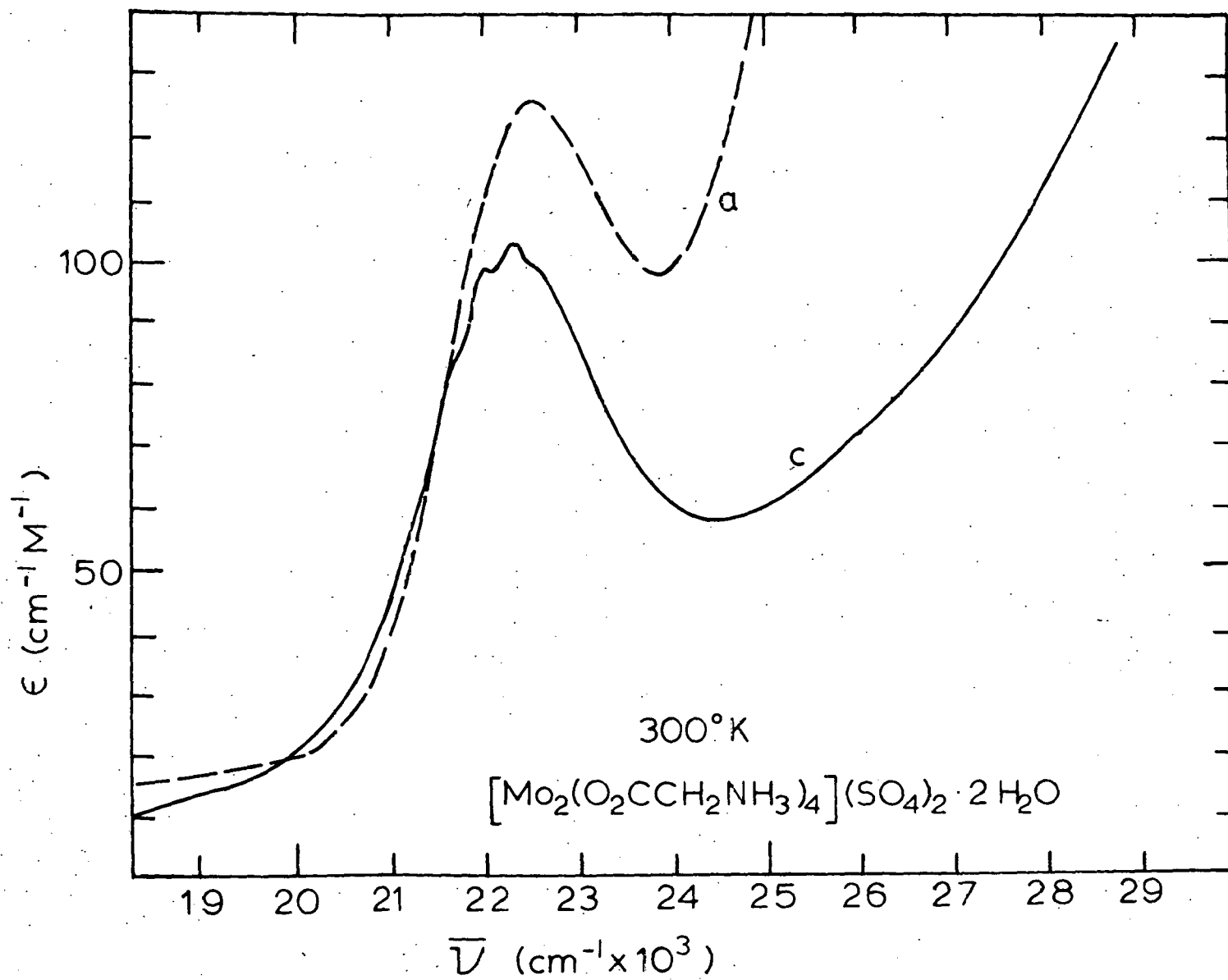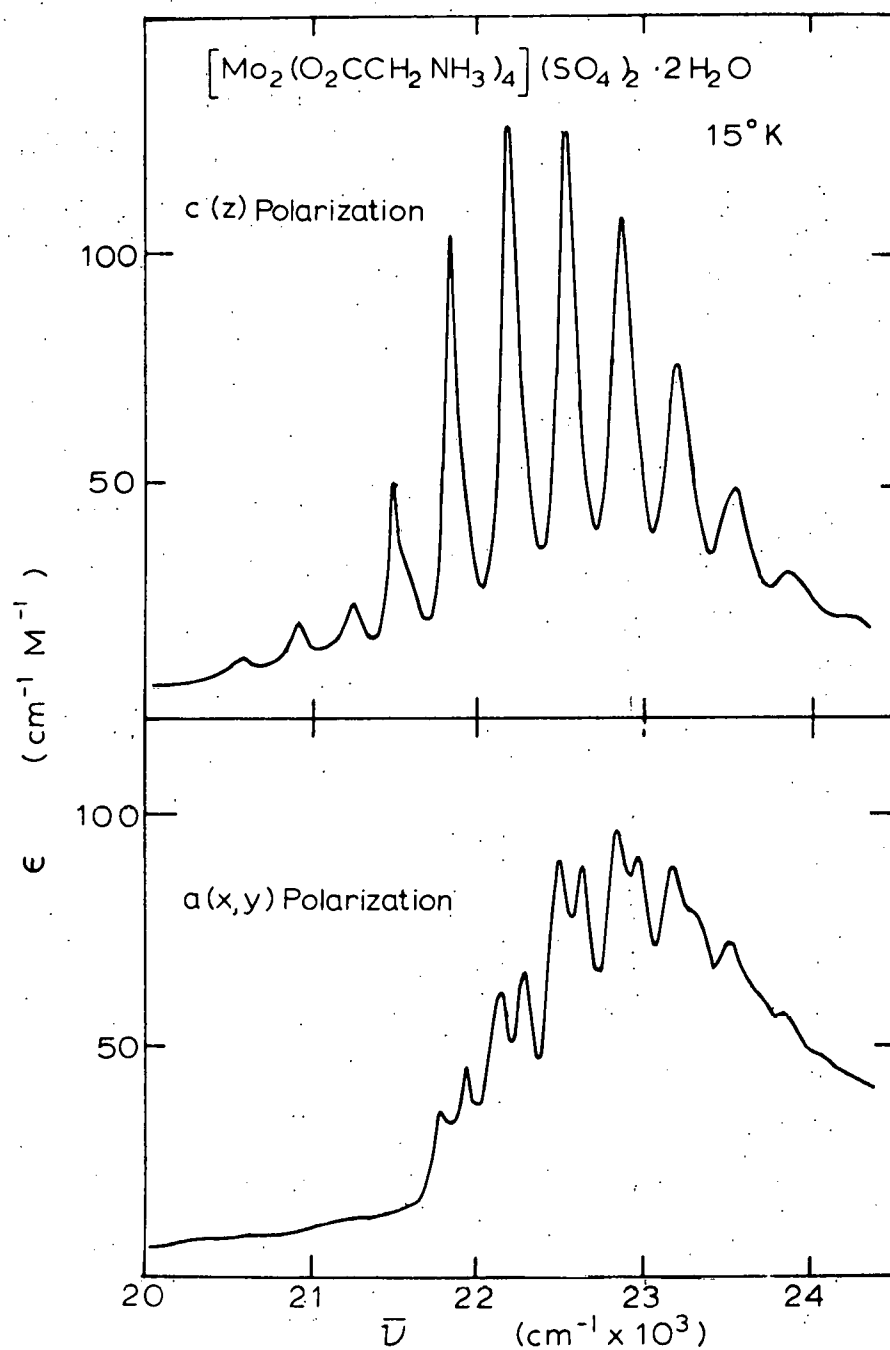
Figure 25. Polarized absorption spectra of
$Mo_2(O_2CCH_2NH_3)_4(SO_4)_2 \cdot 4H_2O$ at 15K

The solution spectrum of Figure 23 is very similar to the solution spectrum of $Mo_2(O_2CCH_3)_4$ in ethanol reported by Dubicki and Martin (33). They also reported similar absorption features for several tetracarboxylatodimolybdenum(II) complexes; and it appeared that the solution spectra of $Mo_2(O_2CR)_4$ are in general closely related.

The space group for crystals of $Mo_2(OCCH_2NH_3)_4(SO_4)_2 \cdot 4H_2O$ was $I\bar{4}$. The primitive unit cell contains only one molecule. The Mo-Mo bond was taken as the molecular z axis and is aligned to the crystallographic c-axis. The site symmetry for the Mo_2^{4+} unit was S_4, but this symmetry is close to D_{4h} about the Mo-Mo bond out as far as the bonds to the α carbon.

The peak positions and peak separations of the vibrational progressions seen in the spectra at 15K are presented in Table 8. Two progressions were discernible in the $\underset{\sim}{c}(z)$-polarized spectrum. The first of these progressions began at 20,570 cm^{-1} and was made up of four lines with a mean energy separation of 343 ± 9 cm^{-1}. The second of these was of much larger intensity and began at 21,510 cm^{-1} and had nine lines with a mean separation of 345 ± 10 cm^{-1}. The fourth and possibly a fifth member of the lower intensity progression appeared as shoulders on the higher intensity vibrational progression. Two overlapping progressions are seen in the $\underset{\sim}{a}(x,y)$-polarization.

Table 8. Vibrational structures for $Mo_2(O_2CCH_2NH_3)_4(SO_4)_2$ $\cdot 4H_2O$

c-polarization		a-polarization				
ν (cm^{-1})	$\Delta\nu$ (cm^{-1})	ν_1 (cm^{-1})	$\Delta\nu_1$ (cm^{-1})	ν_2 (cm^{-1})	$\Delta\nu_2$ (cm^{-1})	$\nu_2-\nu_1$ (cm^{-1})
1st Series						
20,570		21,790		21,930		140
	350		350		350	
20,920		22,140		22,280		140
	350		350		350	
21,270		22,490		22,630		140
	(330)		340		330	
(21,600)		22,830		22,960		130
			340		340	
2nd Series		23,170		23,300		130
			350		350	
21,510		23,520		(23,650)		130
	360		320			
21,870		(23,840)				
	360					
22,230						
	340					
22,570		21,510−20,570 = 940				
	340		21,790−20,570 = 1220			
22,910		21,930−20,570 = 1360				
	350					
23,260						
	340					
23,600						
	330					
23,930						
	340					
24,270						

These two progressions are about ten-fold more intense than the weak progression of the z-polarization, but they are weaker than the strong intensity progression of the z-polarized spectrum. The first progression in the x,y-polarization starts at 21,790 cm^{-1} and consists of seven members with an average energy spacing of 342 ± 11 cm^{-1}. The second progression starts at 21,930 cm^{-1} and consists of six members with an energy separation of 344 ± 8 cm^{-1}.

The first weak progression in z-polarization originating at the lowest energy might be due to an electronic transition which is forbidden under D_{4h} symmetry but allowed due to crystal field perturbation of the S_4 site symmetry. The small deviation from D_{4h} in the vicinity of the Mo-Mo bond would explain the weakness of this progression. The peak seen at 20,570 cm^{-1} would presumably be the 0-0 line. The other more intense progression seen in z-polarization and the ones in x,y-polarized progressions could be due to vibronic perturbation by the asymmetric vibrations under D_{4h}. The energy of the asymmetric vibration in the excited electronic state indicated by the difference of the first member in each progression from the 0-0 band at 20,570 cm^{-1} would be 940 cm^{-1} for the z-polarized progression, 1,220 cm^{-1} for the first x,y-polarized progression, and 1,360 cm^{-1} for the second x,y-polarized progression. The magnitude of these vibrations in the

excited state are high and are probably not due to bending

vibrational modes of Mo-Mo-O distortion which would be

lower in energy. The Mo-Mo-O distortions are present in

the molybdenum(II) acetate compound as reported by Bratton,

Cotton, Debeau, and Walton (54). In view of the large

number of vibrational modes for the ion relatively simple

electronic excitation spectra indicate that the electronic

excitation is probably quite localized in the ion. The

vibrational spacing in the progressions average 340 -

345 cm^{-1} and are presumably associated with the mode of

Mo-Mo stretching. This particular mode has a ground state

energy of 393 cm^{-1}. This lowering of the energy spacing

in the excited state progressions is most likely due to

the promotion of an electron from an Mo-Mo bonding orbital

or into an antibonding Mo-Mo orbital or both.

Possible assignments for the electronic transition

under this assignment forbidden in D_{4h} and allowed in the

z-polarized spectrum under S_4 are $^1A_{1u}$, $^1B_{1g}$, $^1B_{2g} \leftarrow ^1A_{1g}$.

Under the preceding considerations, the transition could

not be due to the $\delta^* \leftarrow \delta$ transition and the orbital ordering

in Figure 6 would need revision. Recently, spectra have

been recorded for a series of molybdenum(II) carboxylates

which contain the $Mo_2(O_2CR)_4$ molecular units (55,56). In

each case strong vibronic structure is seen for a weak

transition. Although the molecule has occupied sites of

low symmetry, no weak progressions corresponding to crystal field perturbations originating so far below the first vibronic state despite the fact that considerably more progressions originating from correspondingly more vibrations have been seen. Although the spectra shown in Figure 25 were reproduced from three different crystals; since they all were prepared from a single synthesis, the possibility exists that they might have contained an impurity component.

IV. CONCLUSIONS

The crystal structure of $K_2PtBr_4 \cdot 2H_2O$ was determined and was found to have an orthorhombic unit cell with two molecules per unit cell.

The absorption spectra for $K_2PtBr_4 \cdot 2H_2O$, $[N(C_2H_5)_4]_2Pt_2Br_6$, and $Mo_2(O_2CCH_2NH_3)_4(SO_4) \cdot 4H_2O$ have been recorded at 300 and 15K. In the case of $K_2PtBr_4 \cdot 2H_2O$ polarized spectra were obtainable for the a-, b-, and c-directions. The spectra of crystals of $[N(C_2H_5)_4]_2Pt_2Br_6$ were recorded for both the high and low extinctions of the 001 cleavage face. The polarized spectra of $Mo_2(O_2CCH_2NH_3)_4(SO_4)_2 \cdot 4H_2O$ were obtained for the a- and c-polarizations.

In $K_2PtBr_4 \cdot 2H_2O$ crystals the spectra were quite similar to the corresponding spectra in anhydrous K_2PtBr_4. Vibrational structure at 15K was resolved for two of the d←d bands. A study of the vibrational structure provided a distinction between K_2PtBr_4 and $K_2PtBr_4 \cdot 2H_2O$. The $^1A_{2g} \leftarrow {}^1A_{1g}$ transition was identified by its absence from the c-polarization spectrum. Davydov splitting of transition energies was not discernible in the crystal spectra of $K_2PtBr_4 \cdot 2H_2O$.

The polarized absorption spectra of crystals of $[N(C_2H_5)_4]_2Pt_2Br_6$ were recorded in the region 15,000 – 40,000 cm^{-1}. The excited states of $Pt_2Br_6^{2-}$ were assigned

under the D_{2h} point group. The delocalization of the
platinum(II) d electrons was found to enhance the inten-
sities of both spin-forbidden and spin-allowed d←d
transitions and permit some dipole-allowed character in
these transitions. The M←L charge-transfer transitions
occur at lower energies for $Pt_2Br_6^{2-}$ than for $PtBr_4^{2-}$.
These intense charge-transfer transitions were found to
originate from the terminal bromide ligands.

The polarized single crystal spectra of
$Mo_2(O_2CCH_2NH_3)_4(SO_4)_2 \cdot 4H_2O$ revealed the presence of strong
vibrational structure at 15K. The very simple inter-
actions with the available vibrational modes is probably
indicative of the localization of the electronic
excitation in the ion. The observations reported for the
crystal spectra of $Mo_2(O_2CCH_2NH_3)_4(SO_4)_3 \cdot 4H_2O$ are incon-
sistent with the assignment of the absorption band as the
$\delta^* \leftarrow \delta$ transition.

V.   ACKNOWLEDGEMENTS

VI. BIBLIOGRAPHY

1. D. P. Craig and S. H. Walmsley, "Excitons in Molecular Crystals," W. A. Benjamin, Inc., New York, N.Y., 1968.

2. D. S. McClure, Solid State Phys., 9, 399 (1959).

3. R. M. Hochstrasser, "Molecular Aspects of Symmetry," W. A. Benjamin, Inc., New York, N.Y., 1966, Chapter 10.

4. D. S. Martin, Jr., Inorganica Chimica Acta Reviews, 5, 107 (1971).

5. L. F. Phillips, "Basic Quantum Chemistry," J. Wiley and Sons, Inc., New York, N.Y., 1965, p. 126.

6. A.B.P. Lever, "Inorganic Electronic Spectroscopy," Elsevier Publishing Co., New York, N.Y., 1968, p. 123.

7. C. J. Ballhausen, "Introduction to Ligand Field Theory," McGraw Hill Book Co., New York, N.Y., 1962, p. 187.

8. J. Chatt, G. O. Gamlen and L. E. Orgel, J. Chem. Soc., 1958, 486.

9. C. K. Jorgensen, "Absorption Spectra and Chemical Bonding in Complexes," Pergamon Press, London, England, 1961, p. 169.

10. H. B. Gray and C. J. Ballhausen, J. Amer. Chem. Soc., 85, 260 (1963).

11. H. Basch and H. B. Gray, Inorg. Chem., 6, 369 (1967).

12. W. R. Mason and H. B. Gray, J. Amer. Chem. Soc., 90, 5721 (1968).

13. F. A. Cotton and C. B. Harris, Inorg. Chem., 6, 369 (1967).

14. A. J. McCaffery, P. N. Schatz and P. N. Stephens, J. Amer. Chem. Soc., 90, 5730 (1968).

15. R. F. Fenske, D. S. Martin, Jr., and K. Ruedenberg, Inorg. Chem., 1, 441 (1962).

16. S. Yamada, J. Amer. Chem. Soc., 73, 1182 (1951).

17. C. K. Jorgensen, Adv. Chem. Physics, 5, 33 (1963).

18. D. S. Martin, Jr., and C. A. Lenhardt, Inorg. Chem., 3, 1368 (1964).

19. O. S. Mortensen, Acta Chem. Scand., 19, 1500 (1965).

20. D. S. Martin, Jr., M. A. Tucker and A. J. Kassman, Inorg. Chem., 4, 1682 (1965).

21. P. Day, A. F. Orchard, A. J. Thompson and R.J.P. Williams, J. Chem. Phys., 42, 1973 (1965).

22. D. S. Martin, Jr., M. A. Tucker and A. J. Kassman, Inorg. Chem., 5, 1298 (1966).

23. D. S. Martin, Jr., J. G. Foss, M. E. McCarville, M. A. Tucker and A. J. Kassman, Inorg. Chem., 5, 491 (1966).

24. B. G. Anex and N. Takeudhi, J. Amer. Chem. Soc., 96, 4411 (1974).

25. H. H. Patterson, J. J. Godfrey and S. M. Khan, Inorg. Chem., 11, 2872 (1972).

26. H. H. Patterson, T. G. Harrison and R. J. Belair, Inorg. Chem., 15, 1461 (1976).

27. R. F. Kroening, R. M. Rush, D. S. Martin, Jr., and J. C. Clardy, Inorg. Chem., 13, 1366 (1974).

28. E. Biilman and A. C. Anderson, Ber. Deut. Chem. Ges., 36, 1565 (1903).

29. N. C. Stephenson, Acta Crystallogr., 17, 587 (1964).

30. P. Day, M. J. Smith and R.J.P. Williams, J. Chem. Soc. A, 668 (1968).

31. C. D. Cowman, J. C. Thibeault, R. F. Ziolo and H. B. Gray, J. Amer. Chem. Soc., 98, 3209 (1976).

32. F. A. Cotton, Inorg. Chem., 4, 334 (1965).

33. L. Dubicki and R. L. Martin, Aust. J. Chem., 22(8), 1571 (1969).

34. J. G. Norman, Jr. and H. J. Kolari, J. Chem. Soc. Chem. Comm., 649 (1975).

35. C. D. Cowman and H. B. Gray, J. Amer. Chem. Soc., 95, 8177 (1973).

36. F. A. Cotton, B. A. Frenz, B. R. Stults and T. R. Webb, J. Amer. Chem. Soc., 98, 2768 (1976).

37. F. A. Cotton and T. R. Webb, Inorg. Chem., 15, 68 (1976).

38. C. M. Harris, S.E.M. Livingstone and N. C. Stephenson, J. Chem. Soc., 3697 (1958).

39. F. D. Bloss, "An Introduction to the Methods of Optical Crystallography," Holt, Rinehart and Winston, Inc., New York, N.Y., 1961, p. 50.

40. D. S. Martin, Jr., R. M. Rush and T. J. Peters, Inorg. Chem., 15, 669 (1976).

41. L. E. Alexander and G. S. Smith, Acta Cryst., 15, 983 (1962).

42. "International Tables of X-Ray Crystallography," Vol. III, 2nd ed., Kynoch Press, Birmingham, England, 1968, p. 157.

43. D. J. Wehe, W. R. Busing and H. A. Levy, "OR ABS, A Fortran Program for Calculating Single Crystal Absorption Corrections," USAEC Report ORNL-TM-229, Oak Ridge National Laboratory, Oak Ridge, Tennessee, 1962.

44. J. D. Scott, Queen's University, Kingston, Ontario, Canada, private communication, 1971.

45. S. L. Lawton and R. A. Jacobson, Inorg. Chem., 7, 2124 (1968).

46. M. M. Woolfson, "An Introduction to X-Ray Crystallography," Cambridge University Press, London, England, 1970, p. 244.

47. C. R. Hubbard, C. O. Quicksall and R. A. Jacobson,
     "The Fast Fourier Algorithm and the Programs ALFF,
     ALFFDP, ALFFPROJ, ALFFT and FRIEDEL," USAEC Report
     IS-2625, Ames Laboratory, Iowa State University,
     Ames, Iowa, 1971.

48. W. R. Busing, K. O. Martin and H. A. Levy, "OR FLS,
     A Fortran Crystallographic Least-Squares Program,"
     USAEC Report ORNL-TM-305, Oak Ridge National
     Laboratory, Oak Ridge, Tennessee, 1962.

49. P. A. Doyle and P. S. Turner, Acta Cryst., A24, 390
     (1968).

50. P. Hendra, J. Chem. Soc. A, 1298 (1967).

51. P. E. Fanwick and D. S. Martin, Jr., Inorg. Chem., 12,
     24 (1973).

52. P. A. Vaughan, J. H. Sturdivant and L. Pauling,
     J. Amer. Chem. Soc., 72, 5477 (1950).

53. F. A. Cotton, D. S. Martin, Jr., T. R. Webb and
     T. J. Peters, Inorg. Chem., 15, 1199 (1976).

54. W. K. Bratton, F. A. Cotton, M. Debeau and
     R. A. Walton, J. Coord. Chem., 1, 121 (1971).

55. P. E. Fanwick and D. S. Martin, Jr., Iowa State
     University, Ames, Iowa, private communication, 1977.

56. W. C. Trogler, E. I. Solomon, I. Trajberg,
     C. J. Ballhausen and H. B. Gray, California Institute
     of Technology, Pasadena, California, private
     communication, 1977.